

Evaluating the interaction of heavy metals and biocides with dissolved organic matter in building runoff and their adsorption onto granular activated carbon

Panfeng Zhu

Complete reprint of the dissertation approved by the TUM School of Engineering and Design of the Technical University of Munich for the award of the

Doktor der Ingenieurwissenschaften (Dr.-Ing.).

Chair: Prof. Dr.-Ing. habil. Konrad Koch

Examiners:

1. Prof. Dr. Brigitte Helmreich
2. Prof. Dr. An Liu

The dissertation was submitted to the Technical University of Munich on 30 August 2024 and accepted by the TUM School of Engineering and Design on 4 December 2024.

Abstract

Water scarcity is a worldwide concern expected to affect more than three billion people in 2050. Hence, addressing the water crisis is an urgent task that is of high priority. Besides reusing treated wastewater, building runoff harvesting and reuse is a promising alternative to mitigate water stress. However, stormwater runoff from buildings is usually contaminated by heavy metals and biocides/transformation products (TPs) released from construction materials. Therefore, appropriate treatment is required to remove the pollutants and improve runoff quality for reuse and safe discharge to groundwater. To achieve efficient removal performance, we need a better understanding of pollutants' environmental behaviors. By now, their release from buildings and occurrence in urban water systems have been widely studied. However, the interaction with ubiquitously present dissolved organic matter (DOM) is scarcely addressed. This study aims to investigate the interaction of heavy metals and biocides/TPs with DOM and evaluate their adsorption onto granular activated carbon (GAC) as a treatment step. The mechanistic research could provide detailed insights into pollutant-DOM interactions in building runoff and the consequent influence on the adsorption process, providing fundamental knowledge for developing or improving treatment technologies for building runoff.

Firstly, the interaction of dissolved heavy metals (Cu^{2+} and Zn^{2+}) and biocides (benzyl-dimethyl-tetradecyl ammonium chloride dihydrate (BAC), mecoprop-p (MCP)) with DOM (commercial humic substance as representative) at pH 5–9 was studied by using excitation-emission matrix and parallel factor analysis (EEM-PARAFAC). Meanwhile, mechanisms involved in the interaction between BAC/MCOP with DOM were revealed by Fourier-transform infrared spectroscopy (FTIR) and two-dimensional correlation spectrum (2D-COS) analysis. Results showed that the DOM used in this study can be separated into two fluorescent components, C1 and C2. Of these two components, C1 interacted stronger with heavy metals and biocides than C2, indicated by more quenched fluorescence. Increasing pH enhanced the interaction between heavy metals and DOM; for component C1, a sample with $66.9 \mu\text{mol/L}$ of Cu^{2+} at pH 9 quenched 12.7% more fluorescence than at pH 5. Contrarily, higher pH impaired the interaction between BAC/MCOP and DOM; a 21.3% increase in fluorescence was observed for the MCOP-C1 group from pH 5 to 9. FTIR coupled with 2D-COS analysis revealed that

hydrogen bonding, π - π interaction, and electrostatic effect are involved in the interaction between BAC/MCPP and DOM.

Quantitative analysis was carried out to evaluate the extent of interaction after qualitatively determining the interaction between building runoff pollutants with DOM. In present study, diuron, MCPP, terbutryn, BAC, 1-(3,4-dichlorophenyl)-3-methylurea, 1-(3,4-dichlorophenyl) urea, 3,4-dichloroaniline, atra-zine-desisopropyl-2-hydroxy, and terbutylazine-2-hydroxy were introduced as biocides and TPs. To investigate the effect of DOM molecular weight (MW) on the interaction with heavy metals and biocides/TPs, DOM was separated by centrifugal fractionation according to MW difference and was then characterized. After that, the binding of heavy metals and biocides/TPs with DOM fractions was analyzed using dialysis equilibrium. The results showed that the UV absorbance of different DOM fractions was similar. Their $SUVA_{254}$ values were in the range of 7.5–8.2 L/(mgC·m). The highest total acidity was found for DOM fraction 3–10 kDa with 22.9 mmol/gC, followed by DOM fraction >100 kDa (18.0 mmol/gC) and DOM fraction 10–30 kDa (15.2 mmol/gC). For the binding of Cu^{2+} to DOM, it was found that Cu^{2+} prefers to bind with DOM fraction with higher MW; however, this trend was not observed for Zn^{2+} , which showed weaker DOM binding than Cu^{2+} . For the binding of biocides/TPs with DOM, parent biocides showed a higher affinity to DOM than corresponding TPs. Additionally, parent biocides-DOM binding affinity was found following a decreasing order of MCPP > terbutryn > diuron, and hydrogen bonding played an important role in the binding of MCPP with DOM. The presence of Cu^{2+} inhibited the binding of biocides to the DOM fraction >100 kDa. In contrast, the binding of biocides to DOM fractions <100 kDa was enhanced.

GAC is a promising adsorbent for removing both organic and inorganic pollutants. In this study, we investigated its adsorption of heavy metals and biocides and evaluated the influence of DOM (5 mgC/L) during this process. Langmuir and Freundlich models fitted the adsorption processes. The results showed that more than half of DOM at low concentration (5 mgC/L) was adsorbed by GAC, and the adsorption was greater for low MW (3–10 kDa) of DOM. The maximum adsorption of Cu^{2+} and Zn^{2+} in the absence of DOM influence estimated by the Langmuir model were 157 and 85.7 μ mol/g, respectively. The Freundlich model well explained the GAC adsorption difference between Cu^{2+} and Zn^{2+} . The presence of 5 mgC/L DOM improved the adsorption of Cu^{2+} , whereas Zn^{2+} was less affected due to its weaker affinity to GAC. When DOM

was absent for adsorption of biocides/TPs onto GAC, GAC adsorbed more diuron-related compounds than terbutryn-related compounds. Additionally, DOM affected slightly on diuron adsorption but enhanced terbutryn adsorption and inhibited MCPP adsorption. The impact of Cu^{2+} and Zn^{2+} on biocides adsorption was similar to those of DOM.

In summary, this dissertation investigated the interactions between building runoff pollutants (i.e., heavy metals and biocides/TPs) and DOM and their adsorption onto GAC. Involved interaction mechanisms and pollutant binding/adsorbing preference were revealed. The obtained results can supplement our understanding of the behaviors of building runoff pollutants and provide guidance for building runoff treatment system design. Briefly, adsorption treatment is recommended for building runoff pollutants removal and adsorbent material with abundant oxygen-containing functional group is suggested. Meanwhile, to improve treatment efficiency, sequential adsorption of building runoff pollutants can be considered.

Zusammenfassung

Wasserknappheit ist ein weltweites Problem, das im Jahr 2050 voraussichtlich mehr als drei Milliarden Menschen betreffen wird. Daher ist die Bewältigung der Wasserkrise eine dringende Aufgabe mit hoher Priorität. Neben der Wiederverwendung von gereinigtem Abwasser ist die Sammlung und Wiederverwendung von Niederschlagsabfluss von Gebäuden eine vielversprechende Alternative, um den Wasserstress zu mindern. Der Niederschlagsabfluss von Gebäuden ist jedoch in der Regel durch Schwermetalle und Biozide/Transformationsprodukte (TPs) verunreinigt, die aus Baumaterialien freigesetzt werden. Daher ist eine geeignete Behandlung erforderlich, um die Schadstoffe zu entfernen und die Qualität des Abwassers für die Wiederverwendung zu verbessern. Eine Behandlung ist auch notwendig, wenn die Einleitung des Niederschlagswassers in das Grundwasser erfolgt. Um eine effiziente Reinigungsleistung in Behandlungsanlagen zu erzielen, müssen wir das Verhalten der Schadstoffe und Interaktionen mit anderen Inhaltsstoffen besser verstehen. Ihre Freisetzung aus Gebäuden und ihr Vorkommen in städtischen Gewässern sind inzwischen weitgehend erforscht, doch die Wechselwirkung mit der allgegenwärtigen gelösten organischen Substanz (DOM) ist kaum untersucht worden. Ziel dieser Studie ist es, die Wechselwirkung von Schwermetallen und Bioziden/TPs mit DOM zu untersuchen und ihre Adsorption an körniger Aktivkohle (GAC) als Behandlungsstufe zu bewerten. Die mechanistische Forschung könnte detaillierte Einblicke in die Wechselwirkungen zwischen Schadstoffen und DOM in Gebäudeabflüssen und den daraus resultierenden Einfluss auf den Adsorptionsprozess liefern, was grundlegende Erkenntnisse für die Entwicklung oder Verbesserung von Behandlungstechnologien für Gebäudeabflüsse liefern könnte.

Zunächst wurde die Wechselwirkung von Schwermetallen (Cu^{2+} und Zn^{2+}) und Bioziden (Benzyl-Dimethyl-Tetradecylammoniumchlorid-Dihydrat (BAC), Mecoprop-p (MCP)) mit DOM (handelsüblicher Huminstoff als Vertreter) bei einem pH-Wert von 5-9 mittels Anregungs-Emissions-Matrix und paralleler Faktorenanalyse (EEM-PARAFAC) untersucht. In der Zwischenzeit wurden die Mechanismen, die an der Interaktion zwischen BAC/MCOP und DOM beteiligt sind, durch Fourier-Transformations-Infrarotspektroskopie (FTIR) und zweidimensionale Korrelationsanalyse (2D-COS) ermittelt. Die Ergebnisse zeigten, dass das in dieser

Studie verwendete DOM in zwei fluoreszierende Komponenten C1 und C2 aufgeteilt werden kann. Von diesen beiden Komponenten zeigte C1 eine stärkere Wechselwirkung mit Schwermetallen und Bioziden als C2, was sich in einer stärker gelöschten Fluoreszenz resultierte. Ein steigender pH-Wert verstärkte die Wechselwirkung zwischen Schwermetallen und DOM. Für die Komponente C1 löschte eine Probe mit $66,9 \mu\text{mol/l Cu}^{2+}$ bei pH 9 12,7 % mehr Fluoreszenz als bei pH 5. Im Gegensatz dazu beeinträchtigte ein höherer pH-Wert die Wechselwirkung zwischen BAC/MCPP und DOM; für die MCPP-C1-Gruppe wurde ein Anstieg der Fluoreszenz um 21,3 % von pH 5 auf pH 9 beobachtet. Die FTIR-Analyse in Verbindung mit der 2D-COS-Analyse ergab, dass Wasserstoffbrückenbindungen, π - π -Wechselwirkungen und elektrostatische Effekte an der Wechselwirkung zwischen BAC/MCPP und DOM beteiligt sind.

Nach der qualitativen Bestimmung der Wechselwirkung zwischen Schadstoffen aus dem Gebäudeabfluss und DOM wurde eine quantitative Analyse durchgeführt, um das Ausmaß der Wechselwirkung zu bewerten. In der vorliegenden Studie wurden Diuron, MCPP, Terbutryn, BAC, 1-(3,4-Dichlorphenyl)-3-methylharnstoff, 1-(3,4-Dichlorphenyl)-Harnstoff, 3,4-Dichloranilin, Atra-Zin-Desisopropyl-2-hydroxy und Terbutylazin-2-hydroxy als Biozide und TPs eingesetzt. Um die Auswirkungen des Molekulargewichts (MW) des DOM auf die Interaktion mit Schwermetallen und Bioziden/TPs zu untersuchen, wurde das DOM durch Zentrifugalfraktionierung nach MW-Differenz getrennt und anschließend charakterisiert. Anschließend wurde die Bindung von Schwermetallen und Bioziden/TPs an die DOM-Fractionen durch ein Dialysegleichgewicht analysiert. Die Ergebnisse zeigten, dass die UV-Absorption der verschiedenen DOM-Fractionen ähnlich war, ihre SUVA₂₅₄-Werte lagen im Bereich von 7,5-8,2 L/(mgC·m). Der höchste Gesamtsäuregehalt wurde für die DOM-Fraktion 3-10 kDa mit 22,88 mmol/gC festgestellt, gefolgt von der DOM-Fraktion >100 kDa (18,02 mmol/gC) und der DOM-Fraktion 10-30 kDa (15,22 mmol/gC). Bei der Bindung von Cu^{2+} an DOM wurde festgestellt, dass Cu^{2+} bevorzugt an die DOM-Fraktion mit höherem MW bindet; dieser Trend wurde jedoch nicht für Zn^{2+} beobachtet, welches eine schwächere DOM-Bindung als Cu^{2+} aufwies. Bei der Bindung von Bioziden/TPs an DOM hatten die Ausgangs-Biozide eine höhere Affinität zu DOM als die entsprechenden TPs. Darüber hinaus wurde festgestellt, dass die Bindungsaffinität zwischen Bioziden und DOM in abnehmender Reihenfolge MCPP > Terbutryn >

Diuron ist, und dass die Wasserstoffbrückenbindung eine wichtige Rolle bei der Bindung von MCPP an DOM spielt. Die Anwesenheit von Cu^{2+} hemmte die Bindung von Bioziden an DOM-Fractionen >100 kDa, im Gegensatz dazu wurde die Bindung von Bioziden an DOM-Fractionen <100 kDa verstärkt.

GAC ist ein vielversprechendes Adsorptionsmittel zur Entfernung organischer und anorganischer Schadstoffe. In dieser Studie haben wir die Adsorption von Schwermetallen und Bioziden untersucht und den Einfluss von DOM (5 mgC/L) während dieses Prozesses bewertet. Die Adsorptionsprozesse wurden durch Langmuir- und Freundlich-Modelle beschrieben. Mehr als die Hälfte des DOM wurde bei niedriger Konzentration (5 mgC/L) von GAC adsorbiert. Die Adsorption war größer für DOM mit niedrigem MW (3-10 kDa). Die nach dem Langmuir-Modell geschätzte maximale Adsorption von Cu^{2+} und Zn^{2+} ohne Einfluss von DOM betrug 157 bzw. 85,7 $\mu\text{mol/g}$. Der Unterschied in der GAC-Adsorption zwischen Cu^{2+} und Zn^{2+} wurde durch das Freundlich-Modell gut erklärt. Die Anwesenheit von 5 mgC/L DOM verbesserte die Adsorption von Cu^{2+} , während Zn^{2+} aufgrund seiner schwächeren Affinität zu GAC weniger betroffen war. Bei der Interaktion von Bioziden/TPs und AKPF adsorbierte die AKPF in Abwesenheit von DOM mehr Diuron-Verbindungen als Terbutryn-Verbindungen. Darüber hinaus wirkte sich DOM geringfügig auf die Diuron-Adsorption aus, verstärkte jedoch die Terbutryn-Adsorption und hemmte die MCPP-Adsorption. Die Auswirkungen von Cu^{2+} und Zn^{2+} auf die Adsorption von Bioziden waren ähnlich wie die von DOM.

Zusammenfassend wurden in dieser Dissertation die Wechselwirkungen zwischen Schadstoffen aus dem Niederschlagsabfluss von Gebäuden (Schwermetalle und Biozide/TPs) und DOM sowie deren Adsorption an GAC untersucht. Die beteiligten Interaktionsmechanismen und die Präferenz der Schadstoffinteraktion wurden aufgedeckt. Die erzielten Ergebnisse können unser Verständnis des Verhaltens von Schadstoffen im Gebäudeabfluss während einer Behandlung durch Adsorption ergänzen und eine Anleitung für die Weiterentwicklung von Behandlungsanlagen bieten. Kurz gesagt, die Adsorptionsbehandlung wird für die Beseitigung von Schadstoffen aus dem Gebäudeabfluss empfohlen, und es wird ein Adsorptionsmittel mit einer reichlich vorhandenen sauerstoffhaltigen funktionellen Gruppe vorgeschlagen. Um die Effizienz der Behandlung zu verbessern, kann eine sequentielle Adsorption von Schadstoffen aus dem Gebäudeabfluss in Betracht gezogen werden.

Acknowledgments

Firstly, I would like to say thank you to my supervisor Prof. Dr. Brigitte Helmreich, thank you for giving me the chance studying at Chair under your supervision, leading me explore the unknow, and giving me great support during my PhD time.

I also would like to thank the China Scholarship Council for their financial support and the help from Prof. Nian Hong and Prof. An Liu in my scholarship application.

My research work gained much support from Dr. Oliver Knoop, Myriam Reif, Wolfgang Schröder, Dr. Philipp Sperle, Philipp Stinshoff, Tong Zhang, and Jianyuan Bi; I am very thankful for their help.

Special thanks are given to Dr. Ignacio Sottorff Neculhueque. Without his help, I couldn't finish my research and publications.

I am also happy to be an office colleague to Dipl.-Ing. (FH) Claus Lindenblatt. Thank you for his help during my stay.

I was on a great team, the STORMWATER GROUP; we helped each other as much as possible, and I am very happy to be with all of you.

And, of course, I must thank Lijia Cao and my family. With their support, I can finally finish my PhD trip.

Contents

Abstract	I
Zusammenfassung.....	IV
Acknowledgments.....	VII
Contents	VIII
List of Figures	XII
List of Tables	XV
Abbreviations.....	XVI
1. Introduction.....	1
2. State-of-the-art	5
2.1 Heavy metals in roof runoff.....	5
2.2 Biocides leaching from building façades and their environmental behaviors .7	
2.2.1 Leaching of biocides from building façades	7
2.2.2 Factors affecting biocide leaching	9
2.2.3 Occurrence of biocides in urban water systems.....	10
2.2.4 Degradation of biocides and formation of TPs	12
2.2.5 Ecotoxicity and ecological influence of biocides and their TPs	13
2.3 Green infrastructure removing pollutants in runoff.....	15
2.4 GAC as a promising adsorbent removing pollutants	17
2.5 DOM influencing pollutant removal.....	18
3. Research objectives and hypotheses	21
3.1 Research objective #1	21
3.2 Research objective #2	22
3.3 Research objective #3	23
4. Interaction of heavy metals and biocide/herbicide from stormwater runoff of buildings with dissolved organic matter	26
Abstract	27

4.1 Introduction.....	28
4.2 Material and methods.....	30
4.2.1 Chemicals.....	30
4.2.2 Titration experiments setup.....	31
4.2.3 3D-EEM and PARAFAC analysis.....	32
4.2.4 Quenching processes modeling.....	32
4.2.5 FTIR and 2D-COS analysis	33
4.3 Results and discussion	34
4.3.1 Characterization of the applied DOM.....	34
4.3.2 Heavy metals complexation with DOM	35
4.3.3 Interaction of BAC and MCPP with DOM.....	39
4.3.4 BAC, MCPP-HS interactions investigated by FTIR coupling 2D-COS analysis.....	44
4.4 Conclusion	48
4.5 Acknowledgement	49
5. Determining the binding of heavy metals, biocides, and their transformation products with dissolved organic matter – understanding pollutants interactions in building façade runoff.....	50
Abstract.....	51
5.1 Introduction.....	52
5.2 Material and methods.....	54
5.2.1 Fractionation and Characterization of DOM	54
5.2.2 Dialysis bag preparation and DOM retention	55
5.2.3 Dialysis of heavy metals-DOM mixture	56
5.2.4 Dialysis of biocides/transformation products-DOM mixture	56
5.2.5 Solid phase extraction and HPLC-MS analysis	57
5.3 Results and discussion	58
5.3.1 Hydrophobicity and acidity of DOM fractions.....	58
5.3.2 DOM dialysis retention and heavy metals binding to DOM fractions	60

5.3.3 Binding of biocides and transformation products to DOM fractions .	62
5.3.4 Effect of Cu ²⁺ on the binding of biocides to DOM fractions.....	65
5.4. Conclusion	68
5.5 Acknowledgement	69
6. Adsorption of Heavy Metals and Biocides from Building Runoff onto Granular Activated Carbon—The Influence of Different Fractions of Dissolved Organic Matter	70
Abstract	71
6.1 Introduction.....	72
6.2 Material and methods.....	74
6.2.1 DOM Fractionation via Centrifugation.....	74
6.2.2 Granular Activated Carbon Preparation.....	74
6.2.3 Adsorption of Fractionated DOM and Pollutants onto GAC.....	75
6.2.4 Pollutants Co-Presence during the Adsorption Process.....	79
6.2.5 Liquid Chromatography–Mass Spectrometry Analysis.....	79
6.2.5 Adsorption Modelling using Freundlich and Langmuir Equations	80
6.3 Results and Discussion	81
6.3.1 DOM and Granular Activated Carbon Prepared.....	81
6.3.2 The Adsorption of DOM onto GAC	81
6.3.3 The Adsorption of Heavy Metals onto GAC	84
6.3.4 The Adsorption of Biocides and Biocide Transformation Products onto GAC	87
6.3.5 The Influence of Co-Presence on the Adsorption Processes	90
6.4 Conclusions.....	93
6.5 Acknowledgments.....	94
7. Overall conclusion and outlook	95
7.1 Overall conclusion	95
7.2 Outlook	98

7.2.1 Interaction of benzyl-dimethyl-tetradecylammonium chloride dihydrate (BAC) with DOM and GAC	98
7.2.2 Interaction of pollutants with natural DOM in building runoff	98
7.2.3 Biocides/TPs adsorption column test and desorption analysis	99
7.2.4 Sequential adsorption of heavy metals and biocides	100
8. Supplementary information	102
Appendix A List of publications.....	102
Appendix B Supplementary information for Chapter 4.....	103
Appendix C Supplementary information for Chapter 5.....	109
References.....	114

List of Figures

- Figure 4.1** Derived components from commercial humic substance (DOM) by PARAFAC modeling. C1 and C2 are derived from DOM, C3 is herbicide MCP.
- Figure 4.2** Remaining fluorescence of each DOM component C1 and C2 in the complexation experiments with Cu^{2+} and Zn^{2+} (Top left: Cu^{2+} complexation with C1; top right: Cu^{2+} with C2; bottom left: Zn^{2+} with C1; bottom right: Zn^{2+} with C2).
- Figure 4.3** Remaining fluorescence of the HS component C1 and C2 in the addition of BAC at various pH conditions and modeling results of the quenching process via the Stern-Volmer equation. (Top left: BAC interaction with C1; top right: BAC interaction with C2; bottom left: modeling of BAC-C1 interaction; bottom right: modeling of BAC-C2 interaction).
- Figure 4.4** Remaining fluorescence of DOM components C1 and C2 in the addition of MCP at various pH conditions and modeling results of the quenching process via the Stern-Volmer equation. (Top left: MCP interaction with C1; top right: MCP interaction with C2; bottom left: modeling of MCP-C1 interaction; bottom right: modeling of MCP-C2 interaction).
- Figure 4.5** Overlaid IR spectrum of BAC, MCP, humic substance and their mixture.
- Figure 4.6** Synchronous (A, C) and asynchronous (B, D) maps generated from FTIR analysis of HS with external perturbation from BAC (A,B) and MCP (C, D).
- Figure 5.1** Characterization of DOM fractions. (A) The UV absorbance of five different DOM fractions (2 mgC/L) at 200–400 nm wavelength. (B) 0.05 M NaOH titration of different DOM fraction solutions from pH 2.6 to 11. DOM fractions 30–100 kDa and <3 kDa were not analyzed.
- Figure 5.2** Binding of heavy metals with DOM fractions. (A) Cu^{2+} ; (B) Zn^{2+} .

- Figure 5.3** Binding of parent biocides (except for BAC) and their transformation products to DOM fractions. (A) >100 kDa; (B) 30–100 kDa; (C) 10–30 kDa; and (D) 3–10 kDa.
- Figure 5.4** The influence of Cu^{2+} on binding of biocides to DOM fractions. (A) DOM fraction >100 kDa; (B) DOM fraction 30–100 kDa; (C) DOM fraction 10–30 kDa; and (D) DOM fraction 3–10 kDa. Orange bars and green bars represented the binding capability mean values of biocides to DOM fractions without adding Cu^{2+} (blank) and with 2 mg/L Cu^{2+} , respectively.
- Figure 6.1** Adsorption curve for DOM and heavy metals. (A) The adsorption of different DOM fractions to 200 mg GAC at various concentrations in 100 mL Milli-Q water (The data point at 600 mgC/L for the 3–10 kDa fraction is an estimated result according to the Langmuir modelling equation, because the stock solution concentration of this fraction was only 567 mgC/L). (B) The adsorption of Cu^{2+} and Zn^{2+} to 200 mg GAC at various concentration in 100 mL Milli-Q water.
- Figure 6.2** The adsorption of biocides/TPs onto GAC and biocides/TPs charge distribution. (A) The adsorption of benzene related biocides and TPs onto 10 mg GAC in 100 mL Milli-Q water; (B) The adsorption of triazine related biocides and TPs onto 10 mg GAC in 100 mL Milli-Q water. (C, D) Charge distribution of biocides and their TPs used in this study, calculated via Materials Studio with module DMol3; blue indicates a charge abundant area.
- Figure 6.3** Influence of co-presence on the adsorption processes. (A) The influence of the presence of various DOM fractions (5 mg/L) on the adsorption of heavy metals (40 mg/L) onto 200 mg GAC in 100 mL Milli-Q water. (B) The influence of the presence of heavy metals (2 mg/L) and various DOM fractions (5 mg/L) on the adsorption of diuron, terbuthryn, and mecoprop-p (40 mg/L) onto 10 mg GAC in 100 mL Milli-Q water. The large deviation for mecoprop-p could also be a result of methodological error.

- Figure 8.1** Linear correlation between UV absorbance at 254nm and DOC concentration.
- Figure 8.2** Fluorescence spectrum of the applied commercial humic substance (DOM) at pH7, 2mgC/L.
- Figure 8.3** Fluorescence of DOM (2mgC/L) before (A) and after (B) dialysis treatment. C, D, and E were fluorescence of Milli-Q water after dialysis treatment for the first, second, and third time.
- Figure 8.4** Ratio of DOM fluorescent components C1 and C2 in dialysis samples. The first two columns are data from DOM before and after dialysis treatment; the following three columns represent samples collected outside the dialysis bag in three sequential dialysis treatments.
- Figure 8.5** Remaining fluorescence of HS component C1 and C2 (before and after the removal of cations by dialysis) with the addition of 46.6 $\mu\text{mol/L}$ MCPP at various pH conditions. Left side: MCPP-C1 interaction; right side: MCPP-C2 interaction.
- Figure 8.6** Characterization of fractionated DOM. (A) Fluorescent components identified by PARAFAC model, C1 and C2 are from DOM used and C3 is from mecoprop. (B) excitation emission matrix of DOM fractions. (C) fluorescent component ratio (C1/C2) of fractionated DOM.
- Figure 8.7** Determined binding of benzyl-dimethyl-tetradecylammonium chloride dihydrate (BAC) with different DOM fractions, with and without the presence of Cu^{2+} .

List of Tables

- Table 3.1** Dissertation structure summarizing research objectives, hypotheses, and corresponding publications.
- Table 4.1** The comparison of maximum peak (peak region) of PARAFAC identified components in different studies
- Table 4.2** LogK value derived from complexation between Cu^{2+} , Zn^{2+} , and DOM at different pH conditions.
- Table 4.3** Quenching conditional constant K from the Stern-Volmer equation in describing the interaction between BAC, MCPP, and each HS component C1 and C2 at different pH conditions.
- Table 6.1** The biocides/TPs used and their physicochemical properties.
- Table 6.2** Pollutants GAC adsorption modelling results by the Langmuir and Freundlich equations.
- Table 8.1** Molecular structures and chemical properties of MCPP and BAC
- Table 8.2** The biocides/TPs used in dialysis study and their physicochemical properties.
- Table 8.3** UV absorbance of DOM fractions at 280 nm before and after dialysis equilibrium.

Abbreviations

2D-COS	Two-dimensional correlation spectrum
BAC	Benzyl-dimethyl-tetradecyl ammonium chloride dihydrate
DCA	3,4-Dichloroaniline
DCPMU	1-(3,4-Dichlorophenyl)-3-methylurea
DCPU	1-(3,4-Dichlorophenyl) urea
DHT	Atra-zine-desisopropyl-2-hydroxy
DOC	Dissolved organic carbon
DOM	Dissolved organic matter
EEA	European environment agency
EEM-PARAFAC	Excitation emission matrix and parallel factor analysis
EM	Emission
EX	Excitation
FTIR	Fourier-transform infrared spectroscopy
GAC	Granular activated carbon
GI	Green infrastructure
HAT	Terbutylazine-2-hydroxy
HPLC-MS/MS	High performance liquid chromatography-mass spectrometry
HS	Humic acid sodium salt
IHSS	International Humic Substances Society
MCPP	Mecoprop-p
MW	Molecular weight
MWCO	Molecular weight cut-off
N,N-DMS	n,n-Dimethyl sulfamide

OIT	Octylisothiazolinone
PAHs	Polycyclic aromatic hydrocarbons
PNEC	Predicted no-effect concentration
RF	Remaining fluorescence
SPE	Solid phase extraction
SUDS	Sustainable urban drainage systems
SUVA	Specific ultraviolet absorbance
TOC	Total organic carbon
TOrCs	Trace organic compounds
TPs	Transformation products
WWTP	Wastewater treatment plant

1. Introduction

Water resources are renewable thanks to the water cycle over the earth, but they can be exhaustible when there is a mismatch between increasing water demand and limited supply. Human activities, including urbanization, socio-economic development, and population growth, have led to increasing water demand, and the demand is predicted to increase by 50-80% in the next thirty years (C. He et al., 2021). Additionally, climate change exacerbates water scarcity by affecting water availability and spatial distribution. Besides water quantity, water scarcity can also be attributed to water quality issues, as anthropogenic pollution reduces the accessibility of clean water. As a consequence, three billion more people are expected to face water scarcity in 2050 (M. Wang et al., 2024). Therefore, addressing global water scarcity has been an urgent and high-prioritized task for achieving sustainable development goals.

European Environment Agency (EEA) reported that around 30% of the EU population and 20% of EU territory were affected by water scarcity yearly (EEA, 2021). With the current consumption rate and pollution situation, the water stress is expected to intensify further, as most EU river basins (an important source of EU freshwater use) will be unhealthy by 2027 (WWF, 2021). To mitigate water scarcity and achieve clean and sustainable water usage, the EU has been making efforts to protect available water resources and expand the water supply. Specifically, water reuse of treated wastewater and other water, including rainwater, which is a feasible way to reduce water abstraction from freshwater resources (e.g., rivers, lakes, and groundwater). The reclaimed water can be applied to agricultural irrigation (Ungureanu et al., 2020), industrial processes (Bauer et al., 2020), and groundwater replenishment (Yu Li et al., 2022). Wastewater reuse not only brings the benefit of reduced stress for freshwater but also has extra advantages. For example, treated wastewater reuse in agricultural irrigation was found to increase crop yield (Yerli et al., 2023; H. Wang et al., 2022). Regarding wastewater reuse in industrial parks, the price of reused water can be nearly halved in comparison with normal factory water, which significantly saves the cost (Boysen et al., 2020).

Apart from wastewater reuse, stormwater runoff from roofs, roads, and other paved surfaces during rain events, as a non-traditional water source, can be harvested to increase water supply if managed appropriately (Quon and Jiang, 2023). Stormwater

harvesting and reuse have attracted rising attention in the aspect of urban water management. In urban areas, according to the ratio of building roofs to total impervious surface (Akbari and Rose, 2008; Akbari and Shea, 2002), building runoff from roofs and façades comprises nearly half of urban stormwater runoff. To date, the reuse of building runoff is mainly for domestic, commercial, irrigation, or livestock purposes (Bañas et al., 2023). Except for these purposes, building runoff can also be reused for groundwater recharge to mitigate water scarcity and protect groundwater. In EU around 65% drinking water is from groundwater, therefore, groundwater protection is of important meaning and necessity. When recharging building runoff, since the natural recharge efficiency of rainwater is only about 20% (Liu et al., 2021; Aju et al., 2021) hence, the loss of stormwater recharge in urban areas owing to impervious surfaces can be compensated and groundwater inflow is secured.

To reuse building runoff as an alternative water supply, proper treatment to remove contained pollutants is required. Building runoff is usually contaminated by a wide range of inorganic and organic pollutants washed off from roofs and façades, such as heavy metals, nutrients, polycyclic aromatic hydrocarbons (PAHs), pesticides, biocides, and their transformation products (TPs) (De Buyck et al., 2021; Degenhart and Helmreich, 2022; Gong et al., 2020). Among these pollutants, dissolved heavy metals (especially copper (Cu^{2+}) and zinc (Zn^{2+})) and dissolved biocides, as well as TPs, should be seriously considered not only due to their frequent detection, high concentrations (for heavy metals), persistent release, non-degradability, and ecotoxicity but also heavy metals and biocides are regarded as key drivers of antimicrobial resistance in aquatic environmental compartments (European Commission, 2018).

Heavy metals in building runoff are mainly from metal material corrosion (FitzGerald et al., 2006; Qiao et al., 2019) and/or leaching of heavy metal-containing preservatives (McIntyre et al., 2019; Clark et al., 2005) in roofs. The concentration of Cu^{2+} and Zn^{2+} in roof runoff can reach several mg/L (Athanasiadis et al., 2007; Athanasiadis et al., 2004; De Buyck et al., 2021; Galster and Helmreich, 2022; Degenhart and Helmreich, 2022), which far exceeds the insignificant threshold values (5.4 $\mu\text{g/L}$ of Cu and 60 $\mu\text{g/L}$ of Zn) drawn up by German federal states water working group (Galster and Helmreich, 2022). Moreover, as heavy metals cannot be further degraded, they persist in the environment and can accumulate in living organisms. Consequently, heavy metals in

roof runoff can pose a significant threat to the ecosystem if directly discharged into receiving environments, e.g., groundwater, without treatment.

Biocides in building runoff are mainly from façades since they are widely applied in building materials to prevent biodeterioration. Biocide concentrations vary a lot due to different environmental exposure times of façades. Commonly, a high leaching amount of biocides can be expected at the beginning of application and decay with exposure time (Schoknecht et al., 2016; Burkhardt et al., 2012). The reported biocide concentrations in runoff range from several ng/L to mg/L differently (Linke et al., 2021; Burkhardt et al., 2012; Vega-Garcia et al., 2020). Obviously, in some cases, the concentration of biocide exceeds the predicted no-effect concentration (PNEC) (the concentration of a chemical below which no toxic effects of exposure in an ecosystem are observed). For example, the PNEC values for diuron, terbutryn, and octhilinone are 20 ng/L, 3 ng/L, and 50 ng/L, respectively (Kresmann et al., 2018; Linke et al., 2021), while previous studies have reported their occurrence in runoff and receiving water bodies with higher concentrations (Burkhardt et al., 2011; Linke et al., 2021). Though biocides can be degraded via physico-chemical or biological processes, the various TPs remain largely unknown not only for their formation but also for their ecotoxicity. Furthermore, the emission of TPs was found to be higher than the parent compounds (Junginger et al., 2023), and they could even be more hazardous (Pacholak et al., 2022). Hence, removing biocides and their TPs in façade runoff is essential for improving stormwater quality.

Currently, there is no treatment facility for stormwater runoff particularly designed for removing heavy metals and biocides simultaneously. In a separate sewer system, building runoff is transported via a drainage system and discharged, often untreated, in urban water bodies, or they are directly infiltrated on-site (Vega-Garcia et al., 2022a; Vega-Garcia et al., 2022b) into the groundwater. It was estimated that 70% of urban stormwater runoff in Berlin is discharged into surface waters without further treatment via the separate sewer system (Wicke et al., 2021). In addition, increasing studies have reported the occurrence of heavy metals or biocides in water bodies originated from building runoff (Hensen et al., 2018; Galster and Helmreich, 2022; Linke et al., 2024). Green infrastructure (e.g., green roofs, rain gardens, constructed wetlands) designed for urban runoff reduction and management is also expected to eliminate pollutants. However, studies have found that existing green infrastructure is not an efficient system

for retaining building runoff pollutants (Rommel et al., 2019; Taguchi et al., 2020; Hensen et al., 2018; Bork et al., 2021). Thus, new strategies must be developed targeting heavy metals and biocides from building runoff.

Granular activated carbon (GAC) can serve as a promising treatment method that effectively adsorbs diverse chemicals and can be used in treatment facilities. As a porous material, GAC has a high surface ratio and is abundant in functional groups providing binding sites (Demiral et al., 2021; Yang et al., 2019). Previous studies have reported that GAC efficiently adsorbed heavy metals from synthetic stormwater (Sountharajah et al., 2015) and retained micropollutants in drinking water treatment (Golovko et al., 2020). However, the adsorption of pollutants onto sorbent can be impacted by dissolved organic matter (DOM), which is ubiquitous in the environment and could influence the removal rate in treatment plants. For instance, a study from Parker et al., 2023 showed that organic matter in stormwater decreased the adsorption of per- and poly-fluoroalkyl substances onto RemBind™ from 84-95% to 0-45%. The negative influence of DOM was also reported by a study using GAC as an adsorbent for removing trace organic chemicals (Kennedy et al., 2021). Prior to applying GAC in building runoff treatment, it is crucial to decipher the bilateral/trilateral interactions between DOM, heavy metals, biocides (as well as TPs), and GAC. With this mechanistic research, the adsorption pattern of building runoff pollutants can be better understood, providing the basis for heavy metals and biocides removal via highly efficient adsorption in stormwater treatment facilities.

Overall, the main research objectives of this dissertation are qualitatively and quantitatively characterizing the interactions among heavy metals, biocides/TPs, DOM, and GAC, meanwhile, revealing the involved interaction mechanisms. The obtained results are expected to contribute to the development of building runoff treatment systems and, finally, relieve the water scarcity in urban area.

2. State-of-the-art

2.1 Heavy metals in roof runoff

Roof runoff contains diverse (micro)pollutants such as heavy metals (Degenhart and Helmreich, 2022; Galster and Helmreich, 2022), biocides and pesticides (Vialle et al., 2013; Polkowska et al., 2009), and polycyclic aromatic hydrocarbons (Hou et al., 2013). Considering the important contribution of roof runoff to stormwater volume (ca. 63%) (Gromaire et al., 2001), the effects of roof runoff on the quality of stormwater and receiving waterbodies should be taken seriously. A meta-analysis of over 100 contaminants by De Buyck et al., 2021 revealed that roof runoff plays a key role in stormwater quality deterioration, acting as a major source of stormwater pollution.

Among roof runoff pollutants, dissolved heavy metals ions like copper (Cu^{2+}) and zinc (Zn^{2+}) have attracted special attention, due to their high concentration level at several mg/L. For instance, the concentrations of Cu^{2+} and Zn^{2+} in roof runoff were determined as 9.7 mg/L and 7.3 mg/L, respectively (Sage et al., 2016; Karlén et al., 2002). The highest concentration was reported to be ten or even a dozen mg/L (Athanasiadis et al., 2006; Galster and Helmreich, 2022). Such a concentration range largely exceeds the no-effect concentration of heavy metals on the environment and could threaten water quality and aquatic ecosystems (Chukwu et al., 2023). As stated by aquatic life ambient freshwater quality criteria from the United States (EPA-822-R-07-001), Cu^{2+} poses acute toxicity to some freshwater animals at the $\mu\text{g/L}$ concentration level. For example, a Worm (*Lumbriculus variegatus*) was found to have an acute value of 48.4 $\mu\text{g/L}$, and for an adult snail (*Lithoglyphus virens*), the acute value was 6.67 $\mu\text{g/L}$. A similar result was reported for Zn^{2+} (EPA-820-B-96-001), with the acute value being 120 $\mu\text{g/L}$ for striped bass (*Morone saxatilis*). Furthermore, a case study from Umbría-Salinas et al., 2021 on the Brazilian coast showed that to protect estuarine areas, the suggested Cu^{2+} predicted no-effect concentration (PNEC) was 0.16 $\mu\text{g/L}$. Another reason for paying close attention to heavy metals is that they are bio-accumulative due to their non-biodegradability, resulting in an increasing total amount in living organisms (i.e., biomagnification) (Madgett et al., 2021; Saidon et al., 2024). Studies from Charters et al., 2021b and Müller et al., 2019 reported that the majority of Cu and Zn in roof runoff

was in a dissolved form, which indicates that they are bioavailable and can undergo the biomagnification pathway.

The origins of heavy metals in roof runoff are diverse, including roof surface, chimneys, gutters, and dormers (Galster and Helmreich, 2022), where copper and/or zinc are used as construction materials or Cu/Zn-containing chemicals are applied to protect the surface from biodeterioration. The atmospheric deposition of Cu^{2+} and Zn^{2+} can be neglected, as their respective mean concentration in roof runoff was lower than $60 \mu\text{g/L}$ (De Buyck et al., 2021). Cu^{2+} and Zn^{2+} released from metal materials can be attributed to corrosion, which results in the formation of patina on the surface of materials. In a study, FitzGerald et al., 2006 examined the patina samples from European countries and found that the patina on the surface of copper had a two-layer structure; the layer contacting with copper consisted of cuprite, and the outer layer was brochantite. In addition, Qiao et al., 2019 stated that in the corrosion of galvanized steel, the main stable compositions in formed patina were $\text{Zn}_5(\text{OH})_6(\text{CO}_3)_2$ and $\text{Zn}_4(\text{OH})_6\text{SO}_4$. The corrosion process facilitates the conversion of copper and zinc into soluble cations; as a consequence, these heavy metal salts dissolve in rainwater and then pollute the roof runoff. The application of Cu/Zn-containing chemicals is mainly in wood products such as wood shingles. Typical compounds include chromated copper arsenate (McIntyre et al., 2019) and ammoniacal copper zinc arsenate (Clark et al., 2005). In this case, when the preservatives impregnated wood materials are exposed to environment, the concentration of heavy metals in runoff can reach the same level of that in metal roof runoff.

Factors affecting the release of heavy metals to roof runoff include roofing materials, exposure time, roof physical properties, and weather conditions (Hedberg et al., 2014; McIntyre et al., 2019). Winters et al., 2015 investigated the release of metals from 14 types of new roofing materials. They found that different materials released distinct metals, e.g., treated wood shakes emitted As^{3+} and Cu^{2+} , copper roofing released Cu^{2+} , and EPDM roofing released Zn^{2+} . Roof physical characteristics such as slope also affect the release of metals, with runoff rates of heavy metals increasing with decreasing inclinations (Odnevall Wallinder et al., 2000). In addition, older roofs often release larger amounts of metals than new roofs, indicated by a 55-year-old galvanized roof releasing 30-45% more Zn^{2+} than a new roof sheet (Wicke et al., 2014). They also determined the effect of rainfall pH on metal mobilization, which is the most influential

weather factor (McIntyre et al., 2019), and found the concentration of dissolved Cu^{2+} and Zn^{2+} increased exponentially with the decrease in pH.

Given the high levels of heavy metals occurring in building runoff and their potential ecotoxicity to aquatic organisms, effective control of Cu^{2+} and Zn^{2+} in building runoff is significant for clean water achievement. Currently, building runoff, together with other sources of runoff, is mixed in stormwater and subjected to further possible stormwater treatment systems (e.g., filtration, constructed wetlands) (Feng et al., 2022), while the treatment designs are not targeting heavy metals. A practicable method for purifying building runoff and mitigating heavy metal pollution is adsorption source control. Such a treatment system removes dissolved Cu^{2+} and Zn^{2+} from roof runoff prior to their entering into stormwater, which is useful especially in urban areas with limited space. Charters et al., 2021a examined the removal of Cu^{2+} and Zn^{2+} by limestone, zeolite, and mussel shells in the downpipe with short-time contact. Over 93% of dissolved Zn^{2+} was removed by mussel shells, and 47-93% of dissolved Cu^{2+} was removed by different materials. Furthermore, various adsorbents such as GAC, silica spongillite, and crab shell were proven to be promising in heavy metal treatment (Chakraborty et al., 2022).

2.2 Biocides leaching from building façades and their environmental behaviors

2.2.1 Leaching of biocides from building façades

Besides the release of some heavy metal ions, runoff from building façades is a reservoir of micropollutants, in particular, various biocides (Paijens et al., 2020; Junginger et al., 2023, Vega-Garcia et al., 2022b; Wicke et al., 2022). Biocides such as terbutryn, diuron, carbendazim, and mecoprop-p (MCP) appear in building runoff because they are used for building materials to prevent undesired growth of microorganisms (i.e., algae and fungi) on building surfaces (Kiefer et al., 2024). Biocides come into effect by mobilizing to the façade surface during rain events. As a result, at the moment that biocides take effect, they are washed off with the stormwater runoff. Therefore, façades are considered to be the major source of biocides in building runoff.

The emission of biocides is discontinuous, a high concentration of biocides in building runoff occurs during the first several months or rain events after application, and the concentration of biocides emitted decreases over time (Bollmann et al., 2016; Kiefer et al., 2024). Consequently, biocides detected in façade runoff were often at the concentration of several mg/L in the early stage of application, and remain at tens/hundreds of $\mu\text{g/L}$ constantly in the long-term performance. For example, concentrations of diuron in façade runoff from different coating systems were 10-25 mg/L in the first month and decreased to 2 mg/L after one year (Burkhardt et al., 2012). Biocide leaching from façades has been proposed by Styszko et al., 2015 of three possible mechanisms: (1) diffusion through the polymer, (2) diffusion through water-filled pores, and (3) evaporative transport. Their experiments showed that soaked renders presented a considerably higher emission than other samples, hence, the evaporating mechanism was identified as not relevant. Diffusion through water-filled pores was suggested as the predominant leaching mechanism, since it was easier to happen than through the render material. Therefore, a decreasing leaching with time could be expected due to the biocide gradients inside the façade material. This expectation was proved by the finding from Schoknecht et al., 2009, where they observed the sharp decrease in the emission rate of terbutryn from renders with increasing experiment time in permanent immersion tests.

Detailed biocide leaching mechanism including five steps was as follow (Uhlig et al., 2019):

(1) Façades contact with rainwater, meanwhile rainwater transports to the coating and fills the pore structure. During this process, a fraction of rainwater turns into porewater. Consequently, total amount of façade runoff is always less than measured wind driven rain, as saturation is a precondition of façade runoff.

(2) Once the pores are filled with rainwater, biocides carried by solid particles start to desorb and transit to the wet phase, i.e. dissolution.

(3) Dissolved biocides in porewater transport through materials, and this process is driven by their concentration gradient, and can be affected by advection.

(4) Biocides are degraded via hydrolysis and photolysis due to water contact and sunlight radiation, resulting in a reduction of total biocides amount and the formation of transformation products (TPs).

(5) Biocides and their TPs transfer to the façade surface and are flushed by runoff. Concentrations of biocides and TPs in runoff decrease with increasing contact time.

2.2.2 Factors affecting biocide leaching

One of the major factors influencing biocide leaching is their physicochemical properties, such as partitioning coefficients and water solubility. In general, biocides with high solubility and low K_{ow} value (< 1) present a preference for an aqueous phase, so they possess a higher possibility of leaching out from building materials to runoff. Schoknecht et al., 2009 found that biocide emission was negatively related to the K_{ow} value (hydrophobicity).

Moreover, weather conditions (e.g., temperature and precipitation) are key drivers for transporting biocides. According to published studies, a more active diffusion and leaching behavior of biocides can be expected at higher ambient temperatures due to decreased interactions. For example, a study from Wangler et al., 2012 indicated that increasing temperature would improve the terbutryn release rate in the next few sprinkling tests. Precipitation patterns such as wind-driven rain and rainfall intensity play a critical role in biocide release as well. Vega-Garcia et al., 2020 pointed out that, with the same exposure surface area, the façade facing wind direction released the highest amount of biocide in rain events. Lebow, 2014 summarized that larger amounts of biocides tend to be emitted from treated wood at a slower rainfall rate of 3 mm/hr, as a more thorough and longer period of soaking is achieved.

In addition, material properties, including organic matter content, service lifetime, and the application method, also have important effects on the biocide leaching process. For instance, Styszko et al., 2015 reported that biocides released from silicone render were usually considerably less than from acrylate render due to the higher content of organic matter in silicone render. Regarding the service lifetime, for newly applied biocides, a high leached concentration in façade runoff can be expected; reversely, for biocides that have been in service for years or even longer, their leaching will be lower. For example, a lab-scale study from Schoknecht et al., 2009 investigated the leaching of biocides by short time immersion (one hour, nine times repeat), showing that at the first contact of water with panels, the release of terbutryn was around 25.6 mg/m², and for the last contact, it was about 5.47 mg/m². The decline of leaching amount with increasing exposure time was also reported by Wangler et al., 2012; they simulated a

total precipitation of 6800 mm, which corresponds to roughly a rainfall of 6 years. At the beginning, the emission rate of terbutryn under given conditions was 14.3 mg/m²; by the end of the experiment, it decreased to 2.28 mg/m². Another important influencing factor is the way biocides are applied to building materials. Compared with freely added biocides in façades, encapsulated biocides tend to release less amount into facade runoff. Results from Vermeirssen et al., 2018 supported such a conclusion. They evaluated the leaching of terbutryn and two other biocides (free and encapsulated) from renders and found that the emission of freely added terbutryn was 4 times higher than the encapsulated one; for the two biocides, the difference was more than 17 fold. Additionally, Pastor et al., 2020 also reported a reduced release of carbendazim from mortar when it formed adsorption complexes with clay.

2.2.3 Occurrence of biocides in urban water systems

Biocides leaching from façades without appropriate treatment will end up in urban water systems. The detection of biocides, as well as the TPs in drainage systems, swales, urban water bodies, wastewater treatment plants (WWTPs), and even groundwater, have been widely reported (Linke et al., 2021; Burkhardt et al., 2011; Becouze-Lareure et al., 2019; Wiest et al., 2018; Linke et al., 2022; Paijens et al., 2021; Wicke et al., 2022; Hensen et al., 2018; Albers et al., 2023).

Linke et al., 2021 investigated the fate of biocides and some of their TPs in a small-scale urban area after initial construction for 13 years. Terbutryn and diuron were constantly detected in standing water of swale during their sampling period of over one year, with concentrations up to 40 ng/L and 174 ng/L, respectively. The expected sources of terbutryn and diuron are from façades, rain downpipes, and drainage pipes, and their TPs (e.g., diuron-desmethyl, terbuthylazine-2-hydroxy, terbutryn-desethyl) were also observed in these sources. Furthermore, detection of biocides in sewer systems was reported by Burkhardt et al., 2011, where they carried out a field survey study in three different sites nearby the city of Zürich. The highest concentrations of terbutryn, carbendazim, and MCPP were monitored to be 1.8, 1.1, and 10 µg/L, respectively, in the effluent of a separate sewer. The presence of biocides in sewer systems was also found by Becouze-Lareure et al., 2019. They collected samples from separate stormwater sewer systems in the Greater Lyon area and found that atrazine and

diuron were frequently quantified (>70%) in urban wet weather discharges. Meanwhile, they also proved the occurrence of these two biocides in the combined sewer systems. Being transported by sewer systems, the following destinations of biocides can be WWTPs and stormwater catchments. The appearance of biocides in stormwater catchments have been detected by recent studies. For example, Wiest et al., 2018 collected sediment samples from a stormwater detention basin located in east Lyon and found the occurrence of diuron at a concentration between 4.4 and 6.6 ng/g. Linke et al., 2022 sampled six stormwater events over 2 years and found that terbutryn existed in the basin sediment at a mean concentration of 2.6 ng/g. In the aspect of biocides in WWTPs, Paijens et al., 2021 collected influents and effluents from *Seine Centre* WWTP during dry weather; they found that most of the analyzed biocides (18-targeted compounds) were quantified in influents. Among these biocides, diuron, terbutryn, carbendazim, and some other biocides were determined at a median concentration between 10 and 100 ng/L. Compared with influents, biocides in effluents presented almost the same quantification frequencies and a very close concentration, which indicated that WWTP treatment processes exhibited limited removal efficiency of biocides.

Despite the already detected biocides in different urban water system compartments, we should be aware that they could only account for a small proportion of the overall released amount. According to the modeling results from Linke et al., 2022, they calculated the terbutryn mass balance for 13 years since the start of construction and took the increased house number into consideration. Results showed that only 11% of leached terbutryn reached the retention pond, and the rest majority of terbutryn was diffusely lost in the residential area. In addition, Wicke et al., 2022 reported that a considerably high proportion (>90%) of biocide is retained near the releasing façades and infiltrated diffusely around buildings, which ends up in soil instead of being discharged into the sewer system. A severe consequence of such environmental behavior is the contamination of biocides in groundwater. In fact, biocides and their TPs have been detected in groundwater. For instance, Hensen et al., 2018 observed the percolation of diuron, terbutryn, octylisothiazolinone (OIT) as well as their TPs into groundwater through stormwater infiltration systems. Samples collected from the downgradient of the swale-trench system exhibited a higher biocide/TP concentration than the upgradient. The contamination of urban groundwater with biocides was also

reported by Albers et al., 2023; they found the wide presence of n,n-dimethyl sulfamide (N,N-DMS) derived from tolylfluanid and dichlofluanid in urban groundwater with a concentration above the quality standards of the European groundwater directive (EU directive 2006/118/EC). Besides, they also found a degradation resistance of N,N-DMS in the subsoil, which indicated a long-term presence of this compound in groundwater under populated areas. Moreover, a most recent study reported that diuron, OIT and terbutryn were detected in groundwater in a southwest German city during a six-year sampling period (Linke et al., 2024).

2.2.4 Degradation of biocides and formation of TPs

Degradation of biocides includes hydrolysis in water matrix, photodegradation and biodegradation either on the façade surface or in the surrounding environments. Although biocides are reduced in such cases, TPs are formed due to incomplete degradation. To predict the fate of biocides in the environment and eliminate contamination, an understanding of the degradation mechanisms regarding parent compounds and TPs is necessary.

Biocides photodegradation occurs at the surface of the building façade during the dry periods and in water bodies in contact with sunlight. Direct photodegradation is the absorption of light by parent compounds, resulting in transforming reactions, and indirect photodegradation is mediated by other aquatic constituents, such as dissolved organic matter (Vione et al., 2024). Studies have been performed to identify TPs and to reveal possible photodegradation pathways for some biocides (e.g., diuron, MCP, terbutryn) (Okamura, 2002; Schoknecht et al., 2021; Minelgaite et al., 2017; Hensen et al., 2019). For example, researchers conducted two experiments to identify the photodegradation TPs of OIT (Bollmann et al., 2017b) and terbutryn (Bollmann et al., 2016) from façade leachates with the irradiation of monochromatic UV-light (254 nm) simulating sunlight. Seven main different TPs were identified for OIT, and terbutryn also produced seven TPs during photodegradation. Moreover, they found that both OIT and terbutryn photodegradation followed a first-order kinetic and had a half-life time of 28 h and 12 h for OIT and terbutryn, respectively. Furthermore, Urbanczyk et al., 2019 found the photodegradation rates of some commonly used biocides were considerably slowed down in the presence of pigments and polymers in the paints of

façade, and transformation patterns were affected by the interactions between pigments and biocides.

Another major degradation pathway for biocides is biodegradation, which relies on the activities of microorganisms and can occur in soil, receiving water, and WWTP under aerobic or anaerobic conditions. Although biocides are toxic to microorganisms, microbes could adapt to diverse biocides and then transform the residues, especially favored by co-metabolism. Junginger et al., 2022 examined the aerobic biodegradation of terbutryn in the laboratory and reported a higher terbutryn biodegradation half-life time than simulated sunlight photodegradation and hydrolysis. Besides, the biodegradation of terbutryn in pond sediment was found to be fastest, followed by in soil and in activated sludge, depending on their different microbial communities. Compound-specific isotope analysis together with TP determination confirmed that the major biodegradation pathway of terbutryn was converting sulfoxide to 2-hydroxy derivate, which is different from the photodegradation pathways producing TerDesEOH and TerOH. Moreover, Chand et al., 2017 investigated the biodegradation of five biocides under three conditions aerobic, anaerobic, and aerobic with substrate. Results showed that a faster decrease of all biocides was observed under aerobic with substrate conditions, indicating the effective biodegradation of biocides was achieved in co-metabolism.

Hydrolysis occurring in water by adding a water molecule is also a possible pathway for biocide transformation. The hydrolysis reaction has been observed in some biocides, such as tralopyril, tolylfluanid, dichlofluanid and bronopol (Cui et al., 2011; Cai et al., 2021; Koning et al., 2021). For example, tolylfluanid underwent a rapid hydrolysis with a half-life time of less than 2h in marine water, resulting in DMST as the TP and DMST is susceptible to further biodegradation (Koning et al., 2021). Hydrolysis of some other biocides strongly depends on environmental conditions e.g., pH and temperature. Junginger et al., 2022 found the hydrolysis of terbutryn was insignificant at pH 7, and it only occurred at extreme pH conditions e.g., pH 1 and pH 13.

2.2.5 Ecotoxicity and ecological influence of biocides and their TPs

The purpose of biocides application is to inhibit organism activities; in other words, they are toxic and hazardous to organisms. Additionally, studies have also indicated the toxicity of biocide TPs, and in some cases, they are even more toxic than the parent

compound (Hensen et al., 2020; Pacholak et al., 2022). Evaluating the ecotoxicity of biocides and their TPs is critical for understanding their environmental influences and eliminating biocide contamination in aquatic environments via a harmless treatment way.

Some lab-scale studies have been carried out to supplement our knowledge. For example, a study by Vermeirssen et al., 2018 investigated toxicity of leachates from renders to aquatic and terrestrial compartments using bioassays. The bioactivities (i.e., photosynthetic yield, bioluminescence, growth rates, and avoidance response) of bacteria, algae, water fleas, earthworms, and springtails were monitored. They found that terbutryn in leachate derived toxicity to algae; meanwhile, OIT derived toxicity toward bacteria and water flea. For terrestrial organisms, earthworms and springtails, due to the low accessibility to biocides in the soil as well as the limited load ability of sample into the soil in tests, they were not affected by biocides. Abreu et al., 2021 assessed the ecological risk of biocides to organisms in the Brazilian coast sediments based on the Risk Quotient and found 4,5-dichloro-2-n-octyl-4-isothiazolin-3-one and diuron posing a high risk on 47% and 35% of 113 sampling sites, respectively. Moreover, Juksu et al., 2019 investigated the occurrence of 19 biocides in Thailand's aquatic systems; nine biocides were detected even in fish. In particular, triclosan was found as the dominant biocide in fish blood, liver, and bile, with a concentration of up to 1.20 µg/g, indicating its high risks to aquatic organisms.

For assessing the ecotoxicity of TPs, Hensen et al., 2020 proposed a tiered approach. At tier I, the bacterial toxicity and genotoxicity of each single TP were predicted based on literature review and *in silico* methods; then, at tier II, a consecutive toxicity test was carried out for photolytic mixtures containing parent biocides and TPs; finally, at tier III, single standard substances were used to conduct toxicity tests. The results showed that strong evidence pointed to around 20% of identified TPs were toxic to environmental bacteria, and TPs of diuron, terbutryn, and MCPP were more toxic than the parent compounds. Meanwhile, they stated that the number of TPs that may pose a risk to the environment was quadrupled compared to the consideration of solely the parent compounds. Pacholak et al., 2022 investigated the toxicity of TPs of four fungicides from both biological and chemical transformation. TPs of fluconazole and epoxiconazole after UV-irradiation had higher cytotoxicity than the parent compounds on tested bacterial strains.

The ecological influences of biocides were reported including changes of microbial composition, functions, diversity, and proliferation (Reiß et al., 2024; Fernández-Calviño et al., 2023) and the resilience of communities (Machate et al., 2021). To be specific, Reiß et al., 2024 characterized the effect of terbutryn, isoproturon, and octhiline (alone and combined) on active soil microbial community composition and functions. Their results showed that gene copy numbers of bacteria and fungi were significantly affected by biocides, as well as biodiversity, richness, composition, and functional patterns of active soil microbiome. Fernández-Calviño et al., 2023 also reported the inhibition effect of isothiazolinone on soil microbial activity. Particularly, they highlighted the “legacy effects” from biocides that, after biocides dissipation, the inhibition of isothiazolinone on soil microbial growth and activity still persisted. Machate et al., 2021 sampled sediments from eight lakes located in North Germany with different macrophytes' ecological statuses and performed a risk assessment based on toxic unit summation. Their study identified biocides irgarol and diuron as the major risk drivers of toxic pressure and concluded that biocides limited the recovery of macrophyte communities.

Until now, ecotoxicity and influence assessment is more focused on parent biocides, and less attention is paid to their TPs. However, as discussed, in some cases, TPs are observed to be more toxic than their parent compounds. Considering an important way of biocides leaching is in the form of TPs, therefore, more efforts are expected in future studies on the ecotoxicity and environmental influence of TPs.

2.3 Green infrastructure removing pollutants in runoff

European Commission defined green infrastructure (GI) as “A strategically planned network of natural and semi-natural areas with other environmental features, designed and managed to deliver a wide range of ecosystem services, while also enhancing biodiversity.” (European Commission, 2013). This definition highlights the aspect of ecosystem services, specifically, improving environmental elements quality (water and air), offering recreation space, and giving assistance in climate mitigation and adaptation. Since urban hydrological systems have been heavily impacted in the past decades, revealed by increasing runoff, decreasing groundwater recharge, and water quality decay, GI is considered a promising stormwater management approach to reduce flooding risk and mitigate water pollution (Meerow and Newell, 2017; Li et al.,

2019). Diverse practices of GI, including constructed wetlands, green roofs, swales, rain gardens, and infiltration zones, have been applied worldwide (Berardi et al., 2014; Pappalardo et al., 2017; Sharma and Malaviya, 2021).

GI is able to remove various pollutants, such as heavy metals, pathogens, nutrients, PAHs, and micropollutants, involving a range of physical and biological processes. Generally, the main removal mechanisms include filtration, sedimentation, adsorption, biodegradation, retention, and vegetation uptake (McFarland et al., 2019; Sharma and Malaviya, 2021). Different studies reported a good performance of green stormwater infrastructures on pollutant removal. For example, Fardel et al., 2020 evaluated the treatment efficiencies of two different pilot swales and found that the standard swale reduced the micropollutant concentration at a range of 35–85% by infiltration, while in overflow, the corresponding value was -13–66% (the negative value of removal efficiency was because of flush-out effect). Furthermore, a city-scale modeling study by W. Yang et al., 2021 proved the effectiveness of GI. In their study, they modeled the migration and removal of four road sediments related to inorganic pollutants under different scenarios. A reduction of stormwater pollution was found to be up to 68% by the downstream-installed GI, which relieved 50% of pollution-mitigation pressure in studied drainage networks. Additionally, the filtering swale showed a better performance than the standard one, with the least micropollutant reduction of 65%, owing to higher infiltration rates of sand media than silt loam soil. The efficient removal of pollutants in stormwater runoff was also found in a rain garden by Jeon et al., 2021. They collected realistic monitoring data from a survey campaign lasting for five years and found that rain gardens effectively reduced 85% of total suspended solids, 91% of chemical oxygen demand, 74% of total nitrogen, and 85% of total phosphorus.

Although GI successfully mitigates pollution in stormwater runoff, achieving the initially designed functional goals, it still has drawbacks. One is the long-term operation of GI without appropriate maintenance, which can lead to the accumulation of undegradable pollutants such as heavy metals. Taguchi et al., 2020 raised the concern for GI infiltration practices, they pointed out that the groundwater contamination risk could enlarge over time as metals accumulate in soil beneath infiltration sites. Moreover, a potential threat to groundwater from the swale that collects and infiltrates zinc roof runoff was reported by Rommel et al., 2019. They collected soil samples from vegetated infiltration swales that served for 15 years and measured the spatial distribution of Zn

horizontally and vertically. A high Zn content of up to 27.9 g/kg in dry soil at the inflow zone of the swale was detected. Considering the locally exceeded soil sorption potential, a high risk of groundwater contamination by Zn^{2+} was expected.

Another drawback of GI removing pollutants is that it is designed to mitigate traditional pollution and lacks a suitable treatment process for emerging contaminants (e.g., biocides in façade runoff). As a result, such pollutants permeate through unsaturated soil and enter into groundwater. According to a study by Hensen et al., 2018, the applied GI for stormwater management consisting of the top soil layer as a 50 cm organic-rich and grass-vegetated soil, the medium layer as a 20 cm fine sand layer, and the bottom layer as 70 cm partly substituted (plastic blocks) gravel, was not able to retain biocides and TPs. It can be noted that the swale was generally built without any matrix amendment; its pollutant removal ability was achieved by particle filtration/sedimentation and solute adsorption onto the soil. However, Bork et al., 2021 concluded that normal soil in GI is not a reliable sink for biocides, as they observed a preferential transport of synthetic stormwater in macropores and reduced solute retention.

In summary, GI practices are protecting the environment as designed, but regular maintenance is also required to avoid the over-accumulation of heavy metals, especially for the runoff from metal roofs; besides, in order to enhance their capability in removing biocides, new designs in GI (e.g., media composition modification) are expected.

2.4 GAC as a promising adsorbent removing pollutants

Generally, contaminant removal methods can be divided into physical, chemical, and biological processes. In the context of pollutants from building surfaces (i.e., heavy metals and biocides), physical elimination methods, especially adsorption, can serve as a cost-effective, flexible, and efficient alternative since heavy metals cannot be degraded, and some biocides are rather resistant to biodegradation (discussed in section 2.1 and 2.2.4). Additionally, simultaneous removal of both inorganic and organic pollutants can be achieved by adsorption.

Among the adsorbent materials, activated carbon with high porosity is frequently used for water and wastewater treatment. Granular activated carbon (GAC), as a main form of activated carbon, is able to adsorb a broad range of substances and can be regenerated

(Katsigiannis et al., 2015). On the surface of GAC, carboxyl groups, phenyl groups, lactone groups, and other functional groups provide binding sites for chemicals (Demiral et al., 2021; Yang et al., 2019). The involved mechanisms include electrostatic interaction, π - π interactions, hydrophobic interactions, and hydrogen bonding (Gayathiri et al., 2022). The great performance of GAC adsorbing pollutants has been widely reported in its diverse applications in water and wastewater treatment (Kalaruban et al., 2019; Cantoni et al., 2021; Jjagwe et al., 2021). In the aspect of stormwater runoff treatment, GAC has shown high removal efficiency of heavy metals and organic pollutants. For example, Sountharajah et al., 2015 evaluated the adsorption of heavy metals in synthetic stormwater by GAC and found that the removal rates of Cu^{2+} , Zn^{2+} , and Cd^{2+} were 99.9%, 53.7%, and 36.7%, respectively. In addition, Ataguba and Brink, 2020 investigated the removal of metals from stormwater runoff by different combined filtration media. The highest adsorption of Cu^{2+} (74%), Fe^{3+} (67%), and Cd^{2+} (46%) were obtained by GAC-gravel and GAC-rice husk. The efficient removal of organic pollutants by GAC was reported by Ekanayake et al., 2021, where they found the addition of a small amount of GAC (0.3%) into the soil-based filter media significantly improved the removal of PAHs from stormwater.

Besides the good performance of GAC in removing pollutants in stormwater, its simple application and flexibility offer the potential for in situ treatment of building runoff (e.g., filtration system in downpipe configuration). However, few studies have investigated the feasibility of such an application. Hence, an overall knowledge of the removal of building runoff pollutants (especially heavy metals and biocides) by GAC and influencing factors is required.

2.5 DOM influencing pollutant removal

Dissolved organic matter (DOM) is a type of compound ubiquitously present in the environment, and due to its complex composition, it cannot be described by a fixed formula. Properties such as fluorescence feature (Peter et al., 2024; Tu et al., 2024), C/H and O/C relation (Wen et al., 2023), carbon stable isotope ratio (Alvarez et al., 2023), molecular weight (MW) difference (Yuanhang Li et al., 2022; Li et al., 2023), and variance in hydrophobicity (Xiao et al., 2020; Ji et al., 2022) can describe DOM. Due to a high carbon proportion in elemental composition (ca. 67%), dissolved organic carbon (DOC, in mgC/L) is commonly used to quantify DOM (Bolan et al., 2011).

The main origins of DOM in building runoff are atmospheric deposition, rainwater background, managed green roofs, and leachate from construction material (De Buyck et al., 2021; Carpenter et al., 2016). The concentration of DOM in building runoff from various surfaces differs. According to the study by Milovanović et al., 2022, DOC values of collected runoff samples from a copper roof were in a range of 2-4.8 mgC/L, while in green roofs, a higher DOC concentration was observed. Ouellet et al., 2021 compared the runoff quality of three roof types (concrete, managed, and unmanaged green roof); the results showed that DOC mean concentration in first-flush from the concrete roof was the lowest of 6.3 ± 0.77 mgC/L, corresponding values from managed and unmanaged green roof were 10.7 ± 0.94 and 17.1 ± 3.11 mgC/L, respectively. In comparison, DOM from building façades is seldom assessed as more attention is paid to the leaching of applied biocides. Due to the vertical surfaces going against the deposition process and without the application of soil-like organic abundant substances, DOM in façade runoff is expected to have a low concentration, and a main source could be rainwater initial background.

According to DOM characterization studies from Nebbioso and Piccolo, 2013, DOM molecules contain hydrophobic structures and hydrophilic functional groups. This molecular structure makes it possible for DOM to interact with other substances via mechanisms such as hydrophobic interaction, hydrogen bonding, and electrostatic interaction (Ding et al., 2022; Dong et al., 2023; B. Yang et al., 2021). Interactions between DOM and pollutants, either directly or indirectly, can enhance the mobilization of pollutants in the environment or, contrarily, improve the adsorption of pollutants to the sorbent. For example, H.-B. Kim et al., 2020 amended soil with different biochars to evaluate the mobility change of arsenic. The results showed that the biochar with lower lignin content released more DOM, and applied biochars enhanced the leaching of arsenic from soil for 3 to 7.4 times differently. On the contrary, DOM enhancing the adsorption of pollutant was reported by Uwayezu et al., 2019. They analyzed the adsorption of perfluorooctanesulfonate isomers onto goethite under the influence of humic acid and fulvic acid. The results showed that humic substance at a concentration of 20 mg/L enhanced the sorption processes, and the increased distribution coefficients were in a range of 9-57%. They assumed that the increased adsorption resulted from the formation of a goethite-DOM-pollutant ternary complex. Furthermore, the degradation and uptake of pollutants by plant are also impacted by DOM. In a

UV/chlorine-induced primidone degradation study, Y. Wang et al., 2020 found that all five applied DOM isolates can considerably inhibit the degradation of primidone, as electron-rich groups and sulfur-containing functional groups in DOM were susceptible to being attacked by radicals ($\cdot\text{OH}$, $\text{Cl}\cdot$, $\text{Cl}_2\cdot$ and $\text{ClO}\cdot$). The degradation decay was observed in a range of 54-74%. Moreover, DOM isolates containing lower SUVA values were generally found to exhibit a weaker inhibitory effect. For the influence of DOM on pollutant uptake by plants, Dinh et al., 2021 investigated the accumulation of selenium in *B. Juncea* tissues where manure from cow/chicken was added to soil. The result showed that the amendment of soil with manure dramatically decreased the uptake of selenium by *B. Juncea* for at least 44.5% in roots (maximal decrease of 94.7% in tubers), and DOM from different manure showed various uptake inhibition effects. The mechanism behind this is that the selenium-DOM complexes have amplified their overall molecular size, which makes the uptake of selenium by root cells become difficult.

In summary, due to the ubiquity of DOM and its physicochemical characteristics, its interaction with other substances can, to a certain extent, affect their environmental behaviors. In particular, the migration and removal of pollutants are impacted by DOM differently under specific circumstances. Therefore, a better understanding of pollutant-DOM interaction mechanisms is important for the development of treatment facilities eliminating contamination of building runoff.

3. Research objectives and hypotheses

Until now, there is no appropriate treatment facility widely applied for building runoff purification. The development of a treatment method for removing heavy metals and biocides simultaneously (e.g., adsorption), is urgently needed. The development of such a treatment facility requires a deep understanding of the behaviors of heavy metals and biocides/TPs, especially in a stormwater matrix with DOM (referred to humic substances in this study). Therefore, the main objectives of this dissertation are to qualitatively and quantitatively determine the bilateral interaction between heavy metals and biocides/TPs with DOM, meanwhile, to evaluate their adsorption onto GAC. For these purposes, the detailed objectives and hypotheses are proposed as follows:

3.1 Research objective #1

Verifying the interaction between biocides and DOM, identifying the preferable fluorescent component of DOM for interaction with heavy metals and biocides, and revealing involved interaction mechanisms.

Currently, studies regarding biocides mainly focus on their leaching under laboratory (Wangler et al., 2012; Styszko et al., 2015) or natural conditions (Vega-Garcia et al., 2020; Schoknecht et al., 2016) and the occurrence in urban water system (Linke et al., 2021; Wiest et al., 2018), less attention is paid to biocide environmental behavior, for example, interactions with DOM. However, the interaction process is expected to impact biocide migration in the environment and their adsorption treatment. Hence, the first objective of this research was to confirm that the interaction occurs between biocides and DOM, and then to reveal the interaction mechanisms. There are two hypotheses regarding **research objective #1**.

***Hypothesis #1.1:** Mecoprop-p and benzyl-dimethyl-tetradecylammonium chloride can interact with DOM, indicated by decreased DOM fluorescence intensity of more than 30% at the end of titration process.*

***Hypothesis #1.2:** Electrostatic interaction and hydrophobic interaction are the two mechanisms involved in interactions between mecoprop-p, benzyl-dimethyl-tetradecylammonium chloride and DOM.*

Research hypotheses #1.1 and **#1.2** are elaborated in **Chapter 4**. For testing research hypothesis #1.1, we prepared a DOM solution and titrated it with mecoprop-p (MCP) and benzyl-dimethyl-tetradecylammonium chloride, respectively. The fluorescence intensity of titrated samples was measured by Aqualog from Horiba Scientific, and collected data was fitted with Ryan-Weber and Stern-Volmer equations to describe the interaction processes. Research hypothesis #1.2 was tested by analyzing freeze-dried humic substance and biocide mixture via ATR-FTIR at wavenumbers from 450 to 4000 cm^{-1} with an increment of 1 cm^{-1} .

3.2 Research objective #2

Quantifying the interaction extent between biocides/heavy metals and DOM at real runoff concentration by dialysis equilibrium, investigating the binding preference of biocides/heavy metals to DOM fractions that separated according to their molecular weight difference, and analyzing the influence of Cu^{2+} on biocides binding to DOM fractions.

Evaluating the interaction between heavy metals/biocides and DOM according to DOM fluorescence change provides qualitative results but less quantitative information. To determine the exact interaction extent of heavy metals/biocides with DOM under realistic similar conditions, a more precise evaluation method is required. Dialysis equilibrium is an appropriate method that has been previously used in some studies (Rizzuto et al., 2021b; Y. Wang et al., 2022). Since DOM is a complex mixture, its interaction with building runoff pollutants differs across various DOM fractions. Furthermore, both heavy metals and biocides can interact with DOM, thus, the presence of heavy metals may affect the binding of biocides to DOM. To gain a better understanding of building runoff pollutants interacting with DOM under realistic conditions, the second objective of this research is quantifying pollutant-DOM interactions by dialysis equilibrium and evaluating the effect of Cu^{2+} on biocides binding to DOM. There are two hypotheses regarding the **research objective #2**.

***Hypothesis #2.1:** Heavy metals and biocides/TPs prefer to bind with DOM fraction having larger molecular weight.*

***Hypothesis #2.2:** The presence of 2mg/L Cu^{2+} reduces 50% of binding between biocides and DOM.*

Research hypotheses #2.1 and **#2.2** are elaborated in **Chapter 5**. For testing research hypothesis #2.1, we separated DOM into five fractions according to the molecular weight difference, and two different dialysis bags were used during dialysis equilibrium. When determining the binding of heavy metals with DOM fractions, DOM was added inside the dialysis bag, and heavy metals were added outside the dialysis bag; differently, in evaluating the binding of biocides/TPs with DOM, premixing was accomplished in a glass bottle, and the mixture was transferred into dialysis bag. Research hypothesis #2.2 was tested following the method of biocides/TPs binding with DOM fractions, where Cu^{2+} , biocides, and DOM were premixed and then dialyzed.

3.3 Research objective #3

Investigating the adsorption of heavy metals, DOM fractions, and biocides/TPs onto GAC and evaluating the influence of the co-existence of pollutants on their adsorption onto GAC.

In general, building runoff is directly discharged without appropriate treatment (Linke et al., 2021; Hensen et al., 2018; Szabó et al., 2023). Consequently, pollutants in building runoff pose potential risks to surface water and groundwater quality. To mitigate building runoff pollution for further reuse, GAC can be considered a promising treatment material since it is porous with a high surface ratio and abundant in functional groups that can provide binding sites for pollutants (Demiral et al., 2021; Yang et al., 2019). The third objective of this research is to evaluate the adsorption of pollutants in building runoff onto GAC and analyze the adsorption process when different pollutants are co-existing. There are two hypotheses regarding the **research objective #3**.

***Hypothesis #3.1:** Transformation products show a better adsorption onto GAC than corresponding parent biocides.*

***Hypothesis #3.2:** The presence of 5 mgC/L DOM fractions or 2 mg/L heavy metals will inhibit the adsorption of biocides onto GAC.*

Research hypotheses #3.1 and **#3.2** are elaborated in **Chapter 6**. For testing research hypothesis #3.1, we prepared 3 biocides (MCCP, terbutryn, diuron) and 5 TPs (derived from terbutryn and diuron). Their respective sample concentration ranged from 5 to 40 mg/L. For each adsorption test, 10 mg GAC was added. Adequate adsorption was achieved by shaking the samples at 120 rpm for 24 h. To test research hypothesis #3.2,

DOM fractions (5 mgC/L) with a molecular weight of >100 kDa, 10–30 kDa, and 3–10 kDa were used, heavy metals (2 mg/L) added in the experiment were Cu²⁺ and Zn²⁺. The concentration of biocides was 40 mg/L. Samples were shaken for 24 h at 120 rpm before analyzing.

Table 3.1: Dissertation structure summarizing research objectives, hypotheses, and corresponding publications.

Chapter	Research objectives	Research hypotheses	Publications
4	#1: Verifying the interaction between biocides and DOM, identifying the preferable fluorescent component of DOM for interaction with heavy metals and biocides, and revealing involved interaction mechanisms.	#1.1: Mecoprop-p and benzyl-dimethyl-tetradecylammonium chloride can interact with DOM, indicated by decreased DOM fluorescence intensity of more than 30% at the end of titration process.	Zhu P., Knoop O., & Helmreich B. Science of The Total Environment, 2022, 814: 152599.
		#1.2: Electrostatic interaction and hydrophobic interaction are the two mechanisms involved in interactions between mecoprop-p, benzyl-dimethyl-tetradecylammonium chloride and DOM	
5	#2: Quantifying the interaction extent between biocides/heavy metals and DOM at real runoff concentration by dialysis equilibrium, investigating the binding preference of biocides/heavy metals to DOM fractions that separated according to their molecular weight difference, and analyzing	#2.1: Heavy metals and biocides/TPs prefer to bind with DOM fraction having larger molecular weight.	Zhu, P., Sottorff, I., Bi, J., & Helmreich, B. Ecotoxicology and Environmental Safety, 291, 117887.
		#2.2: The presence of 2mg/L Cu ²⁺ reduces 50% of binding between biocides and DOM.	

3. Research objectives and hypotheses

	<p>the influence of Cu²⁺ on biocides binding to DOM fractions.</p>		
<p>6</p>	<p>#3: Investigating the adsorption of heavy metals, DOM fractions, and biocides/TPs onto GAC and evaluating the influence of the co-existence of pollutants on their adsorption onto GAC.</p>	<p>#3.1: Transformation products show a better adsorption onto GAC than corresponding parent biocides.</p>	<p>Zhu, P., Sottorff, I., Zhang, T., & Helmreich, B. Water, 2023, 15(11): 2099.</p>
<p>#3.2: The presence of 5 mgC/L DOM fractions or 2 mg/L heavy metals will inhibit the adsorption of biocides onto GAC.</p>			

4. Interaction of heavy metals and biocide/herbicide from stormwater runoff of buildings with dissolved organic matter

This chapter presents investigations related to research hypotheses #1.1 and #1.2:

***Hypothesis #1.1:** Mecoprop-p and benzyl-dimethyl-tetradecylammonium chloride can interact with DOM, indicated by decreased DOM fluorescence intensity of more than 30% at the end of titration process.*

***Hypothesis #1.2:** Electrostatic interaction and hydrophobic interaction are the two mechanisms involved in interactions between mecoprop-p, benzyl-dimethyl-tetradecylammonium chloride and DOM.*

This chapter has been published as follows:

*Zhu, P., Knoop, O., & Helmreich, B. (2022). Interaction of heavy metals and biocide/herbicide from stormwater runoff of buildings with dissolved organic matter. Science of The Total Environment, 814, 152599.
<https://doi.org/10.1016/j.scitotenv.2021.152599>*

Author contributions: P.Z.: Writing – original draft preparation, validation, formal analysis, conceptualization, data curation; O.K.: supervision, reviewing and editing; B. H.: methodology, supervision, writing, reviewing and editing.

Abstract

Stormwater runoff from roofs and façades can be contaminated by heavy metals and biocide/herbicide. High efficiency on-site treatment methods are now urgently needed to safeguard the ecosystem. The basis for developing such treatment facilities is an in-depth understanding of their interactions with dissolved organic matter (DOM), as this affects their migration in the environment. Hence, the interactions between copper (Cu), zinc (Zn), benzyl-dimethyl-tetradecylammonium chloride dihydrate (BAC), mecoprop-P (MCP) and DOM at pH 5 to 9 were investigated separately in this study. The evaluation of the interaction processes was achieved by applying excitation emission matrix and parallel factor analysis (EEM-PARAFAC) to titration samples; obtained data were fitted by two different models. Mechanisms involved in BAC/MCP-DOM interactions were revealed by Fourier-transform infrared spectroscopy (FTIR) and two-dimensional correlation spectrum (2D-COS) analysis. Results showed that the applied DOM was composed of the two different fluorescent components C1 and C2. More interaction with C1 than with C2 was observed for both Cu/Zn and BAC/MCP. Increasing the pH enhanced the interaction between Cu/Zn and DOM. At pH5 with a maximum quencher addition, the remaining fluorescence of Cu-C1 and Zn-C1 were 15.7% and 87.1%, respectively. Corresponding data at pH9 decreased to 3% and 69.5%. Contrarily, interaction between BAC/MCP and DOM was impaired by high pH conditions. The increase of pH from 5 to 9 with maximum BAC and MCP added raised the remaining fluorescence of BAC-C1 and MCP-C1 by 15.9% and 21.3% separately. The fitting outcomes from the Ryan-Weber equation (Cu/Zn titration) and the Stern-Volmer equation (BAC/MCP titration) corresponded well with the titration studies. FTIR coupled with 2D-COS analysis revealed that mechanisms involved in BAC/MCP titration include hydrogen bonding, π - π interaction, and electrostatic effect. The order of mechanisms taking effect during interaction with DOM is affected by the molecular structure of BAC and MCP.

4.1 Introduction

Building surface is an important source of stormwater runoff contamination, especially aged metal roofs and piping materials, bitumen membranes under green roofs as well as newly painted façades. Released pollutants include heavy metals, e.g., copper (Cu), zinc (Zn) (Charters et al., 2016; Rommel et al., 2019; Athanasiadis et al., 2010), biocides, e.g., Benzalkoniumchlorid, Diuron, and Terbutryn, etc. (Pajens et al., 2020; Linke et al., 2021), and herbicides, e.g., mecoprop-P (MCP) (Bucheli et al., 1998; Burkhardt et al. 2007). Results from field investigation showed that the mean concentrations of Cu and Zn in metal roofs runoff can be up to 2.85 mg/L (Athanasiadis et al., 2010) and 6.8 mg/L (Schriewer et al., 2008). Accordingly, concentrations of biocides leached from façades and herbicide leached from bitumen membranes to runoff have been found in hundred µg/L in their early lifetime of application (Gromaire et al., 2015; Burkhardt et al., 2007). At the moment, decentralized treatment facilities like infiltration swales are designed to mitigate heavy metal contamination from roof runoff. Vegetated infiltration swales are an example of decentralized sustainable urban drainage systems (SUDS), which can offer a viable and attractive alternative to managing stormwater runoff from urban areas on-site (Dierkes et al., 2015). However, these SUDS are not designed for the elimination of biocides and herbicides (Bork et al., 2021). Field investigation found that biocides and their transformation products could transport into groundwater via SUDS (Hensen et al., 2018). Combining this knowledge with the finding that antifouling biocides act as a constraint in the recovery of macrophyte communities in some lakes located in Germany (Machate et al., 2021), it is obvious that biocides and herbicides from building runoff pose risks to the ecosystem. Another point of concern is that traditional SUDS may not function well in retaining heavy metals from roof runoff after a long operation period. Rommel et al., 2019 observed that Zn from roof runoff inhibited the growth of swale vegetation due to its high content in the soil; furthermore, there was the possibility that Zn had been transported into the groundwater. In this context, a pressing demand for the development of improved treatment facilities to effectively retain all pollutants coming from building runoffs has arisen.

The successful development of treatment systems relies on a full understanding of the environmental behavior of pollutants, in particular, the interaction with other

substances that could affect their migration into the environment. Many studies have shown that heavy metals (Guo et al., 2020; Wu et al., 2012; Wei et al., 2020; Wang, 2003; Fang et al., 2016) and trace organic compounds (TOrcs) (Christl et al., 2016; Guillosoou et al., 2020) interact with dissolved organic matter (DOM), which occur in all stormwater runoffs from sealed surfaces and also in soils. The interactions are because of the electrostatic complexation and/or non-covalent binding mechanisms. These interactions could result, e.g., in the change of the adsorption properties of pollutants to soils and adsorbents, affecting their environmental behaviors. For instance, investigations from Wang, 2003 have shown that the presence of DOM at alkaline pH values decreased the uptake of heavy metals by sludge particulates due to the formation of heavy metal-DOM complexes. The study from Guillosoou et al., 2020 reported that the interaction of TOrcs with DOM increased their adsorption onto powdered activated carbon. Factors could have significant influence on the interaction processes described above, including the property of DOM (Guo et al., 2020; Ding et al., 2019; Wu et al., 2020), the state of charge of TOrcs (Park et al., 2018), and the pH value (Zhao et al., 2019; Christl et al., 2016).

Overall, many studies focusing on the interaction of heavy metals or TOrcs with DOM have been carried out. However, the majority of them focused on only one category of pollutants, either heavy metals or TOrcs like pesticides. Few studies have considered the investigation on the interaction of these two types of pollutants with DOM with the background of stormwater runoff from buildings. There is a knowledge gap in understanding their interaction with DOM during rain events and during percolation through soil. Furthermore, mechanisms of biocide or herbicide that interact with DOM are not clearly understood. Both of these are of great importance in developing on-site treatment facilities to mitigate pollutants risks to the environment. Therefore, studies on the interaction of building originated pollutants with DOM in stormwater runoff and factors like DOM composition and pH that can affect the interaction processes need to be carried out.

The aim of the present study is to obtain a deeper understanding of the interactions that occur between heavy metals or biocides/herbicides from building runoff and DOM during treatment in decentralized treatment facilities. Which is important for understanding why some treatment facilities do not always work optimally under natural conditions and release heavy metals as well as biocides and herbicides into the

environment in the presence of DOM. In the study, Cu and Zn were selected to represent building runoff heavy metals. To represent TOrCs, benzyl-dimethyl-tetradecylammonium chloride dihydrate (BAC) and MCPP were chosen. The effect of different pH conditions (5 to 9) on pollutant-DOM interaction was evaluated considering the wide pH range in building runoff (Schriewer et al., 2008; Vega-Garcia et al., 2020). To quantify the interaction process, Ryan-Weber equation and Stern-Volmer equation were used. As mechanisms of heavy metals interaction with DOM have been well studied (Huang et al., 2018b; Guo et al., 2020), but those in BAC/MCPP-DOM interaction are still unclear, therefore, fourier-transform infrared spectroscopy (FTIR) coupled with two dimensional correlation spectrum (2D-COS) analysis was applied to gain insight into the interaction mechanisms. The obtained results will contribute to the development of an efficient building runoff pollution treatment system that protects the environment.

4.2 Material and methods

4.2.1 Chemicals

Humic acid sodium salt (HS) was purchased from Carl Roth to act as the representative for DOM. Its stock solution was prepared by dissolving the powder in Milli-Q water and filtering it through 0.45 μm nitrocellulose membrane (Sartorius AG, Germany). The concentration of HS stock solution (mgC/L) was obtained by comparing the UV absorbance at 254 nm (DR6000, Hach) with a calibration curve (**Appendix B, Figure 8.1**). The HS stock solution was stored in the refrigerator at 4 °C before use. As BAC and MCPP are two common TOrCs from the building surface and their charged state make them more easily interact with the DOM, therefore, they were selected in the study and were purchased from Merck and Dr. Ehrenstorfer, respectively. Physicochemical properties of these two substance are listed in **Table 8.1**. Their stock solutions (in methanol) with concentrations of 500 mg/L and 10 mg/mL were prepared and stored in brown glass bottles at room temperature. Because Cu and Zn are relevant pollutants in roof runoff from metal roofs or guttering systems, the heavy metal salts used were copper chloride ($\text{CuCl}_2 \cdot 2\text{H}_2\text{O}$) and zinc chloride (ZnCl_2) purchased from Merck, Germany. The adjustments of pH were performed with 0.1 M HCl (Merck, Germany) and 0.1 M NaOH (Merck, Germany).

4.2.2 Titration experiments setup

Mixture of heavy metals or BAC/MCPPP with HS was accomplished in glass bottles. According to the building runoff quality monitoring result from Vialle et al., 2011 and to minimize the inner filtering influence (Huang et al., 2018b), the concentration of HS was set to 2 mgC/L for all experiments by diluting the HS stock solution. Before the allocation of the HS solution to the sample bottles, the pH was measured by pH electrode (WTW, Germany) and adjusted to the desired values (5.0 ± 0.1 , 6.0 ± 0.1 , 7.0 ± 0.1 , 8.0 ± 0.1 , 9.0 ± 0.1) to evaluate its influence on heavy metal/BAC/MCPPP-DOM interaction. For each sample, 10 mL HS solution was pipetted. In heavy metal titration studies, 50 mg/L and 500 mg/L heavy metal salts stock solutions were used. The addition of these stock solutions was kept less than 0.2 mL to minimize the dilution effect. The final concentrations of Cu^{2+} in the mixture were 0.7, 2.2, 3.7, 5.2, 7.4, 22.3, 37.2, 52.1, and 66.9 $\mu\text{mol/L}$. For Zn^{2+} they were 0.7, 2.2, 3.7, 5.1, 7.3, 22.0, 36.7, 51.4, 66.0, 110.1, and 146.8 $\mu\text{mol/L}$. A thorough mixture of heavy metals with HS was achieved by shaking. Fluorescence from samples was taken after a resting phase of one hour. Accordingly, for BAC/MCPPP titration, concentrations of BAC/MCPPP stock solutions were 500 mg/L. Their addition in samples was kept less than 0.3 mL. Target concentrations of BAC in the mixture were 2.5, 4.9, 7.4, 9.9, 12.4, 14.8, 17.3, 19.8, 22.3, 24.7, 32.2, and 37.1 $\mu\text{mol/L}$. Those for MCPPP were ranged from 4.7 to 47.6 $\mu\text{mol/L}$ with an increment of 4.7 $\mu\text{mol/L}$. An adequate contact of BAC/MCPPP with DOM was achieved by shaking the samples in a reciprocal shaker (Edmund Buhler, Germany) for 24 hours at 150 rpm according to Fu et al., 2016. For a better determination of the interaction between BAC/MCPPP and DOM, all applied BAC/MCPPP concentrations in the titration study were higher than those found in natural samples, but similar to other studies Fu et al., 2016). The preparation of blank samples in study followed the same procedures as titration samples but replaced the additives with the Milli-Q water (0.2 mL for the heavy metals titration and 0.3 mL for the BAC/MCPPP titration). Milli-Q water was also used to offset the small volume difference in titration samples set caused by the addition of different amount of stock solutions to keep them have the same concentration of HS.

4.2.3 3D-EEM and PARAFAC analysis

The fluorescence excitation emission matrixes (EEM) analysis, using an Aqualog (Horiba Scientific, USA) equipped with a 1 × 1 cm quartz glass cuvette at room temperature, was described in detailed by Hellauer et al., 2019. Briefly, the EEM spectrum of titrated samples were obtained by measuring the excitation wavelength at 230–599nm with an increment of 3nm and the emission wavelength at 212–621nm with an increment of 4 pixels (1.64nm). Integration time was set to 1 second and the medium charge coupled device was chosen. In the analysis, Milli-Q water was used as a blank to adjust the EEM spectrum; inner-filter effects together with Rayleigh and Raman scatters that had adverse effects on the results were removed by a proprietary software Aqualog®(V3.6). Fluorescence intensity of the EEM spectra was normalized to Raman Units by dividing the intensity with Milli-Q water Raman peak area at excitation of 350 nm.

Parallel factor analysis (PARAFAC) of EEM data from titration studies was carried out by using the staRdom package in Rstudio. In study, 111 samples (heavy metals or MCPP contained samples) at different pH and with various pollutants concentration were used to build a PARAFAC model. During the PARAFAC model establishment, two to five component models were computed. The appropriate number of components for EEMs was determined by applying a non-negativity constraint, split-half analysis, and residual analysis. More detailed information of PARAFAC analysis can be found elsewhere (Murphy et al., 2013; Pucher et al., 2019). The establishment of PARAFAC model based mostly on the heavy metal-DOM interaction experiments. Meanwhile, this model was directly applied to BAC/MCPP-DOM interaction study as well, due to the same DOM was used in study.

4.2.4 Quenching processes modeling

Fluorescence quenching of PARAFAC-derived DOM components in titration studies was modeled by Ryan-Weber and Stern-Volmer equations, in accordance with Huang et al., 2018b and Wang et al., 2017. Binding parameters for heavy metals titration and BAC/MCPP titration were determined by Eq (1) and Eq (2), respectively.

The Ryan-Weber equation is presented below (Ryan and Weber, 1982):

$$I = \left(\frac{I_{ML} - 100}{2KC_L} \right) * \left[(KC_L + KC_M + 1) - \sqrt{(KC_L + KC_M + 1)^2 - 4K^2C_LC_M} \right] + 100 \quad \text{Eq. (1),}$$

where, I is the remaining fluorescence (RF, in %) of DOM components with and without the addition of heavy metals, K is the conditional stability constant, C_L is the total ligand concentration available for binding, C_M and I_{ML} are the added heavy metals concentration, and the final RF (which does not decrease due to the addition of heavy metals). By substituting the measured I values and corresponding heavy metals concentration (C_M) in the equation, parameters K , C_L , and I_{ML} , can be calculated by nonlinear regression.

The Stern-Volmer equation is shown below (Lakowicz, 2013):

$$\frac{F_0}{F} = 1 + K_{sv}[Q] = 1 + K_q\tau_0[Q] \quad \text{Eq. (2),}$$

where, F_0 and F are fluorescence intensity of DOM components without and with the addition of BAC or MCPP, K_{sv} is the Stern-Volmer conditional quenching constant, Q is concentration of BAC/MCPP, K_q is the bimolecular quenching constant, and τ_0 is the average lifetime of molecule in the absence of quencher, which in this study was the average lifetime of DOM. By using the experimental data and linear fitting, parameters K_{sv} and K_q can be determined.

4.2.5 FTIR and 2D-COS analysis

Solution samples preparation before attenuated total internal reflection (Golden Gate, Specac) FTIR (Spectrum 100, Perkin Elmer) analysis was the same as in the BAC/MCPP titration at pH 7 including the proportion of substances, but with higher concentration to reduce the time consumption during freeze drying (Alpha 1-2 LDplus, Christ). The collected wavenumbers of FTIR spectrum ranged from 450 to 4000 cm^{-1} with an increment of 1 cm^{-1} .

Further decomposition of the IR spectrum was accomplished by applying 2D-COS analysis. The software used was “2D shige” V1.3 developed by Prof. Shigeaki Morita, Osaka Electro-Communication University. During the analysis, the addition of BAC/MCPP were regarded as external perturbations. Synchronous and asynchronous maps were generated to reveal the mechanisms involved in the interaction between BAC/MCPP and DOM. Detailed introduction of 2D-COS analysis and results interpretation are available from Noda, 1990.

4.3 Results and discussion

4.3.1 Characterization of the applied DOM

In this study, commercial HS salt was chosen as the DOM considering its similarity to natural DOM and to keep the consistency in experiments. Its fluorescence spectrum of 2 mgC/L at pH 7 is shown in **Figure 8.2**. Based on the regional integration of fluorescence proposed by Chen et al., 2003, the applied HS is mainly composed of humic acid and fulvic acid. A further decomposition of HS fluorescence through a three-component PARAFAC model with a 98.8% core consistency separated the HS into two groups (**Figure 4.1**). Component 1 (C1) has its fluorescence region at Excitation(EX)/Emission(EM) 230–350(401–500) / 450–620(500–575) and with maximum intensity at 254/544, component 2 (C2) is at EX/EM 230–350 / 374–525 with maximum intensity at 251/422. The third component (C3) identified by the model is MCPP at 230–248(257–293) / (300–343)283–350 with maximum intensity at 230/308. The model derived HS fluorescent components C1 and C2 are similar to those reported previously as shown in Table 4.1. Comparing their maximum peaks with the results from listed PARAFAC studies, the applied model in this study can describe the fluorescence features of DOM very well.

Table 4.1. The comparison of maximum peak (peak region) of PARAFAC identified components in different studies.

Components	EX _{MAX} (nm)	EM _{MAX} (nm)	Sample origin	References
C1	254	544	Commercial HS	This study
C2	251	422	Commercial HS	This study
“C2”	255	498	Lake	Du et al., 2016
“C3”	<250	438	Lake	Du et al., 2016
“C2”	250	515	River	Lin and Guo, 2020
“C3”	250	405	River	Lin and Guo, 2020
“C1”	254	483	Green roof runoff	D’Acunha and Johnson, 2019
“C2”	<250	380	Stormwater runoff	Smith et al., 2021
“C3”	267	460-490	Stormwater runoff	Smith et al., 2021

4. Interaction of heavy metals and biocide/herbicide from stormwater runoff of buildings with dissolved organic matter

“C1”	260	480	Soil	Wu et al., 2021
“C2”	<250	410	Soil	Wu et al., 2021
“C1”	270	510	Soil (IHSS)	Lee et al., 2015
“C3”	250	440	Soil (IHSS)	Lee et al., 2015
“C1”	< 240-250	390-440	Soil	Romero et al., 2019
“C2”	< 240-275	450-540	Soil	Romero et al., 2019
“C1”	250-265	405-445	Soil	Panettieri et al., 2020;
“C2”	250-265	475-515	Soil	Panettieri et al., 2020;

“C1”, “C2” and “C3” represent their original labels in each study, HS: humic substance, IHSS: International Humic Substances Society.

Typically, fluorescence placed in the EEM spectrum is related to HS molecular weight (MW). An increase of the red-shift occurs for HS with a higher MW (Lee et al., 2015; Quang et al., 2016). In this context it was assumed that the MW of C1 is likely larger than for C2. The difference in MW of these two components was later confirmed by a dialysis experiment, reflecting a much higher ratio of C2/C1 outside the dialysis bag with a cutoff MW of 12400 Dalton (**Figure 8.3; 8.4**).

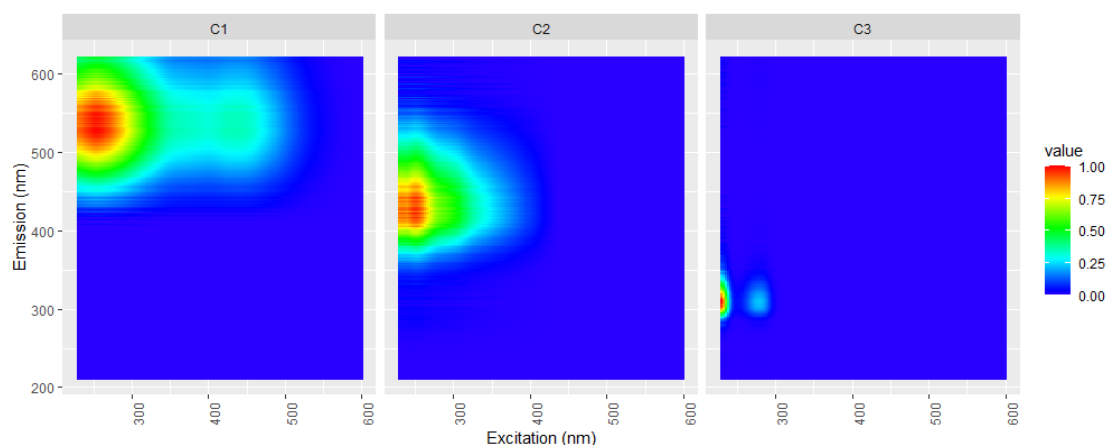


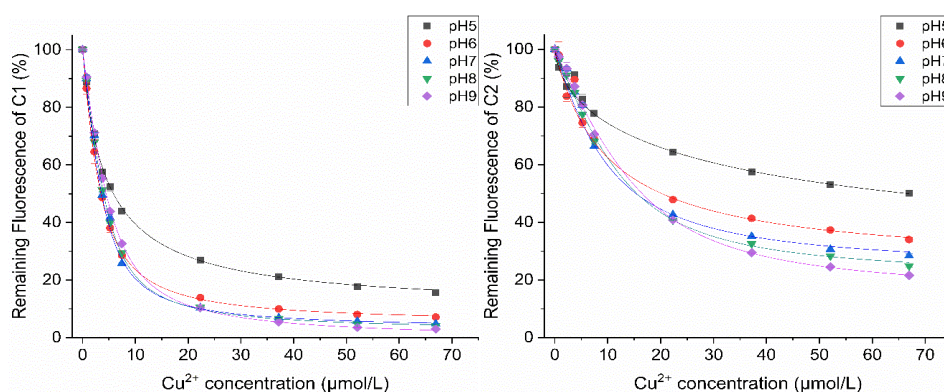
Figure 4.1. Derived components from commercial humic substance (DOM) by PARAFAC modeling. C1 and C2 are derived from DOM, C3 is herbicide MCP. P.

4.3.2 Heavy metals complexation with DOM

To study the interaction of heavy metals with HS, changes of fluorescence from HS when adding different amounts of Cu^{2+} and Zn^{2+} at various pH conditions were

4. Interaction of heavy metals and biocide/herbicide from stormwater runoff of buildings with dissolved organic matter

monitored by EEM analysis. As shown in **Figure 4.2**, a rapid decrease in fluorescence occurs with increasing concentration of Cu^{2+} at all tested pH conditions for both DOM fluorescent components C1 and C2. The fluorescence decreases almost linearly for the lower dosages ($< 7.44 \mu\text{mol/L}$). After the rapid decline, a further increase of Cu^{2+} concentration quenches less fluorescence and RF finally reaches a stable stage. This trend was also observed in a study of Cu^{2+} complexation with compost-derived DOM (Huang et al., 2018b) and digestate DOM (Guo et al., 2020). In our experiments, when maximum Cu^{2+} added RF of HS decreased with the increasing experimental pH. For the Cu^{2+} -C1 interaction at pH 5 the RF was 15.7%, when increased to pH 9 the corresponding value was 3%. This means a stronger interaction happened at a higher pH condition, indicating enhanced complexation between Cu^{2+} and HS. Similar results were observed in Cu^{2+} -C2 interaction experiments as well. For C2 at pH 5, the RF was 50% higher than the value obtained at pH 9 (21.6%). Changes of RF at different pH conditions can be ascribed to a wide pKa range of DOM due to its high complexity in molecular structure. A study from Lu and Allen, 2002 has shown that pKa values of three different DOMs can be well depicted by a 4-site monoprotic discrete-site model with an average range from pH 3.3 to 9.6, the distribution of pKa values has totally covered the pH range used in our experiments. This means when changing pH in our study, DOMs were deprotonated in different degrees. This led to their different capacities in the interaction with Cu^{2+} and finally caused the variance in fluorescence quenching.



4. Interaction of heavy metals and biocide/herbicide from stormwater runoff of buildings with dissolved organic matter

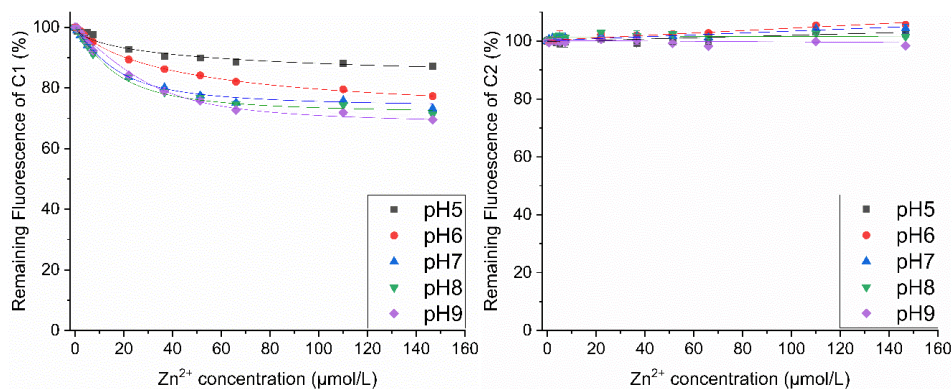


Figure 4.2. Remaining fluorescence of each DOM component C1 and C2 in the complexation experiments with Cu²⁺ and Zn²⁺ (Top left: Cu²⁺ complexation with C1; top right: Cu²⁺ with C2; bottom left: Zn²⁺ with C1; bottom right: Zn²⁺ with C2).

Despite the fluorescence changing trend of C1 and C2 was analogous when adding Cu²⁺ at various pH conditions, it has a distinct difference in extent: the fluorescence intensity of C2 decreased less than that of C1 at the same conditions. For the pH values of 5–9 the RF of C2 at the maximum Cu²⁺ concentration applied was 50%, 34%, 28.4%, 24.9%, and 21.6%, corresponding data from C1 was 15.7%, 7.2% 4.8%, 4.2%, and 3%, respectively. As previously shown in Section 4.3.1, C1 was identified as having higher MW than C2 and exhibited more red shifting in the EEM spectrum. Together with published results which reported that higher DOM MW has more carboxyl in aromatic carbon proportion (Lee et al., 2015), and red shifting in fluorescence was positively correlated with aromatic acidic functions in DOM (Zhrebker et al., 2020). Furthermore, Kikuchi et al., 2017 proved the positive mutuality between the Cu²⁺ binding affinity and the aromaticity of DOM, and suggested a preferential complexation with metal binding ligands close to the aromatic structure. All these findings evinced the difference in quenching of C1 and C2 when complexation with Cu²⁺ due to their various MWs: the higher in MW the more complexation with Cu²⁺ happens. It is always the case as larger MW means more functional groups, i.e., more binding sites. This outcome was consistent with results reported by Chen et al., 2013, which have shown that high MW DOM from size fractionation has a stronger binding affinity to Cu²⁺.

The mechanism for Zn²⁺ complexation with DOM was reported similar to Cu²⁺-DOM complexation evidenced by 2D-FTIR-COS analysis, as they displayed similar signals in the synchronous 2D-FTIR-COS map (Guo et al., 2020). However, Zn²⁺ complexation with DOM was found to be much weaker. As demonstrated in their study with five

4. Interaction of heavy metals and biocide/herbicide from stormwater runoff of buildings with dissolved organic matter

various heavy metal ions, only Zn^{2+} did not lead to a clear trend in DOM quenching with its increasing concentration. In our study, we gained similar results. Zn^{2+} was found to show less of an affinity to HS than Cu^{2+} . As depicted in **Figure 4.2**, complexation of Zn^{2+} with C1 at pH 5 to 9 exhibits a similar quenching trend compared with Cu^{2+} -C1 complexation but with a higher RF. By addition of 147 $\mu\text{mol/L}$ Zn^{2+} the RF of C1 at pH 5–9 were 87.1%, 77.3%, 73.3%, 71.2%, and 69.5%, respectively. These values were much higher than the maximum data obtained from Cu^{2+} -C1 complexation of 15.7%, indicating a weaker capability of Zn^{2+} in complexation with DOM than Cu^{2+} . This is in accordance with the solubility difference between Zn^{2+} and Cu^{2+} showing that Zn^{2+} is more easily dissolved in water. Additionally, no complexation between Zn^{2+} and C2 was observed, indicated by the remaining nearly horizontal fluorescence curve. This further confirms the conclusion that Zn^{2+} has less binding affinity to DOM than Cu^{2+} .

Table 4.2. LogK value derived from complexation between Cu^{2+} , Zn^{2+} , and DOM at different pH conditions.

pH	LogK (L/mol)						
	Cu^{2+} - C1	R^2	Cu^{2+} - C2	R^2	Zn^{2+} - C1	R^2	Zn^{2+} - C2
5	5.26	0.9981	4.32	0.9999	4.14	0.9762	NA
6	5.69	0.9993	4.97	0.9998	4.25	0.9991	NA
7	5.82	0.9990	5.22	0.9981	5.07	0.9977	NA
8	5.80	0.9998	5.33	0.9997	5.08	0.9948	NA
9	5.66	0.9998	5.27	0.9997	5.07	0.9987	NA

NA: not available

Obtained fluorescence data from heavy metals complexation experiments with DOM was fitted through the Ryan-Weber equation by Origin software, which allowed the quantitative comparison of heavy metals complexation with different DOM components at various pH conditions: the higher in logK value the more complexation happens. As listed in Table 4.2, an increase in logK value was observed by the increase of the pH value. For instance, in the Cu^{2+} -C2 complexation experiments from pH 5 to 9, the logK values were 4.32, 4.97, 5.22, 5.33, and 5.27, respectively. Moreover, among different complexation groups logK increased in the sequence of Zn^{2+} -C1, Cu^{2+} -C2, and Cu^{2+} -C1. Data from Cu^{2+} -C1 showed a magnitude larger in the logK value (5.26)

than that from Zn^{2+} -C1 (4.14) at a low pH condition. In comparing the acquired logK values a clear difference between complexations was shown, as obviously the most complexation happened in the Cu^{2+} -C1 group and at the high pH condition. Data in Table 4.2 correspond with those published for Cu^{2+} binding with DOM from compost (Huang et al., 2018b; He et al., 2014; Tang et al., 2019), anaerobic digestate (Guo et al., 2020), and Zn^{2+} binding with DOM from compost (Plaza et al., 2006) as well as municipal solid waste leachate (Wu et al., 2011). Notably, logK values from heavy metal-DOM complexation were not the highest at pH9; commonly they were comparable to those obtained at pH 8 or smaller. At pH 8 logK for Cu^{2+} -C1, Cu^{2+} -C2, and Zn^{2+} -C1 complexations were 5.80, 5.33, and 5.08. Increasing the pH to 9, logK values decreased to 5.66, 5.27, and 5.07, respectively. This does not necessarily mean a decline in complexation behavior, the reason for such a change was that more binding sites were available to heavy metals at the high pH conditions. The assumption for the Ryan-Weber model is a 1:1 binding of the fluorophore and quencher (Ryan and Weber, 1982), but this was definitely not the case for fluorophore from DOM. Meanwhile, fluorescence changing of each heavy metal cation binding to the DOM was not exactly the same. Therefore, the modeled deviation was as expected. Also, in describing the complexation of heavy metals with DOM by the Ryan-Weber equation, the C_L value was always underestimated (Guo et al., 2020; Wu et al., 2012; Plaza et al., 2006) due to the presence of multiple binding sites in the DOM. However, this model still gave a satisfactory result of the quantitative description for the heavy metal-DOM complexation process.

4.3.3 Interaction of BAC and MCPP with DOM

To understand how BAC and MCPP interact with DOM, an experimental setup similar to the complexation of heavy metals with DOM was carried out using different BAC and MCPP concentrations. The results are presented in **Figure 4.3** and **Figure 4.4**. As shown in **Figure 4.3**, with the increase of BAC concentration from 2.5 to 37.1 $\mu\text{mol/L}$ the RF of C1 and C2 gradually decreases. In contrast to the quenching processes observed from the heavy metals complexation with DOM, the quenching with a small dosage of BAC is less dominant. Furthermore, the RF obtained at maximum BAC addition is found to increase with the raising pH value. For C1 at pH 5 to 9 the RF values are 19.8%, 23.6%, 29.0%, 30.1%, and 35.7%, for C2 they are 55.2%, 59.0%,

4. Interaction of heavy metals and biocide/herbicide from stormwater runoff of buildings with dissolved organic matter

73.2%, 70.6% and 80.4%, respectively. This finding indicates a negative correlation between pH increase and BAC-HS interaction intensity ($r= 0.99$ for BAC-C1 and 0.94 for BAC-C2). It was adverse to the obtained result for the complexation of heavy metals and DOM presented in Section 4.3.2 showing more complexation at a higher pH.

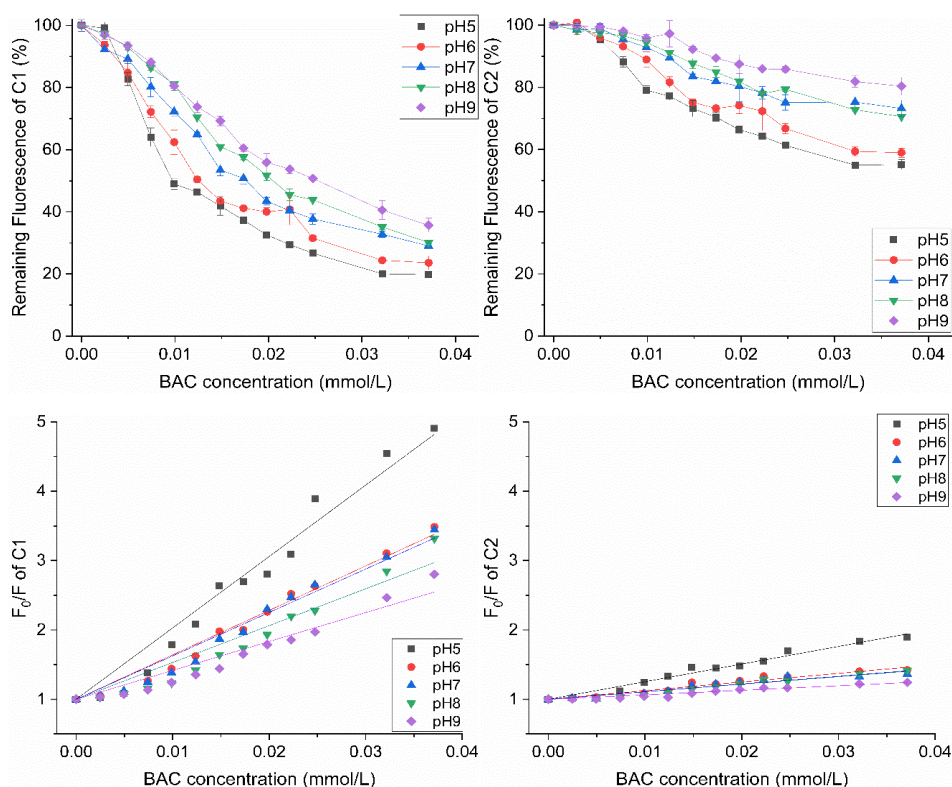


Figure 4.3. Remaining fluorescence of the HS component C1 and C2 in the addition of BAC at various pH conditions and modeling results of the quenching process via the Stern-Volmer equation. (Top left: BAC interaction with C1; top right: BAC interaction with C2; bottom left: modeling of BAC-C1 interaction; bottom right: modeling of BAC-C2 interaction).

The above-mentioned two properties in BAC-DOM interaction different from those in heavy metal-DOM complexation due to the involvement of additional mechanisms. The mechanism for the heavy metals complexation with DOM is electrostatic interaction. Correspondingly, according to the literatures those for interaction between BAC and DOM contain not only electrostatic interaction but also hydrogen bonding and π - π interaction (Chianese et al., 2020; Wu et al., 2020; Liu et al., 2019). Since more pathways were available for BAC-DOM interaction, in combination with the difference in the quenching capability of each interaction pathway, the quenching of DOM from

BAC addition was consequently moderate at the start. Similar results were obtained in studies of atrazine (Wang et al., 2017) and roxarsone (Fu et al., 2016) interaction with soil-derived DOM, where main fluorescence peaks identified from the EEM spectra were found to be less quenched by the same proportion of additives in the beginning of the experiments. In the aspect of adverse impact from a high pH condition on BAC-DOM interaction, with increasing pH values from 5 to 9 the acidic functional groups in DOM were deprotonated gradually on account of their distinctive pKa values. The deprotonation process destroyed the hydrogen bonding, while at the same time more electrostatic binding sites (-) were exposed to BAC (+) due to the oppositely charged state. Increasing the pH value brought two contrasting impacts to the BAC-DOM interaction. Among them the destruction of hydrogen bonding played a more important role than electrostatic attraction and then led to less quenching at higher pH conditions. The failure in utilization of negatively charged binding sites by BAC results due to steric hindrance from the long hydrocarbon chain (C₁₂) in the BAC molecule. Such an influence from pH changes on ionizable TOrCs interaction with DOM was also reported by Zhao et al., 2019 and Christl et al., 2016. They studied the interaction of fluoroquinolones having different pKa values with DOM and found their various affinities to DOM at changing pH conditions.

Comparing the interaction of BAC with C1 and C2, BAC showed more affinity to C1. This was comparable to heavy metals complexation with DOM. More interaction between BAC and C1 than C2 could be attributed to the larger MW of C1 and its higher aromaticity. This phenomenon was also reported by Chen et al., 2010, where they found that herbicide prometryne prefers interacting with high MW DOM that contains a more aromatic framework.

In contrast to BAC, the herbicide MCPP was negatively charged under the experimental conditions. As presented in **Figure 4.4**, RF of both C1 and C2 decrease with increasing MCPP concentration (from 4.7 to 46.6 $\mu\text{mol/L}$ MCPP). In comparison to the quenching process in BAC-DOM interaction, the one in MCPP-DOM interaction is almost linear. At maximum MCPP concentration and pH range from 5 to 9 the RF of C1 are 70.0%, 62.0%, 61.9%, 72.5%, and 91.3%, for C2 they are 81.7%, 77.0%, 76.4%, 79.3%, and 88%, respectively. Similar to BAC-DOM interaction, MCPP has shown more affinity to C1 than C2 at pH 5 to 7 but at pH 8 and pH 9 more interaction with C2 rather than C1 is observed. Meanwhile, MCPP-C1 is found more susceptible to the pH change than

4. Interaction of heavy metals and biocide/herbicide from stormwater runoff of buildings with dissolved organic matter

MCPP-C2. With increasing the pH value from 7 to 9 at an addition of 46.6 $\mu\text{mol/L}$ MCPP, the RF for C1 increases by 29.4% and for C2 by 11.6%. Furthermore, in contrast to the BAC-DOM interaction at the end of MCPP dosage, the most quenching is found at pH7 for MCPP-DOM interaction.

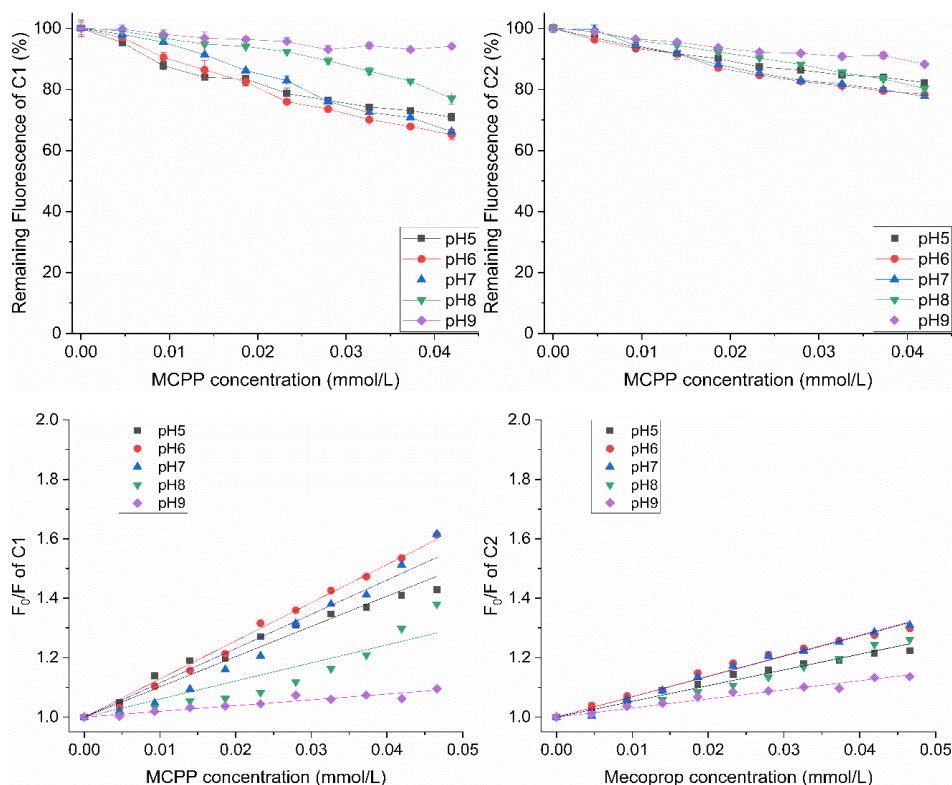


Figure 4.4. Remaining fluorescence of DOM components C1 and C2 in the addition of MCPP at various pH conditions and modeling results of the quenching process via the Stern-Volmer equation. (Top left: MCPP interaction with C1; top right: MCPP interaction with C2; bottom left: modeling of MCPP-C1 interaction; bottom right: modeling of MCPP-C2 interaction).

All these results were related to the negative charge of MCPP. The more abundant of acidic groups in C1 rather than C2 led to a stronger electrostatic repulsion in MCPP-C1 at high pH conditions. Hence, less interaction was found in MCPP-C1 than in MCPP-C2 at pH 9. For the same reason, it was not difficult to understand why the interaction of MCPP-C1 was more vulnerable than MCPP-C2 to pH changings. The disorder of RF ranking for MCPP-DOM interaction (with MCPP addition over 23.3 $\mu\text{mol/L}$) at the pH from 5 to 9 comparing with BAC-DOM interaction was because of the involvement of the cation bridge mechanism, among which, e.g., Ca^{2+} from the HS solution helped

to form a ternary complex of MCPP-Ca-DOM. The capability of Ca^{2+} acts as a bridge in the ternary complexation was previously suggested by Sowers et al., 2018b. They found the adsorption of organic carbon to ferrihydrite increased 52% at pH9 by the addition of 30 mM Ca^{2+} . Additionally, the presence of the ternary complexation was confirmed by some advanced analysis methods (Sowers et al., 2018a). Similar ternary complexation induced by polyvalent metals was also proposed by other researchers. Elkins et al., 2011 found a signal shift in the EEM spectrum which suggested herbicide dichlorprop bound to fulvic acid through an Al^{3+} ion bridge, and Pan et al., 2012 found the reinforcement of ofloxacin-DOM interaction by the presence of Cu^{2+} . More interestingly, the result from the interaction of MCPP (46.6 $\mu\text{mol/L}$) with DOM had cations removed supports our ternary interaction assumption. As shown in **Figure 8.5**, the removal of cations in the HS solution weakens the interaction between the MCPP and DOM at high pH conditions. For MCPP-C1 at pH 7, 8, and 9, the exclusion of cations increases the RF of C1 by 13.9%, 14.7%, and 5.1%, respectively. For MCPP-C2, the RF of C2 increases synchronously with the increasing pH value. These findings evidence the presence of ternary interaction in MCPP-DOM interaction.

As several mechanisms are involved in BAC-DOM and MCPP-DOM interactions, the Ryan-Weber equation failed to model their quenching processes. Therefore, the Stern-Volmer equation was used. Linear fitting results are listed in Table 4.3. The conditional constants K_{sv} range from 1.9 to 104 L/mmol and are in the same scope as the results found in Wang et al., 2017 and Huang et al., 2018a, which studied the interaction between TOrCs and DOM. In this study, the minimum K_{sv} value was found in MCPP-C1 at pH 9; correspondingly, the maximum was obtained from BAC-C1 at pH 5. The higher in K_{sv} values, the more interaction happens. Differences in the interaction of BAC and MCPP with DOM as well as the influence of pH changes on these processes were well described by the calculated K_{sv} values. For example, K_{sv} values from the BAC-DOM interaction were always larger than those from the MCPP-HS interaction, indicating a higher affinity of BAC than MCPP to DOM at all pH conditions. Moreover, the adverse impact from pH increasing to the BAC-DOM interaction was reflected by the decreasing K_{sv} values.

4. Interaction of heavy metals and biocide/herbicide from stormwater runoff of buildings with dissolved organic matter

Table 4.3. Quenching conditional constant K from the Stern-Volmer equation in describing the interaction between BAC, MCP, and each HS component C1 and C2 at different pH conditions.

pH	K_{sv} (L/mmol)							
	BAC				MCP			
	C 1	R ²	C 2	R ²	C1	R ²	C2	R ²
5	103.5 ± 3.7	0.9921	25.4 ± 0.8	0.9987	10.2 ± 0.3	0.9994	5.3 ± 0.1	0.9999
6	64.1 ± 1.9	0.9960	12.5 ± 0.5	0.9991	12.8 ± 0.2	0.9998	6.9 ± 0.2	0.9999
7	62.6 ± 2.1	0.9950	11.1 ± 0.5	0.9991	11.5 ± 0.5	0.9985	6.8 ± 0.1	0.9999
8	53.1 ± 2.8	0.9894	10.9 ± 0.5	0.9994	6.1 ± 0.5	0.9982	5.3 ± 0.2	0.9998
9	41.7 ± 2.0	0.9932	6.5 ± 0.3	0.9996	1.9 ± 0.1	0.9999	3.1 ± 0.1	0.9999

Bimolecular quenching constants (K_q) for each sub-interaction groups could be derived by dividing their respective K_{sv} values with average fluorescence lifetime of DOM (τ_0). In general, 1×10^{-8} S was taken as the reference for τ_0 (Huang et al., 2018a). Recently, a more precise value of 1.53×10^{-9} S measured from soil DOM was acquired by Wang et al., 2020. Based on the order of magnitude of τ_0 , all K_q values from BAC-DOM, MCP-DOM interactions were believed to be larger than $1 \times 10^{11} \text{ M}^{-1}\text{S}^{-1}$. For a diffusion-controlled quenching process, typically its K_q is near $1 \times 10^{10} \text{ M}^{-1}\text{S}^{-1}$; apparently larger values usually indicate the occurrence of binding interaction (Lakowicz, 2013). This means the decline of DOM fluorescence with the addition of BAC or MCP were static quenching processes.

4.3.4 BAC, MCP-HS interactions investigated by FTIR coupling 2D-COS analysis

Interaction between functional groups can be monitored by FTIR analysis. Hence, FTIR analysis was used to verify the mechanisms involved in BAC-DOM (HS), MCP-DOM (HS) interactions as described in Section 4.3.3. IR spectrum ($450\text{-}4000 \text{ cm}^{-1}$) of HS, BAC, MCP and their mixture in different ratios were collected in analysis. However, due to the overlaid spectrum at wavenumber larger 2500 cm^{-1} provided limited useful information, only the range of $450\text{-}2500 \text{ cm}^{-1}$ is presented in **Figure 4.5**. Separately mixing BAC and MCP with HS led to different changes at the IR spectrum. For BAC-

4. Interaction of heavy metals and biocide/herbicide from stormwater runoff of buildings with dissolved organic matter

HS samples, pronounced changes in peak location and/or peak intensity were observed at 1667–1630, 1590–1550, 1505–1430, 1069–996, and 900–845 cm^{-1} . Generally, the first three bands were assigned to aromatic “-C=C-” stretching from different molecule structures (Caglayan et al., 2017; Liu et al., 2013), two following bands were assigned to “-C-O-” stretching (Schmidt and Martínez, 2019) and aromatic “-C-H” stretching (Hussan et al., 2016). Among these stretchings, aromatic “-C=C-” stretching resulted from π - π interaction (Yang et al., 2005), “-C-O-” stretching due to “-O-H/O \cdot \cdots π ” hydrogen bonding, and aromatic “-C-H” stretching was from the aromatic interaction. These observed molecule vibrations support the mechanisms proposed for BAC-HS interaction. Despite the useful information obtained, some key points were still missing due to ambiguous vibrations at the BAC-HS IR spectrum. For instance, reactions of covalent bonds “-C=O” and “-C-N-” to BAC/HS mixture ratio alteration were not clearly identified, and these were related to electrostatic attraction mechanism (Keshavarz et al., 2013).

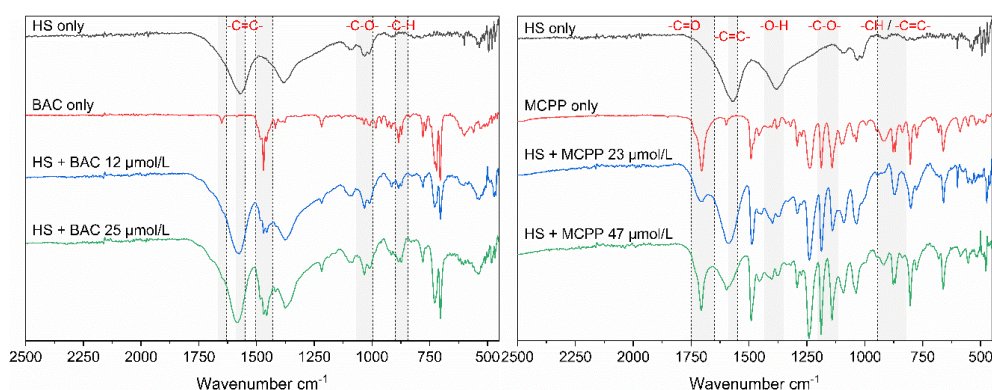


Figure 4.5. Overlaid IR spectrum of BAC, MCPP, humic substance and their mixture.

For MCPP-HS samples, molecule vibrations were found at 1750–1650, 1590–1550, 1435–1350, 1205–1115, and 945–820 cm^{-1} . These bands were assigned to carboxyl “-C=O” stretching (Garrido et al., 2012), aromatic “-C=C-” stretching (Liu et al., 2017), “-O-H” bending (Kaal et al., 2017), “-C-O-” stretching, aromatic “-C-H” stretching (Hussan et al., 2016), and “-C=C-” bending, respectively. The observed molecule vibrations suggest the existence of π - π interaction (aromatic “-C=C-” stretching, aromatic “-C-H” stretching and “-C=C-” bending), hydrogen bonding (carboxyl “-C=O” stretching, “-C-O-” stretching and “-O-H” bending), and the possible involvement of the cation bridging effect (carboxyl “-C=O” stretching and “-C-O-” stretching) in MCPP-HS.

4. Interaction of heavy metals and biocide/herbicide from stormwater runoff of buildings with dissolved organic matter

As a powerful tool, FTIR analysis successfully identified active functional groups in BAC-HS and MCPP-HS. However, there was an obstacle that could not be ignored, and that was the overlap of peaks. As DOM has broad peaks in FTIR spectra, in mixed samples some small changes in peak intensity or position are easily covered over and become unrecognizable. Therefore, useful information is missing. To overcome this obstacle, application of 2D-COS analysis was suggested. Another benefit from 2D-COS analysis was that it gave sequential information about molecule vibrations and helped to reveal the interaction processes in BAC-HS and MCPP-HS.

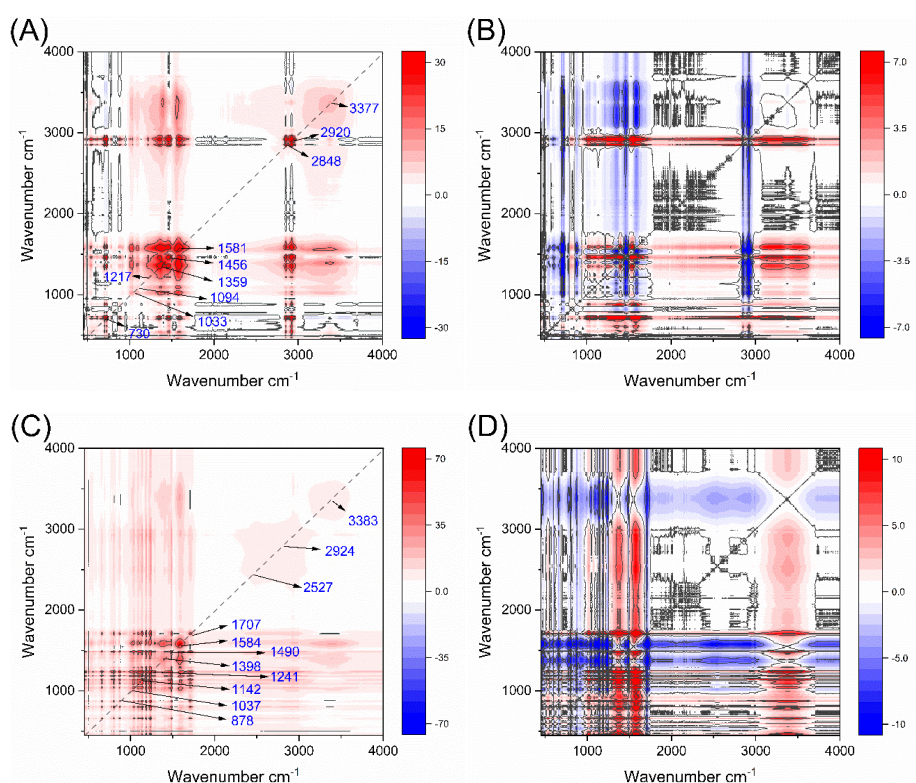


Figure 4.6. Synchronous (A, C) and asynchronous (B, D) maps generated from FTIR analysis of HS with external perturbation from BAC (A,B) and MCPP (C, D).

Figure 4.6 shows the FTIR synchronous and asynchronous maps from the interaction between HS and BAC / MCPP. The analyzed FTIR spectrum range was 450–4000 cm⁻¹ to collect as much useful information as possible. Several peaks were observed and marked at the diagonal in synchronous maps (**Figure 4.6A** and **C**). These peaks are called autopeaks, representing functional groups affected by the addition of BAC or MCPP. Notably different from heavy metal salts, BAC and MCPP themselves have some characteristic peaks from certain structures within the acquired FTIR spectrum. Increasing the proportion of these two substances in mixture with HS will definitely

enhance the FTIR signal of these characteristic peaks. For structures that did not play a role in interaction with HS, gradually increasing their FTIR signal in the data set would be erroneously defined as active functional groups by 2D-COS analysis. Such interference should be carefully discriminated and excluded. In **Figure 4.6A**, autopeak noise from BAC is found at 2920, 2848 and 730 cm^{-1} , where they are assigned to “-C-H” stretching/bending. For the rest, seven identified autopeaks are at 3377, 1581, 1456, 1359, 1217, 1094, and 1033 cm^{-1} . The first five autopeaks are assigned to “-OH” stretching from intermolecular bonded, aromatic “-C=C-” stretching, “-OH” bending from carboxylic acid, “-OH” bending from alcohol, and “-C-N-” stretching from amine, respectively. The last two autopeaks are most likely “-C-O-” stretching from carboxylic acid/alcohol. These identified autopeaks correspond well with the observed molecule vibration bands at the FTIR spectrum. 2D-COS did give a better resolution in the identification of functional groups as “-C-N-” stretching was not recognized in **Figure 4.5**. However, overlapping of autopeaks is still found in **Figure 4.6A** according to cross-peaks aside the diagonal around 1640–1720 cm^{-1} , this indefinite autopeak corresponds to carboxyl “-C=O” stretching. Similar overlapping of autopeaks was also reported by Liu et al., 2017 in studying the interaction between DOM and organic cation. All cross-peaks related to identified active functional groups are positive. According to asynchronous map **Figure 4.6B**, together with Noda’s rule (Noda, 1990) that asynchronous cross peak (assuming its X axis is W_1 ; Y axis is W_2 ; $W_1 > W_2$) which locates at the lower right section of the spectrum with positive (negative) sign means change at higher wavenumber W_1 happens before (later than) the change at W_2 . The susceptibility of functional groups to BAC addition from high to low is $3377 > 1094 > 1033 > 1217 > 1581 > 1359 > 1456 \text{ cm}^{-1}$. This has well described the interaction sequence when mixing BAC with HS. The first wavenumber 3377 cm^{-1} implying intermolecular hydrogen bonding was the first structure affected by BAC addition, and a possible result was the formation of new intermolecular hydrogen bondings between HS and the BAC aromatic part. This suggestion was further proved by cross-peaks in the asynchronous map located roughly at 1554 cm^{-1} indicating “-C=C-” stretching from the aromatic structure. The following was the electrostatic attraction between BAC and HS, evidenced by the changes from “-C-O-” and “-C-N-” stretching as well as the ambiguous carboxyl “-C=O” stretching. The third involved interaction was the π - π interaction as aromatic “-C=C-” stretching was found at 1581 cm^{-1} . The last was hydrogen bonding of BAC with residual free hydroxyl. These findings were in

accordance with results published by Liu et al., 2017, but our results stress the role of hydrogen bonding in the interaction of BAC with HS.

According to the same analysis procedure, autopeaks of MCPP-HS were marked and shown in **Figure 4.6C**. After excluding the noise, autopeaks related to active functional groups were found at 3383, 2924, 1707, 1584, 1398, 1241, 1142, and 1037 cm^{-1} . They were assigned to “-OH” stretching from intermolecular bonded, “-OH” stretching from carboxylic acid, “-C=O” stretching from carboxyl, aromatic “-C=C-” stretching, “-OH” bending from carboxylic acid/alcohol, “-C-N-” stretching from amine, and “-C-O-” stretching from carboxylic acid/alcohol (for both 1142 and 1037 cm^{-1}), respectively. All cross-peaks in the synchronous map off the diagonal are positive. In combining results from the asynchronous map **Figure 4.6D** and Noda’s rules (Noda, 1990), the susceptibility of functional groups to MCPP addition followed the order 3383 > 1584 > 1398 > 2924 > 1037 > 1241 > 1142 > 1707 cm^{-1} . This descending sequence has accurately depicted the interaction process when mixing MCPP with HS. First, intermolecular hydrogen bonding in HS was destroyed, followed by π - π interaction between MCPP and HS. Next occurred the formation of new hydrogen bonding between “-OH”/“-NH” (from HS) and MCPP; the last was the formation of cation bridge connection between MCPP and HS.

In comparing the interactions between BAC and MCPP with HS, involved mechanisms were the same but different in the sequence of taking effect. This was because of the difference in molecule structures between BAC and MCPP.

4.4 Conclusion

We offer the following conclusions and an outlook:

1. Two different fluorescent components C1 and C2 were identified within the applied HS by EEM-PARAFAC. The surrogate runoff pollutants prefer to interact with C1 than C2 due to C1 has larger MW and more abundant functional groups.
2. Increasing the pH from 5 to 9 enhanced the interaction between heavy metals and DOM as more binding sites are available to cations at higher pH condition, except for Zn^{2+} -C2 group (no complexation was observed throughout the study). However, the interaction between BAC/MCPP and DOM were impaired as hydrogen bonding was destroyed with increasing pH.

4. Interaction of heavy metals and biocide/herbicide from stormwater runoff of buildings with dissolved organic matter

3. Pollutant-DOM interactions could be well described by models. For heavy metal-DOM interaction the Ryan-Weber equation is eligible; however, for BAC/MCPP-DOM interactions the Stern-Volmer equation was more appropriate due to the presence of other interaction mechanisms.

4. Mechanisms involved in the BAC/MCPP-HS interaction include hydrogen bonding, π - π interaction, and electrostatic effect. Among these three mechanisms the role of hydrogen bonding was emphasized. The order of mechanisms that came into effect was different in BAC/MCPP titration studies and this relates to the molecular structure of BAC and MCPP. For the BAC-HS group it was intermolecular hydrogen bonding > electrostatic attraction > π - π interaction > hydrogen bonding with residual free hydroxyl. For the MCPP-HS group it was intermolecular hydrogen bonding > π - π interaction > hydrogen bonding with residual free hydroxyl > cation bridge effect (electrostatic attraction).

5. Retention of large MW DOM in SUDS, e.g., by filtration or addition of sorption materials, and maintenance a neutral condition would help to reduce the migration of both heavy metals and TOCs into the environment.

The next step is to investigate how the interactions or complexations between Zn^{2+} or Cu^{2+} and DOM are influenced if biocides or herbicides are present at the same time. This will be the topic of a separate publication.

4.5 Acknowledgement

The author wishes to thank the China Scholarship Council for the sholarship fund of Panfeng Zhu. FTIR spectra were acquired at the Center for Building Materials and Material Testing, TUM, under the supervision of Dr. Harald Hilbig and Caroline Herzinger.

5. Determining the binding of heavy metals, biocides, and their transformation products with dissolved organic matter – understanding pollutants interactions in building façade runoff

This chapter presents investigations related to research hypotheses #2.1 and #2.2:

***Hypothesis #2.1:** Heavy metals and biocides/TPs prefer to bind with DOM fraction having larger molecular weight.*

***Hypothesis #2.2:** The presence of 2mg/L Cu^{2+} reduces 50% of binding between biocides and DOM.*

This chapter has been published as follows:

*Zhu, P., Sottorff, I., Bi, J., & Helmreich, B. (2025). Determining the binding of heavy metals, biocides, and their transformation products with dissolved organic matter– Understanding pollutants interactions in building façade runoff. *Ecotoxicology and Environmental Safety*, 291, 117887.*

<https://doi.org/10.1016/j.ecoenv.2025.117887>

Author contributions: P.Z.: Conceptualization, data curation, funding acquisition, methodology, validation, visualization, investigation, methodology, writing – original draft; I.S.: Methodology, supervision, writing – review and editing; J.B.: Investigation, writing – review and editing; B.H.: Resources, supervision, writing – review and editing

Abstract

Understanding the interaction between biocides and heavy metals with dissolved organic matter (DOM) is the basis of building runoff treatment facility development. In the present study, we aimed to quantitatively determine the binding of biocides/heavy metals with DOM and evaluate the effect of Cu^{2+} on biocides-DOM interaction. We hypothesize that biocides prefer to bind with DOM having a larger molecular weight (MW), and this binding can be inhibited by Cu^{2+} . In experiments, DOM was separated into different fractions according to their MW difference, then we investigated the binding of Cu^{2+} , Zn^{2+} , biocides, and their transformation products (TPs) to different DOM fractions by dialysis equilibrium. According to the results, Cu^{2+} was found having the highest affinity for DOM fraction >100 kDa with the mean binding value of $2.65 \mu\text{mol}/\text{mgC}$, which reduced with decreasing DOM MW. Zn^{2+} binding to DOM was much weaker than Cu^{2+} with a mean value below $0.296 \mu\text{mol}/\text{mgC}$ and Zn^{2+} did not show a clear preference for DOM MW. Parent biocides showed higher DOM affinity than their TPs. The binding affinity of biocides to DOM followed the order mecoprop-p > terbutryn > diuron. Hydrogen bonding was found to play an important role in biocides-DOM binding. Moreover, the opposite effect of Cu^{2+} on biocides-DOM binding was observed, with inhibition for DOM fractions >100 kDa and enhancement for DOM fractions <100 kDa. Our findings suggest that source control of biocides/TPs pollution is important because a relatively high mobility of biocides/TPs in the environment is expected due to their limited interaction with DOM.

5.1 Introduction

Biocides (e.g., Diuron and terbutryn) are widely applied in façade renders and paints to prevent algae and mold growth on building surfaces. Frequently used biocides include diuron, terbutryn, mecoprop-p, isoproturon, and carbendazim, among others (Vega-Garcia et al., 2022a; Wicke et al., 2022; Reiß et al., 2021). When rainwater contacts with façades and fills the pore structures of the coating, applied biocides diffuse into rainwater and mobilize to the façade surface (Styszko et al., 2015; Vega-Garcia et al., 2020). This mechanism determines that building façade runoff is polluted by leached biocides. According to published studies, the leaching of biocides from façades into the environment can reach a high concentration. For example, Vega-Garcia et al., 2020 found that diuron had a concentration of 2.8 mg/L in façade runoff. Bollmann et al., 2016 reported that the concentration of terbutryn could be up to 5 mg/L at the early contact of the façade with rainwater. Moreover, Wicke et al., 2022 showed that an exposition time longer than one year can produce concentrations of diuron in runoff as high as 900 µg/L. These findings suggest that releasing biocides from buildings toward the environment is a constant process characterized by a large amount of initial leaching. Leached biocides are transferred to the soil surrounding the building or into Sustainable Urban Drainage Systems (SUDS) such as infiltration swales (Linke et al., 2021; Bollmann et al., 2017a). More importantly, Bork et al., 2021 pointed out that SUDS can't well retain these pollutants, and as a result, biocides could permeate into groundwater. Another study by Hensen et al., 2018 also concluded that detecting biocides and their transformation products (TPs) in groundwater from SUDS was possible. Furthermore, recent studies have shown that biocides have toxic effects on sediment and aquatic organisms (Reiß et al., 2021; Kiefer et al., 2024). In brief, for biocides in the environment, the pollution source keeps releasing biocides without appropriate treatment, and biocides fail to be retained by SUDS and cannot be eliminated by wastewater treatment plants (Paun et al., 2022). Additionally, current researches mainly focus on degradation studies, field surveys, and leaching modeling; biocide environmental behaviors are barely investigated and still unclear. Together, these emphasize that developing appropriate treatment facilities for controlling biocide pollution is necessary, and further research is needed.

In revealing the environmental behaviors of biocides, studying their interaction with other substances in building runoff is an important part. Here, it refers to heavy metals and dissolved organic matter (DOM), as they are often present in building runoff together with biocides. The origins of heavy metals are metal roofs, gutters, chimneys, and dormers due to corrosion (Galster and Helmreich, 2022; Degenhart and Helmreich, 2022). The leading players are Cu^{2+} and Zn^{2+} ; the concentration of Cu^{2+} in runoff can reach 4.9 mg/L (Athanasiadis et al., 2010), and Zn^{2+} can be up to 32 mg/L (Charters et al., 2021b) in metal roof runoff. The concentration of DOM in non-vegetated building runoff was reported as 4 mgC/L (Ouellet et al., 2021). Investigating the interaction of biocides and heavy metals with DOM can be accomplished by applying excitation-emission matrix (EEM) analysis (Schmidt et al., 2024; Ren et al., 2022), Fourier transform infrared (FTIR) spectroscopy analysis (D. Wang et al., 2020; Zhu et al., 2022), or by dialysis equilibrium (Rizzuto et al., 2021b; Zhang et al., 2021). EEM analysis can provide a half-quantified interaction result, and FTIR focuses more on revealing the interaction mechanism. Only dialysis equilibrium can precisely quantify the interaction among substances, even at very low concentrations. According to previous studies, dialysis equilibrium has been successfully used to determine the binding strength of Mn^{2+} and DOM (H. Wang et al., 2024) and assess the binding association between isoproturon and DOM (Rizzuto et al., 2021b). Therefore, dialysis equilibrium is a practicable method to investigate the binding interaction of biocides and heavy metals with DOM.

In the present study, we aim to quantify the interaction extent between biocides/heavy metals and DOM at real runoff concentration by dialysis equilibrium and investigate the binding preference of biocides/heavy metals to DOM fractions. Consequently, DOM was first separated into fractions according to their MW difference and then characterized. Subsequently, the binding of heavy metals and biocides with DOM fractions was quantified via dialysis equilibrium. Finally, the influence of Cu^{2+} on the biocides' binding process was investigated. The novelty of this research is the quantitative description of binding between biocides/TPs and DOM fractions under conditions that are close to reality. The tested hypothesis was that heavy metals and biocides/TPs bind the most, with DOM fraction having the largest MW, and the presence of Cu^{2+} impairs the binding between biocides and DOM. The obtained results

in the present study can provide the basis for the development of building runoff treatment systems to remove biocides.

5.2 Material and methods

5.2.1 Fractionation and Characterization of DOM

The DOM used in our experiments was prepared by commercial humic acid sodium salt (Carl Roth, Karlsruhe, Germany). The fractionation of DOM was described in our previous study (Zhu et al., 2023). After the dissolution of humic acid into Milli-Q water, the solution was centrifugated ($5000 \times g$, 10 min, twice) and filtered with 0.45 μm cellulose nitrate membrane (Sartorius, Göttingen, Germany) to remove particles. Then, the DOM stock solution was separated by centrifugal fractionation, where different pore sizes of membranes (3 kDa, 10 kDa, 30 kDa, and 100 kDa) were used. After this procedure, five different MW DOM fractions were obtained: <3 kDa, 3–10 kDa, 10–30 kDa, 30–100 kDa, and >100 kDa. Meanwhile, sodium azide was added into the obtained DOM fraction solutions (0.2 mM) to prevent biodegradation (S. He et al., 2021).

DOM fractions' characterization was related to their hydrophobicity, acidity, and fluorescence features (**Figure 8.6**). The hydrophobicity of DOM fractions was determined according to their UV-VIS absorbance behavior. After an appropriate dilution of the DOM fraction samples, their UV absorbance was measured in the 200–400 nm range with an interval of 1 nm (Hach DR6000, Colorado, USA). The DOC concentration of the corresponding sample normalized the absorbance to compare the hydrophobicity difference of the DOM fractions. The quantitative description of the DOM fraction hydrophobicity was achieved by calculating the specific ultraviolet absorbance (SUVA) at 254 nm since previous research (Weishaar et al., 2003) reported that SUVA₂₅₄ was strongly correlated with the percent aromaticity of DOM.

The acidity of DOM fractions was determined by base titration using an Eco titrator (Metrohm, Filderstadt, Germany). In the experiments, the prepared DOM fraction samples had a volume of 100 mL (10 mmol/L NaCl) and their concentrations were up to 100 mgC/L. Before titration, the DOM fraction samples were acidified with 10.2 M concentrated HCl (Merck, Darmstadt, Germany) to reach a pH of 2.5. Then, the samples were titrated with 0.05 M NaOH (Merck, Darmstadt, Germany) to reach a pH

of 11. The used titration mode was dynamic equivalence point titration, and the stirring speed was set to the maximum of the titrator. DOM fraction acidity was estimated by applying the acid neutralization capacity method. In this study, the acidity refers to carboxyl and phenolic content, where pH 8 was taken as the titration endpoint for carboxyl content, and phenolic content was from pH 8 to 10 (twice the base consumption) (Lu and Allen, 2002). The acidity analysis did not include DOM fractions <3 kDa and 30–100 kDa. Because DOM fraction <3 kDa had too low stock solution concentration to be precisely determined and DOM fraction 30–100 kDa (accounting for 1.4% of total DOM) had a limited sample amount. Additionally, DOM fraction 30–100 kDa had similar UV and fluorescence features compared with DOM fraction 10–30 kDa; therefore, the acidity of DOM fraction 10–30 kDa can be taken as a reference for DOM fraction 30–100 kDa.

5.2.2 Dialysis bag preparation and DOM retention

To lower the experiment cost, the dialysis bags used in this study had two different pore sizes, 12.4 kDa and 2 kDa (Merck, Darmstadt, Germany). The preparation of the dialysis bags with 12.4 kDa pore size followed the instructions from the supplier, including the removal of glycerol and sulfur compounds, followed by the acidification and rinse steps. For the dialysis bags with 2 kDa pore size, only Milli-Q water was used for cleaning.

A good retention performance for different DOM (humic acid) fractions inside the dialysis bag was required in this study. Therefore, a DOM fraction retention test was carried out for all four DOM fractions, except for DOM fraction <3 kDa since it wasn't used later in this study. In the experiments, 2 mgC/L DOM fraction solutions were prepared and transferred into dialysis bags. Those DOM fractions with MW > 10 kDa were placed in a 12.4 kDa dialysis bag. The DOM fraction 3–10 kDa was placed in a 2 kDa dialysis bag. Those dialysis bags filled with DOM solution were subsequently immersed in Milli-Q water for 24 hours to reach equilibrium. The mass loss was evaluated by comparing the absorbance at 280 nm before and after the dialysis treatment. The 280 nm wavelength selected was to prevent interference from sodium azide (strong UV absorbance at 254 nm). All samples were prepared and analyzed in triplicate.

5.2.3 Dialysis of heavy metals-DOM mixture

The binding capacity of heavy metals to DOM (humic acid) fractions was determined using dialysis equilibrium. In this study, the heavy metal salts selected were ZnCl₂ and CuCl₂, purchased from Merck (Darmstadt, Germany). As Zn²⁺ and Cu²⁺ can easily cross the dialysis bag membrane, Zn²⁺ and Cu²⁺ were added directly to the 1 L solution (Milli-Q water with 10 mM NaCl, pH 7) outside the dialysis bag to a 1 mg/L concentration. Inside the dialysis bag, the added DOM fractions (<3 kDa was not studied) were 25 mL, and the concentrations of DOM fractions were 1, 2, 3, 4, and 5 mgC/L, respectively. DOM concentration doubled for DOM fraction 3–10 kDa due to its weaker binding affinity to heavy metals. The equilibrium time of dialysis treatment was 24 hours. After the dialysis equilibrium, 20 mL solution inside the dialysis bag was collected and processed with acid digestion to remove the DOM. Meanwhile, 50 mL samples outside the dialysis bag were collected and filtered through a 0.45 µm syringe filter (Sartorius, Göttingen, Germany); they were used as blank samples to represent the freely dissolved Cu²⁺ (without interaction with DOM fractions). The concentration of Cu²⁺ was determined by atomic absorption spectroscopy analysis (Rommel et al., 2019). For the equilibrium of Zn²⁺, all experimental conditions were the same as Cu²⁺, except for the volume of added DOM fractions. Because Zn²⁺ had a minor affinity to DOM than Cu²⁺, and to avoid the undesired dilution in the acid digestion step, the volume of DOM fractions in Zn²⁺ equilibrium was increased to 60 mL, and the sample solution collected after dialysis was 50 mL. All samples were prepared and analyzed in triplicate.

5.2.4 Dialysis of biocides/transformation products-DOM mixture

Nine biocides and TPs purchased from Merck and Dr. Ehrenstorfer (Augsburg, Germany) were used in our study, and their stock solutions were prepared in methanol at a concentration of 100 mg/L. Four of the nine chemicals are parent biocides, i.e., diuron, mecoprop-p, terbutryn, and benzyl-dimethyl-tetradecylammonium chloride dihydrate (BAC). The other five chemicals were transformation products (TPs) of diuron (i.e., 1-(3,4-Dichlorophenyl)-3-methylurea (DCPMU), 1-(3,4-Dichlorophenyl) urea (DCPU), and 3,4-Dichloroaniline (DCA)) and terbutryn (i.e., Atra-zine-desisopropyl-2-hydroxy (DHT) and Terbutylazine-2-hydroxy (HAT)). Detailed

information on these nine chemicals is listed in **Table 8.2**. The quantitative assessment of the interaction between each biocide/TP and DOM (humic acid) fractions was also achieved by dialysis equilibrium. In biocides/TPs equilibrium, the addition of biocides/TPs was different from that of heavy metals described in section 2.3. Specifically, before the dialysis, each biocide/TP was premixed with 15 mL DOM fractions (<3 kDa was not studied) in brown glass bottles. The concentration of DOM fractions ranged from 1 to 5 mgC/L with an interval of 1 mgC/L, and the amount of biocides/TPs added was 1 µg for samples containing $\text{DOM} \leq 3$ mgC/L and 2 µg for samples with 4 and 5 mgC/L DOM. These mixtures were later shaken in a reciprocal shaker (Edmund Buhler®, Germany) for 24 h to achieve adequate interaction between biocides/TPs and DOM fractions. Afterward, the mixtures were transferred into different dialysis bags according to the MW of DOM fractions. Then, all the dialysis samples were immersed in 100 mL solution (Milli-Q water with 10 mM NaCl, pH 7) for 24 h, respectively, to reach the equilibrium. After the equilibrium, the samples inside the dialysis bag were collected, purified with solid phase extraction (SPE), and analyzed by high-performance liquid chromatography coupled with mass spectrometry (HPLC-MS/MS) to determine the concentration of biocides/TPs. The solutions outside dialysis bags were also analyzed and used as blanks representing the freely dissolved biocides/TPs.

In studying the influence of Cu^{2+} on the interaction between biocides and DOM fractions, Cu^{2+} was added to the biocides-DOM fraction mixture before the shaking step. The concentration of DOM fractions added inside the dialysis bag was 4 mgC/L, and the concentration of Cu^{2+} was 2 mg/L. The rest of the settings were the same as the biocides-DOM dialysis experiment. All samples were prepared and analyzed in triplicate.

5.2.5 Solid phase extraction and HPLC-MS analysis

To minimize the influence of DOM (humic acid) on the detection of biocides/TPs during HPLC-MS/MS analysis, a cleanup process was performed through SPE using a cartridge Oasis® HLB 6cc (200 mg, Waters, Eschborn, Germany) to reduce the interferences and the carbon load. The cleanup steps were as follows: Firstly, the conditioning of the cartridge was done with 10-volume methanol followed by 10-volume Milli-Q water. Secondly, the cartridge was equilibrated with 20 volumes of

Milli-Q water. Then, the loading step was performed by loading 4 mL of sample; loaded cartridges were kept flowing slowly for 4 min. Subsequently, the washing step was performed by adding ten volumes of Milli-Q water to eliminate the polar carbon load and the interferences. Then, the samples were dried using a vacuum. Next, the elution step was performed by adding 4 mL of methanol, which was left in the cartridge for 5 min to increase the recovery of the analytes. Finally, the biocides/TPs were eluted. It should be noted that Atrazine-desisopropyl-2-hydroxy (DHT) and benzyl-dimethyl-tetradecylammonium chloride dihydrate (BAC) had relatively low recovery in this SPE treatment. Therefore, samples containing these two compounds were directly analyzed without SPE treatment.

The method for analyzing the biocides/TPs using targeted HPLC-MS/MS was the same as that described in our previous study (Zhu et al., 2023). Briefly, a PLATINblue (Knauer®, Germany) HPLC system coupled with a 150 x 3 mm 2.6 µm PFP 100Å Kinetex® chromatographic column (Phenomenex®, Germany) was used. The mass spectrometer detector was a Triple Quad 6500 from Sciex® (Framingham, MA, USA). Each analyte was identified by two fragments: a quantifier and a qualifier. Additionally, the analytes were confirmed and corrected using heavy isotope internal standards. The mobile phases were Milli-Q water and LC-MS grade methanol in a gradient manner; both solvents contained 0.1% formic acid. The flow rate of solvent was 0.7 mL/min.

5.3 Results and discussion

5.3.1 Hydrophobicity and acidity of DOM fractions

The UV absorbance of different DOM (humic acid) fractions is shown in **Figure 5.1A**. For all the DOM fractions, except for DOM fraction <3 kDa, their normalized absorbance curves exhibited a similar trend, especially for DOM fractions 30–100 kDa and 10–30 kDa, where their normalized absorbance curves overlapped. DOM fraction <3 kDa showed a lower normalized absorbance than other DOM fractions. According to a previous study by Dilling and Kaiser, 2002, UV absorbance was positively correlated with hydrophobicity. Hence, it can be concluded that DOM fraction <3 kDa has the lowest hydrophobicity. Since the absorbance curves of other DOM fractions (>3 kDa) were not separated distinctly, a more obvious index to compare their

5. Determining the binding of heavy metals, biocides, and their transformation products with dissolved organic matter – understanding pollutants interactions in building façade runoff

hydrophobicity is required. Here, specific ultraviolet absorbance (SUVA) at 254 nm was used. The $SUVA_{254}$ values for DOM fractions, MW from large to small, were 7.85, 8.20, 8.20, 7.50, and 1.65 L/(mgC·m), respectively. Therefore, the DOM fractions 30–100 kDa and 10–30 kDa were considered to have the highest hydrophobicity, followed by DOM fractions >100 kDa, 3–10 kDa, and <3 kDa.

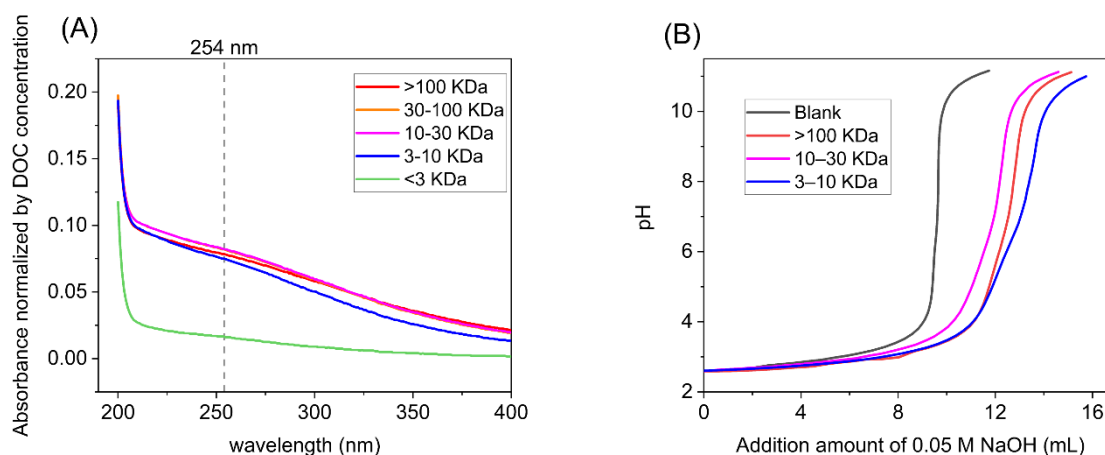


Figure 5.1. Characterization of DOM fractions. (A) The UV absorbance of five different DOM fractions (2 mgC/L) at 200–400 nm wavelength. (B) 0.05 M NaOH titration of different DOM fraction solutions from pH 2.6 to 11. DOM fractions 30–100 kDa and <3 kDa were not analyzed.

Generally, the $SUVA_{254}$ value of DOM from terrestrial ecosystems (D'Andrilli et al., 2022) or stormwater runoff (Lin et al., 2022) is no larger than 6 L/(mgC·m). In this study, although the DOM fractions used (excluding DOM fraction <3 kDa) showed $SUVA_{254}$ values higher than 7 L/(mgC·m), the obtained interaction results were still representative and meaningful because the $SUVA_{254}$ value of DOM in green roof runoff and surface runoff sometimes can be higher than 7 L/(mgC·m) (Ouellet et al., 2021; Xian et al., 2018). In addition, since DOM is a substance with a complex composition, the $SUVA_{254}$ value only reflects an average absorbance of all components. Thus, a certain proportion of DOM can have a relatively high $SUVA_{254}$ value. Investigating high $SUVA_{254}$ value fractions is necessary to comprehensively understand DOM interaction with biocides.

The result of DOM fractions base titration was depicted in **Figure 5.1B**. Generally, it is expected that more abundant carboxyl or phenolic groups provide more potential binding sites for pollutants. It can be seen that to reach pH 8, DOM fraction

3–10 kDa consumed the most of the base, followed by DOM fraction >100 kDa and DOM fraction 10–30 kDa, suggesting that DOM fraction 3–10 kDa has the highest carboxyl content. The calculated carboxyl content for each DOM fraction was 18.9 (3–10 kDa), 15.5 (>100 kDa), and 12.7 mmol/gC (10–30 kDa), respectively. Corresponding phenolic contents were 3.98 (3–10 kDa), 2.50 (>100 kDa), and 2.50 mmol/gC (10–30 kDa). It can be noted that the carboxyl content was more abundant than the phenolic content in all DOM fractions. The carboxyl content accounted for around 84% of total acidity. Previous studies have suggested that the acidity of DOM and its acidic group composition was sample-specific. For example, a high proportion of carboxyl group in DOM was also reported by Lu and Allen, 2002, who found that carboxyl group comprised 70% of total acidic sites in natural DOM. Meanwhile, (Ren et al., 2017) found that in fractionated humic acid (>1 kDa), carboxyl group only accounted for around 51% of total acidity. Moreover, Engel and Chefetz, 2015 showed that DOM derived from composted biosolids had a low total acidity of 4.3 mmol/gC.

Previous studies have reported that hydrophobicity and acidity can influence the interaction of DOM with pollutants; for example, Mei et al., 2016 stated that pyrene preferred to bind with the hydrophobic neutral DOM fraction than more polar acidic DOM fraction; a study from Ren et al., 2017 found that binding of As(III) and As(V) to DOM had a positive correlation with total acidity. Therefore, these two characteristics of DOM fractions were analyzed in this study to illustrate the differences between the pollutants and the interaction of DOM fractions.

5.3.2 DOM dialysis retention and heavy metals binding to DOM fractions

According to the results from DOM (humic acid) fractions dialysis experiments, all tested DOM fractions were well retained by the dialysis bag (**Table 8.3**). The minimum retention ($85.1\% \pm 0.7\%$) was found in the equilibrium of DOM fraction 3–10 kDa in a dialysis bag having a molecular weight cut-off (MWCO) of 2 kDa. For DOM fractions >10 kDa, their retention in the dialysis bag (MWCO 12.4 kDa) was 95.5–97.1%.

The results of investigating the interaction between heavy metals and DOM are shown in **Figure 5.2**. It can be found that Cu^{2+} presented a much stronger DOM binding

capability than Zn^{2+} . The mean values of Cu^{2+} binding to DOM fractions were 2.65 (>100 kDa), 2.79 (30–100 kDa), 1.97 (10–30 kDa), and 1.38 $\mu\text{mol}/\text{mgC}$ (3–10 kDa), respectively. The corresponding binding capabilities of Zn^{2+} to DOM fractions were 0.097, 0.296, 0.093, and 0.064 $\mu\text{mol}/\text{mgC}$, which were a magnitude lower than that of Cu^{2+} . The higher binding capability of Cu^{2+} to DOM than Zn^{2+} was also observed by S. He et al., 2021. This phenomenon can be attributed to the higher electronegativity of Cu^{2+} over Zn^{2+} , which brings about the more vital interaction of Cu^{2+} with the carboxyl group (Pan et al., 2022). Another reason is that phenolic groups in DOM have a higher affinity to Cu^{2+} than Zn^{2+} (Adusei-Gyamfi et al., 2019).

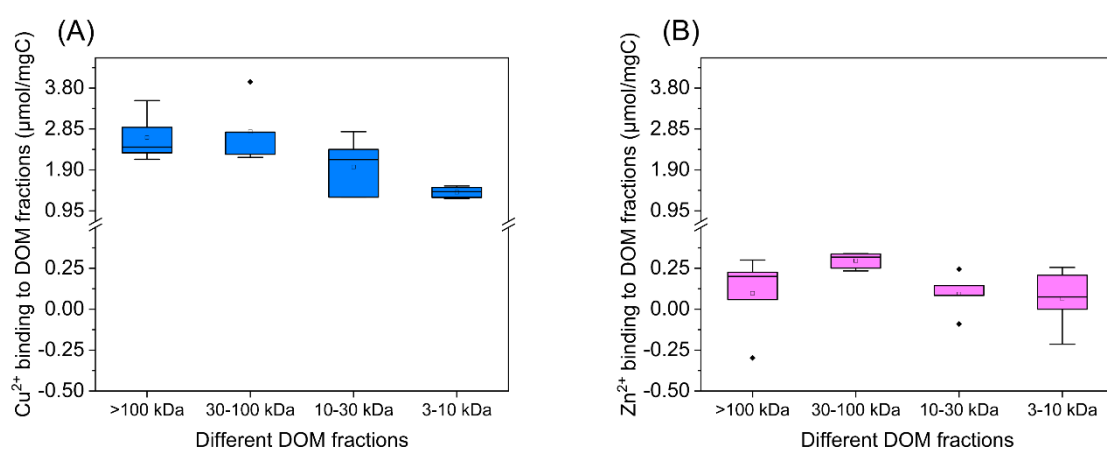


Figure 2. Binding of heavy metals with DOM fractions. (A) Cu^{2+} ; (B) Zn^{2+} .

In principle, Cu^{2+} interacts with DOM through carboxyl and phenolic functional groups (M. Huang et al., 2018), which means that higher DOM total acidity leads to a higher Cu^{2+} binding amount. Interestingly, our results showed that the binding of Cu^{2+} to DOM fractions was not positively correlated with the calculated total acidity, carboxyl, or phenolic content (**Figure 5.1B**, **Figure 5.2A**). Specifically, the DOM fraction >100 kDa, which had the largest MW but with a median total acidity, provided the most abundant binding sites for Cu^{2+} (DOM fraction 30–100 kDa had an outlier that raised the mean value, **Figure 5.2A**). The DOM fraction 3–10 kDa containing the highest carboxyl content complexed the least Cu^{2+} . Such binding preference was also observed when evaluating the correlation between Cu^{2+} binding and phenolic content. According to **Figure 5.2A**, it can be concluded that Cu^{2+} binding capability was positively related to DOM MW instead of total acidity. The possible reason for MW-dependent Cu^{2+} -DOM binding, which was also observed by previous studies (W. B. Chen et al., 2013; Fan et al., 2022), could be that the Cu^{2+} binding process is selective,

where only partial carboxyl or phenolic sites in DOM are preferred. These sites are more prevalent in large molecules. As a result, DOM fractions with larger MW tend to bind more Cu^{2+} , while the total acidity does not indicate Cu^{2+} binding preference. To be more specific, the selectivity of Cu^{2+} binding to DOM attributes to aromatic structure in DOM, binding sites close to aromatic structure are more popular for Cu^{2+} . Large DOM fraction having more aromatic structures, therefore, shows a higher Cu^{2+} binding capability. This is supported by a study from Kikuchi et al., 2017, their findings suggested that Cu^{2+} preferred to complex with acidic functional groups near the aromatic structure of humic materials.

Since the binding capability of Zn^{2+} to all DOM fractions was relatively low (**Figure 5.2B**), it was hard to observe the correlation of total acidity and DOM MW with Zn^{2+} binding affinity. This circumstance resulted from the high similarity of DOM fractions; for comparison, S. He et al., 2021 prepared different DOM samples, which varied a lot in the composition, and found a distinct difference in binding with Zn^{2+} .

Considering the large DOM binding capability difference between Cu^{2+} and Zn^{2+} , in designing the treatment facility, it is suggested that applying more retaining material (e.g., organic abundant topsoil) for Zn^{2+} treatment than Cu^{2+} treatment. As for applying the conclusion to other heavy metals, considering the physical and chemical difference, individual investigation rather than direct reference is recommended.

5.3.3 Binding of biocides and transformation products to DOM fractions

The binding capabilities of parent biocides (except for benzyl-dimethyl-tetradecylammonium chloride dihydrate (BAC) in supplementary **Figure 8.7**) and their transformation products (TPs) to different DOM (humic acid) fractions are shown in **Figure 5.3**. We found that BAC had the highest binding capability among all compounds, with a binding capability mean value of around several hundred $\mu\text{mol/gC}$ (supplementary **Figure 8.7**). This could be because BAC is a positively charged chemical that can interact with DOM through the electrostatic mechanism, which was qualified in our previous study by FTIR (Zhu et al., 2022). This mechanism is considered to cause a strong interaction, which can be reflected by heavy metal-DOM binding; as shown in **Figure 5.2**. The determined binding capabilities were in the range of mmol/gC . However, other compounds can only interact with DOM through non-

5. Determining the binding of heavy metals, biocides, and their transformation products with dissolved organic matter – understanding pollutants interactions in building façade runoff

covalent bonding (e.g., hydrophobic interaction and hydrogen bonding) (Ma and Yates, 2018; Chianese et al., 2020; Wu et al., 2020); therefore, their binding capabilities were much lower than BAC, for example, with corresponding mean values below 12.1 $\mu\text{mol/gC}$ when interacting with DOM fraction >100 kDa. This study's determined non-covalent binding affinities were in the range of previously reported results (Rizzuto et al., 2021b; Rizzuto et al., 2021a; Li et al., 2020).

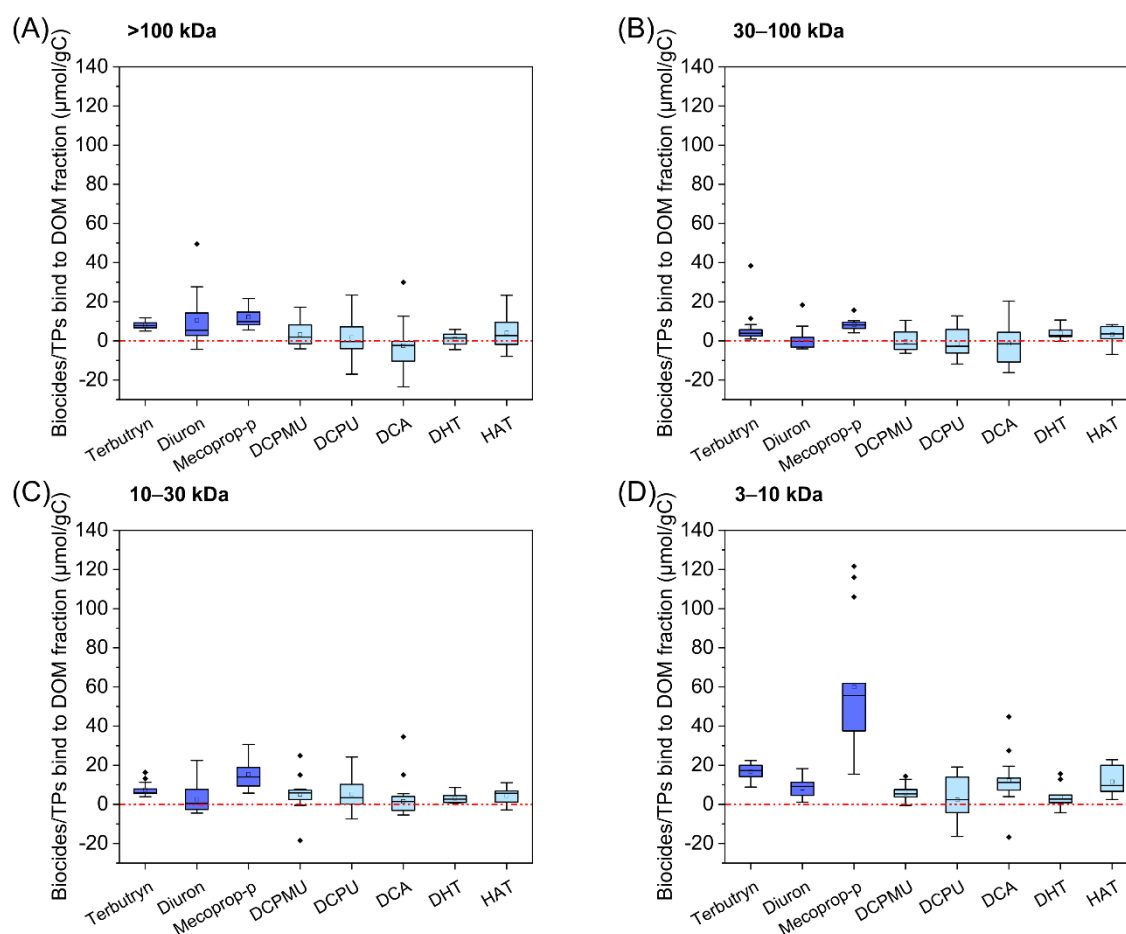


Figure 5.3. Binding of parent biocides (except for BAC) and their transformation products to DOM fractions. (A) >100 kDa; (B) 30–100 kDa; (C) 10–30 kDa; and (D) 3–10 kDa.

Notably, parent biocides showed higher binding capabilities for all DOM fractions than TPs (**Figure 5.3**). The decline of DOM binding affinity in TPs can be attributed to the change of molecular structure compared with parent compounds, which resulted in decreased hydrophobicity and increased water solubility of TPs (supplementary **Table 8.2**). For example, the hydrophobicity of terbutryn represented by LogD value (pH=7) was 2.7, and corresponding values of terbutryn TPs were 0.59 (DHT) and 1.94 (HAT),

respectively. Their calculated water solubility LogS in ascending sequence were -3.65 (terbutryn), -2.67 (HAT), and -1.8 (DHT), individually.

Regarding parent biocides, mecoprop-p showed higher DOM binding capability than terbutryn and diuron, and the affinity followed the order mecoprop-p > terbutryn > diuron. For instance, the mean binding value of mecoprop-p, terbutryn, and diuron to DOM fraction 10–30 kDa was 15.3, 7.49, and 2.61 $\mu\text{mol/gC}$, respectively. It can be seen that the binding abilities of parent biocides were inconsistent with their hydrophobicity (LogD, **Table 8.2**), and mecoprop-p, having the lowest LogD value, interacted the most with DOM. This indicated that an additional interaction mechanism, except for hydrophobic interaction, was involved. Based on the molecular structure of mecoprop-p, its carboxyl group is believed to interact with DOM via hydrogen bonding and, finally, result in the strongest DOM binding. Organic pollutants interacting with DOM via the carboxyl group have been previously proposed by Wu et al., 2020; in their study, they investigated the interaction of 4-chloro-2-methylphenoxyacetic acid with DOM.

Furthermore, in comparing the binding of parent biocides to different DOM fractions, we found that the used parent compounds exhibited an apparent higher affinity to DOM fraction 3–10 kDa, especially for mecoprop-p, whose binding capability was roughly four times higher than those found in other DOM fractions. Given the similar SUVA_{254} of DOM fractions, hydrophobic interaction was identified as not the main mechanism leading to the discrepancy of biocides-DOM fractions binding. At the same time, considering DOM fraction 3–10 kDa, which has a more significant amount of carboxyl and phenolic groups, it is assumed that the stronger interaction of biocides with DOM fraction 3–10 kDa than other DOM fractions was because of enhanced hydrogen bonding. The enhancement of pollutant-DOM binding due to a more abundant carboxyl functional group was also mentioned by Liu et al., 2019; they found DOM having higher dimer $-\text{COOH}$ content presented a larger erythromycin-DOM interaction coefficient.

All of the above findings suggested that electrostatic interaction, hydrophobic interaction, and hydrogen bonding were involved mechanisms in biocides/TPs-DOM binding, and the extent of interaction was dependent on the characteristics (e.g., molecule charge state, hydrophobicity, total acidity, and molecular structure) of both biocides/TPs and DOM. Moreover, hydrogen bonding was a mechanism that should be

carefully considered in evaluating the interaction between organic pollutants with DOM. However, it is also noteworthy that the proportion of biocides/TPs binding to DOM is low <10% (except for BAC, not precisely measured), most of which is dissolved in water. Hence, in setting up a building runoff treatment facility, applying adsorption material (e.g., granular activated carbon) is suggested, because the retention of biocides/TPs by topsoil has challenge.

5.3.4 Effect of Cu^{2+} on the binding of biocides to DOM fractions

The effect of Cu^{2+} on the binding interaction of terbutryn, diuron, and mecoprop-p to different DOM (humic acid) fractions is shown in **Figure 5.4**. We only presented the results of three parent compounds since TPs-DOM interaction was too weak to observe their responses to Cu^{2+} addition. Due to the analysis deviation, biocide BAC was also excluded in this study.

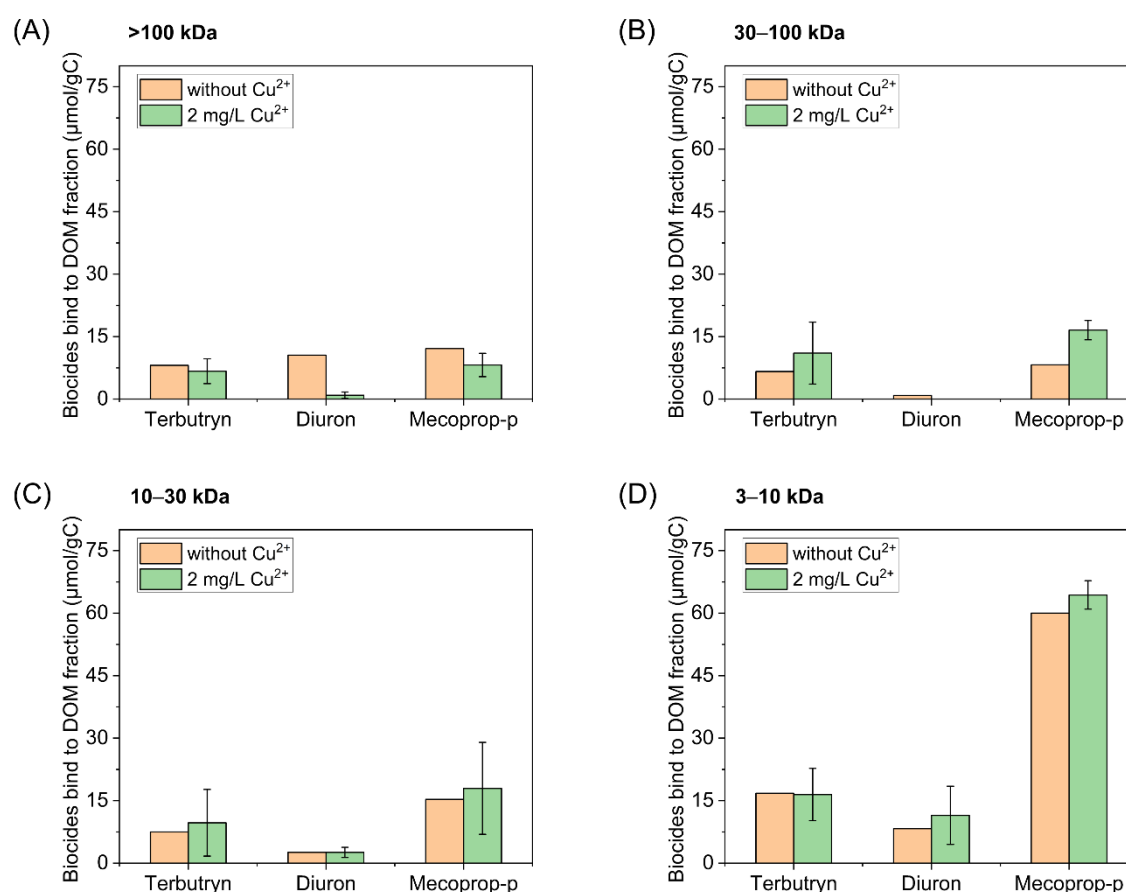


Figure 5.4. The influence of Cu^{2+} on binding of biocides to DOM fractions. (A) DOM fraction >100 kDa; (B) DOM fraction 30–100 kDa; (C) DOM fraction 10–30 kDa; and (D) DOM fraction 3–10 kDa. Orange and green bars represented the binding capability

mean values of biocides to DOM fractions without adding Cu^{2+} (blank, from **Figure 5.3**) and with 2 mg/L Cu^{2+} , respectively.

For DOM fraction >100 kDa, the addition of Cu^{2+} inhibited the biocides binding process, with a decrease of 1.41 $\mu\text{mol/gC}$ for terbutryn and 3.94 $\mu\text{mol/gC}$ for mecoprop-p (**Figure 5.4A**). Although the observed decline of diuron binding capability was obvious, it did not imply such a strong inhibition effect of Cu^{2+} but, in fact, less inhibition. The diuron blank's mean binding capability was overestimated (**Figure 5.3A**, the diuron data set has a significant deviation). Overall, the presence of Cu^{2+} impaired the binding of these three biocides with DOM fraction >100 kDa. The negative effect of metal cations on organic pollutants-DOM interactions was also reported by Pan et al., 2012 and S. Wang et al., 2024, who found that Mg^{2+} inhibited the binding of ofloxacin and tetracycline to DOM. Pan et al., 2012 attributed the inhibition to Mg^{2+} competing or shielding the binding sites on DOM. In contrast, Wang et al., 2024 pointed out that Mg^{2+} posed an inhibitory effect at alkaline conditions due to the formation of a tetracycline- Mg^{2+} complex. In our study, considering the strong binding of Cu^{2+} to DOM fraction >100 kDa (**Figure 5.2A**), it is possible that Cu^{2+} binding with DOM competed with biocides for binding sites (e.g., oxygen-containing functional groups) and thus impeded biocides-DOM combination. As a result, the mobility of biocides in the environment is expected to increase under this context.

However, for DOM fraction <100 kDa, it can be noted that the binding of biocides with DOM fractions was enhanced by Cu^{2+} supplementation (**Figure 5.4B, C, D**), which was opposite to DOM fraction >100 kDa (**Figure 5.4A**). Specifically, the binding of terbutryn and mecoprop-p with DOM fraction 30–100 kDa increased by 4.44 and 8.35 $\mu\text{mol/gC}$, respectively (**Figure 5.4B**). Correspondingly, the improvement of terbutryn and mecoprop-p binding to DOM fraction 10–30 kDa were 2.20 and 2.63 $\mu\text{mol/gC}$ (**Figure 5.4C**). The enhanced biocides-DOM (30–100 kDa and 10–30 kDa) binding was because Cu^{2+} destroyed DOM's inter- or intramolecular hydrogen bonding. Therefore, extra binding sites for biocides were exposed. This kind of additional binding site was not expected in DOM fraction >100 kDa since Cu^{2+} bound is stronger with DOM fraction >100 kDa, and this DOM fraction has fewer inter- or intramolecular hydrogen bonding interactions. More abundant inter- or intramolecular hydrogen bonding in DOM fraction 30–100 kDa and 10–30 kDa than in DOM fraction >100 kDa was due to their higher hydrophobicity (indicated by SUVA_{254} , **Figure 5.1A**). The

relationship between inter- or intramolecular hydrogen bonding and hydrophobicity was supported by a previous study that found strengthened water hydrogen bonds near purely hydrophobic solutes (Grdadolnik et al., 2017).

For DOM fraction 3–10 kDa, with the addition of Cu^{2+} , the binding between diuron and DOM fraction increased by $3.20 \mu\text{mol/gC}$. Meanwhile, the binding of terbutryn and mecoprop-p to DOM fraction was less affected (mecoprop-p blank has a significant deviation, **Figure 5.3D**). As stated previously, DOM fraction 3–10 kDa has the lowest hydrophobicity. Theoretically, this fraction should be negatively affected by Cu^{2+} addition, like DOM fraction >100 kDa. However, an opposite result was obtained because DOM fraction 3–10 kDa has the highest total acidity among these DOM fractions, leading to the strongest hydrogen bonding interaction between biocides and DOM fraction. Furthermore, according to section 3.2, Cu^{2+} interacted the least with DOM fraction 3–10 kDa compared to other DOM fractions. These two reasons make biocides-DOM (3–10 kDa) binding less affected by Cu^{2+} addition. As for enhanced diuron-DOM binding, which was because diuron has a lower DOM binding affinity than terbutryn and mecoprop-p, as a result, diuron is susceptible to hydrogen bonding sites change. Adding Cu^{2+} destroyed some weakly formed inter- or intramolecular hydrogen bonding in DOM fraction 3–10 kDa. These weak inter- or intramolecular hydrogen bonds can also be destroyed by terbutryn and mecoprop-p. Consequently, only diuron presented enhanced binding to DOM fraction 3–10 kDa when Cu^{2+} was added.

Besides our research, another study also reported the positive effect of Cu^{2+} on organic molecules binding to DOM. Specifically, Yi et al., 2023 found that Cu^{2+} promoted the sorption of sulfamethoxazole onto DOM. However, they attributed the enhanced binding to the formation of the sulfamethoxazole- Cu^{2+} -DOM ternary complex, which differs from our hydrogen bonding assumption.

In reality, it is expected that the presence of Cu^{2+} enhances the retention of biocides in stormwater treatment systems because of the improved DOM binding. Whereas, the influence of Cu^{2+} is limited due to the low binding proportion of biocides (section 5.3.3). Therefore, in developing building runoff treatment facilities, more effort should be paid in selecting appropriate adsorption material.

5.4. Conclusion

In summary, this study characterized centrifugally fractionated DOM (humic acid) and investigated the binding of heavy metals and biocides/TPs with different DOM fractions. Based on the obtained results, our hypothesis is rejected, and it can be concluded that DOM fractions with different molecular weights had similar optical properties, expressed in terms of UV absorbance curves and a narrow range of SUVA₂₅₄ values. The binding of Cu²⁺ with DOM fraction was positively related to DOM MW rather than total acidity. We assumed that the binding of Cu²⁺ with DOM was selective, and those preferential binding sites were more abundant in large molecules. For the binding of heavy metals with DOM, Cu²⁺ had a much higher affinity to DOM than Zn²⁺, hence, in retaining Zn²⁺ applying more organic abundant topsoil is suggested.

In the aspect of biocides binding to DOM fractions, electrostatic interaction was much more efficient than non-covalent binding, and the corresponding binding capability can be more than an order of magnitude higher. For binding between neutral or negatively charged biocides with DOM, hydrogen bonding played an important role, and a higher content of total acidity in DOM fraction enhanced such a hydrogen bonding process. Moreover, parent biocides had a higher DOM binding capability than TPs due to the decreased hydrophobicity and increased water solubility of TPs. The influence of Cu²⁺ supplementation on biocides binding to DOM was related to DOM MW. Cu²⁺ enhanced the interaction of biocides with DOM fraction <100 kDa and impaired the interaction with DOM fraction >100 kDa. It is necessary to consider the hydrophobicity (related to the amount of inter- or intramolecular hydrogen bonding) as well as total acidity (related to hydrogen bonding) of DOM to have a full view of the influence of Cu²⁺. Since the simultaneous presence of Cu²⁺ increases the binding of biocides to DOM in the fractions < 100 kDa, the enhancement of biocide retention in treatment systems can be expected.

Our results suggest that source control of biocides/TPs pollution is important because a relatively high mobility of biocides/TPs in the environment is expected due to their limited interaction with DOM. For this problem, a practicable way is to apply granular activated carbon in treatment because it has strong adsorption of organic compounds. Moreover, adsorption material with higher content of oxygenated functional groups is preferred, as it can enhance biocides retention by forming hydrogen

5. Determining the binding of heavy metals, biocides, and their transformation products with dissolved organic matter – understanding pollutants interactions in building façade runoff

bonding. For this aspect, surface modification of granular activated carbon can be considered.

5.5 Acknowledgement

The author wishes to thank the China Scholarship Council for the sholarship fund of Panfeng Zhu.

6. Adsorption of Heavy Metals and Biocides from Building Runoff onto Granular Activated Carbon—The Influence of Different Fractions of Dissolved Organic Matter

This chapter presents investigations related to research hypotheses #3.1 and #3.2:

***Hypothesis #3.1:** Transformation products show a better adsorption onto GAC than corresponding parent biocides.*

***Hypothesis #3.2:** The presence of 5 mgC/L DOM fractions or 2 mg/L heavy metals will inhibit the adsorption of biocides onto GAC.*

This chapter has been published as follows:

*Zhu, P., Sottorff, I., Zhang, T., & Helmreich, B. (2023). Adsorption of Heavy Metals and Biocides from Building Runoff onto Granular Activated Carbon—The Influence of Different Fractions of Dissolved Organic Matter. *Water*, 15(11), 2099.*

<https://doi.org/10.3390/w15112099>

Author contributions: P.Z.: methodology; validation, formal analysis, investigation, data curation, writing—original draft preparation, visualization, funding acquisition; T.Z.: formal analysis, investigation; I.S.: validation, data curation, writing—review and editing, supervision; B.H.: validation, resources, writing—review and editing, supervision, project administration, funding acquisition.

Abstract

Building runoff presents a good opportunity for water reuse in urban infrastructures; however, it is often polluted by biocides and heavy metals. In order to mitigate the pollution and improve water quality, we analysed the adsorption of heavy metals and biocides onto granular activated carbon (GAC) and investigated the influence of dissolved organic matter (DOM) fractions (>100 kDa, 10–30 kDa, and 3–10 kDa). In addition to our experimental work, we also studied the adsorption process by applying the Langmuir and Freundlich models. The results showed that $\geq 50\%$ of DOM was adsorbed at low concentrations (5 mgC/L). We also observed that DOM at a small molecular size exhibits improved adsorption. The adsorption capacity estimated by the Langmuir equation for Cu^{2+} and Zn^{2+} in the absence of DOM influence was 157 and 85.7 $\mu\text{mol/g}$, respectively. The presence of DOM at 5 mgC/L improved the adsorption of Cu^{2+} . Zn^{2+} adsorption was less sensitive to the presence of DOM than Cu^{2+} . Interestingly, without the influence of DOM, diuron-related compounds have a higher affinity toward GAC than terbutryn-related compounds. DOM affected the adsorption of diuron slightly. For terbutryn, the adsorption was enhanced, whereas mecoprop-p exhibited a strong competition with DOM. The presence of Cu^{2+} and Zn^{2+} presented a similar effect on the adsorption of biocides like DOM. Overall, GAC is an ideal adsorbent material for use in retaining building runoff pollutants.

6.1 Introduction

Runoff from buildings (roof and façade runoff) is a non-negligible part of urban stormwater runoff. It can be considered a water supply source for the urban water cycle (Luthy et al., 2019; Zhang et al., 2017). A basic requirement for the utilization of runoff water is its good quality. However, building runoff presents drawbacks, including heavy metal and biocide pollution. The release of heavy metals comes from metal roofs, gutters, chimneys, and dormers as a result of corrosion (Galster and Helmreich, 2022). The main players are Cu^{2+} and Zn^{2+} . The reported concentrations of these two heavy metals can be up to 4.9 mg/L for Cu^{2+} (Athanasiadis et al., 2010) and 32 mg/L for Zn^{2+} (Charters et al., 2021b) in copper and zinc roof runoff, respectively. It has been observed that more than 80% of copper and zinc were in the dissolved form as Cu^{2+} and Zn^{2+} ions (Charters et al., 2021b). This finding indicates that the majority of copper and zinc in metal roof runoff is bioavailable. A high proportion (>90%) of dissolved heavy metals in metal roof runoff was also reported by (Müller et al., 2019). This untreated metal roof runoff poses a huge threat to surface water quality and even to groundwater. The appropriate removal of heavy metals is required before the runoff water enters the environment and/or the runoff is reused.

Additionally found in building runoff are biocides, which leach from the building façades during rain events (Styszko et al., 2015; Vega-Garcia et al., 2020) through the water-filled pores (Styszko et al., 2015; Vega-Garcia et al., 2020). In general, biocides are described as substances used to control unwanted organisms that are harmful to human or animal health or to the environment, or that cause damage to human activities. Some well-known biocides found in construction materials include isoproturon, diuron, carbendazim, terbutryn, and others. (Styszko et al., 2015),(Vega-Garcia et al., 2020; Wicke et al., 2022a). The concentration of these chemicals in façade runoff is high in the early lifetime of the painting material and decreases with increasing exposure time. Previous research has shown that the diuron and terbutryn concentration in runoff can reach around 20 mg/L and 2 mg/L, separately, upon initial contact of the façade with rainwater (Burkhardt et al., 2012). In a case study with an exposure time of 1.5–3 years, it was discovered that diuron and terbutryn in the façade runoff still yielded concentrations around 900 µg/L and 20 µg/L, respectively (Wicke et al., 2022).

Also noteworthy is the biocide mecoprop-p (MCP), which is used on roofing materials. This biocide is added to bitumen roof sealing membranes in the form of esters in order to protect them against root penetration on flat green roofs (Bucheli et al., 1998). The amount of MCP emitted in runoff is not always constant and largely depends on the rain event (Paijens et al., 2020; Burkhardt et al., 2007; Schwerd et al., 2018). In a given roof, a higher emission level is initially observed after the new installation (Schwerd et al., 2018), followed by a decrease in the washout concentration and load after several years (Burkhardt et al., 2007).

Considering the damaging effects of biocides on the ecosystem (e.g., the inhibition of soil microbial activity (Fernández-Calviño et al., 2023)), their penetration through sand/clayey soil (Vega-Garcia et al., 2022a), and the unreliable retention by urban stormwater infiltration systems (Bork et al., 2021), an appropriate mitigation method for the biocides from runoff is needed to prevent the contamination of soil, aquatic environment, and groundwater.

In this context, a granular activated carbon (GAC)-based decentralized on-site runoff treatment is a promising option in the mitigation of building runoff pollution because such a system has the advantages of high efficiency, cost-effective, and flexibility in construction. As a porous material with a large surface ratio, GAC has been previously applied in stormwater pollution elimination (Ekanayake et al., 2021; Ko et al., 2018) and water quality assurance (Belkouteb et al., 2020; Vatankhah et al., 2019).

Research on building runoff has thus far mainly focused on the field pollution survey, pollutant leaching simulations, and modelling. Less effort has been made regarding the aspect of decentralized on-site building runoff treatments or to the aspect that both heavy metals and biocides are present in the runoff, not just one or the other. Moreover, there is also the possibility of an additional influence from naturally occurring dissolved organic matter (DOM) on the sorption behaviour onto GAC, which could lead to a reduction in sorption capacity. The utilization of building runoff has been limited by insufficient study of above aspects; therefore, our study aims to fulfil the knowledge gaps and remove the barrier in building runoff reuse.

In this research, we evaluated the adsorption capacity of pollutants in building runoff toward GAC, with a particular focus on biocides, biocide transformation products (TPs), heavy metals, and DOM occurring both alone and simultaneously. The present study consists of three main parts. Firstly, the investigation of the adsorption of each pollutant

onto GAC at different concentrations. Secondly, the quantitative description of adsorption processes via the Langmuir and Freundlich models. Thirdly, studying the influence of the presence of DOM on the adsorption of heavy metals and biocides. We further study the influence of heavy metals on the adsorption of biocides without DOM. The results from this research will contribute to the development of new strategies for the treatment of building runoff, thus achieving pollution source control and the protection of urban environment.

6.2 Material and methods

6.2.1 DOM Fractionation via Centrifugation

DOM was obtained from Carl Roth® (Karlsruhe, Germany) in the form of humic acid sodium salt, which was previously used in a study focused on proving the interaction between biocides and DOM via fluorescence changes (Zhu et al., 2022). The fractionation of DOM was performed using centrifugation according to their differences in molecular weight. Before the centrifugal fractionation, DOM stock solution (around 2 g/L) was first particle-cleaned via centrifugation (Centrifuge 5804R; Eppendorf, Berzdorf, Germany) twice in 50 mL tube at 5000× *g* for 10 min. The supernatant was then filtered through a 0.45 μm nitrocellulose membrane (Sartorius®, Goettingen, Germany) to remove the remaining particles and to avoid clogging the membranes for further fractionation. The fractionation membranes used (from Pall®, Ann Arbor, MI, USA and Sartorius®) had molecular weight cut offs at 100 kDa, 30 kDa, 10 kDa, and 3 kDa. A sequential centrifugation process was accordingly adopted, where the centrifugation speed was 6000× *g*, the time of centrifugation ranged from 4 to 60 min, which increased with decreasing DOM fraction size. At the end, the DOM fractions >100 kDa, 30–100 kDa, 10–30 kDa, 3–10 kDa, and <3 kDa were obtained and stored in glass bottles at 4 °C. After an appropriate dilution, the concentrations of dissolved organic carbon (DOC) in these five DOM fractions were measured using a total organic carbon (TOC) analyser (vario, Elementar®, Langenselbold, Germany).

6.2.2 Granular Activated Carbon Preparation

The GAC used in this study was Cyclecarb 301 (Chemviron®, Hattersheim, Germany). In order to avoid the influence from large GAC particles and maintain consistency

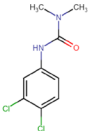
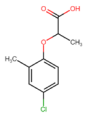
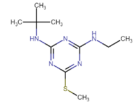
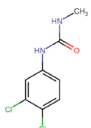
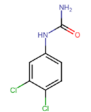
between each experiment, the GAC in the adsorption experiments was separated using a vibratory sieve shaker (AS200, RETSCH®, Haan, Germany). The sieves used had four different mesh sizes, 0.5, 0.71, 1.0, and 1.4 mm, respectively. The parameters used for the vibratory sieve shaker were 10 min for the sieving process with a 10 s interval, and the amplitude for sieving was 1.2 mm. The GAC used for sieving was around 250 g. All fractions were weighed after the separation process to calculate the ratio between each part to the total amount (this step was repeated three times). Of the five fractions thereby obtained, one or two fractions, which accounted for more than 50% of the total GAC, were selected as the working adsorbent (0.71–1.4 mm). Before applying the GAC in adsorption experiment, the GAC was dried at 105 ± 1 °C to a constant weight and later stored in a desiccator.

6.2.3 Adsorption of Fractionated DOM and Pollutants onto GAC

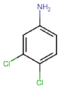
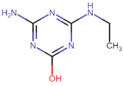
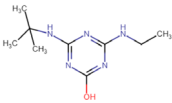
In order to study the adsorption of pollutants in building runoff onto GAC, we selected three fractionated DOM (>100 kDa, 10–30 kDa, and 3–10 kDa), two heavy metals (Cu^{2+} and Zn^{2+}) relevant to metal roof runoff, as well as three different biocides and their respective biocide transformation products (TPs). See Table 6.1. All experiments were performed in triplicate.

6. Adsorption of Heavy Metals and Biocides from Building Runoff onto Granular Activated Carbon—The Influence of Different Fractions of Dissolved Organic Matter

Table 6.1. The biocides/TPs used and their physicochemical properties.

Chemicals	Molecular Structure ^b	Molecular Formula ^a	Molecular Weight ^a	Water Solubility (mg/L) ^a	LogD (pH = 7) ^b
Diuron		C ₉ H ₁₀ Cl ₂ N ₂ O	233.09	37.4–42 (–3.11) ^c	2.53
Mecoprop-p		C ₁₀ H ₁₁ ClO ₃	214.64	880 (0.0) ^c	–0.25
Terbutryn		C ₁₀ H ₁₉ N ₅ S	241.36	35.9 (–3.65) ^c	2.7
1-(3,4-Dichlorophenyl)-3-methylurea (DCPMU)		C ₈ H ₈ Cl ₂ N ₂ O	219.06	(–3.08) ^c	2.31
1-(3,4-Dichlorophenyl)urea (DCPU)		C ₇ H ₆ Cl ₂ N ₂ O	205.04	(–3.08) ^c	2.09

6. Adsorption of Heavy Metals and Biocides from Building Runoff onto Granular Activated Carbon—The Influence of Different Fractions of Dissolved Organic Matter

3,4-Dichloroaniline (DCA)		$C_6H_5Cl_2N$	162.01	$(-2.75)^c$	2.35
Atrazine-desisopropyl-2-hydroxy (DHT)		$C_5H_9N_5O$	155.16	$(-1.8)^c$	0.59
Terbutylazine-2-hydroxy (HAT)		$C_9H_{17}N_5O$	211.26	$(-2.67)^c$	1.94

Notes: a: data from Pubchem; b: calculated data from ChemAxon; c: calculated solubility LogS from ChemAxon.

The investigation of the adsorption of fractionated DOM onto GAC was performed in glass bottles under shaking conditions of 120 rpm, 24 h (Orbital shaker, SM25, Bühler®, Bodelshausen, Germany). The solid-to-liquid ratio (GAC/Milli-Q water) of this reaction system was maintained at 2 mg/mL. The concentrations of DOM in the adsorption batch tests were 2, 4, 6, 8, 10, 20, 30, 40, 50, 100, 200, 400, and 600 mgC/L (DOM fraction 3–10 kDa did not include the maximum concentration). For samples with a DOM concentration of less than 40 mgC/L, the test volume was 100 mL (200 mg GAC added); for samples with a DOM concentration of 50 and 100 mgC/L, it was 50 mL (100 mg GAC added); the remaining tests were performed using a volume of 15 mL (30 mg GAC added). The decline in test volume was determined by the limited amount of fractionated DOM stock solution. All of the samples in these experiments contained 10 mM NaCl (Merck®, Darmstadt, Germany) in order to simulate environmental ionic strength. The pH value of samples with a volume larger than 50 mL was adjusted to 7.0 ± 0.2 . Since the sieved GAC comprised some fine particles which could not be removed using a 0.45 μm filter, measurement of the remaining DOM after adsorption was achieved by calibrating the sample (0.45 μm filtered) absorbance through calibration curves, which were acquired at 254 nm.

The experiments concerning the adsorption of Cu^{2+} and Zn^{2+} onto GAC were similar to the DOM adsorption experiments. The study was carried out in glass bottles, and the heavy metals added were CuCl_2 (Merck®, Germany) and ZnCl_2 (Merck®, Germany). The stock solutions were at a concentration of 5 g/L. In the experiments, 200 ± 0.2 mg GAC was added into 100 mL Milli-Q water containing 10 mM NaCl. The concentration of Cu^{2+} and Zn^{2+} in the samples was 5, 10, 15, 20, 30, and 40 mg/L, respectively. The pH value of the samples was adjusted to 6.0 ± 0.2 to minimize the precipitation of Cu^{2+} . All of the samples were shaken at 120 rpm for 24 h to achieve adequate adsorption. The concentration of the remaining heavy metals in each sample was determined via atomic absorption spectroscopy analysis after filtration through a 0.45 μm syringe filter and acidification with HNO_3 (Merck®, Germany) (Rommel et al., 2019).

The organic chemicals used to study the adsorption of biocides and their TPs onto GAC were purchased from Dr. Ehrenstorfer® (Augsburg, Germany). In the experiment, 10 ± 0.2 mg of GAC was weighed and added into a 100 mL solution of 10 mM NaCl. The concentrations of biocides and TPs in the experiments were 5, 10, 15, 20, 30, and 40 mg/L. The stock solution of biocides and TPs was prepared in methanol (Merck®,

Germany) at a concentration of 10 g/L, except for atrazine-desisopropyl-2-hydroxy and terbutylazine-2-hydroxy. These two chemicals had lower solubility in methanol; therefore, their stock solutions were prepared at a lower concentration of 2 g/L and was dissolved in a mix of water/MeOH (1:1) containing 0.4% formic acid (Merck[®], Germany). The pH value of the samples was adjusted to 7.0 ± 0.2 before shaking at 120 rpm for 24 h. Regarding those samples containing Terbutylazine-2-hydroxy, it was observed that the chemical formed a floccule after pH adjustment. To overcome this issue, we added 20 μ L of formic acid (Merck[®], Germany) into these samples ($V_T = 100$ mL) after the shaking process and before sampling in order to return it to a dissolved form. The collected samples were analysed via liquid chromatography coupled with mass spectrometry (LC-MS) after a filtration step using 0.22 μ m syringe filters.

6.2.4 Pollutants Co-Presence during the Adsorption Process

The evaluation mainly focused on the influence of DOM on the adsorption of heavy metals and biocides onto GAC. We also studied the influence of heavy metals on the adsorption of biocides onto GAC. The concentrations of DOM fractions in the experiments were maintained at 5 mgC/L, which approached the actual concentration in building runoff (Ouellet et al., 2021). The concentration of heavy metals and biocides was 40 mg/L. The experimental settings were the same as those in Section 6.2.3 with the highest pollutant concentration, i.e., 40 mg/L of heavy metals and biocides. With regard to studying the influence of heavy metals on biocide adsorption onto GAC, the experiment setting was similar. The heavy metals concentration was set to 2 mg/L, which mimics the concentration found in metal roof runoff (Galster and Helmreich, 2022). The biocide concentrations were prepared at 40 mg/L. Bearing in mind the similarity between TPs and their parent compounds, only the parent biocides were studied in this section. All experiments were performed in triplicate.

6.2.5 Liquid Chromatography–Mass Spectrometry Analysis

Targeted LC-MS analysis features high levels of resolution and accuracy for detecting trace organic pollutants in environmental and experimental samples, and it has been widely used to analyse biocides (Schoknecht et al., 2021; Urbanczyk et al., 2019). In the present study, it was applied in order to quantify the concentrations of biocides and their transformation products (TPs) in our samples. The UPLC system used was a

PLATINblue from Knauer[®] (Berlin, Germany). The chromatographic column was a 150 × 3 mm, Kinetex[®] 2.6 μm PFP 100 Å from Phenomenex[®] (Aschaffenburg, Germany).

The mass spectrometer used was a triple Quad 6500 from Sciex[®] operated with Analyst (version, 1.6.2, Sciex[®], Framingham, MA, USA). The instrument was operated using a Turbo V[®] ion source with a TurboIonSpray[®] ESI probe (Framingham, MA, USA). For the detection of the analytes, we used a targeted MRM method with optimized values for DP, CE, and CXP. Each analyte was identified using a quantifier and qualifier transition, in addition to a heavy isotope internal standard. The mobile phase was composed of a gradient of Milli-Q water and LC-MS grade methanol (Merck[®], Germany). Both solvents were supplemented with formic acid to reach a final concentration of 0.1%. The flow rate used was 0.7 mL/min.

6.2.5 Adsorption Modelling using Freundlich and Langmuir Equations

The Langmuir and Freundlich equations are the two most frequently used models in adsorption studies (Wang and Guo, 2020), in the literature; they have been used to describe the adsorption of pollutants onto GAC (Kalaruban et al., 2019),(Cai et al., 2020), powder activated carbon (Peñañiel et al., 2021), and biochar (Solanki and Boyer, 2019).

The expression of the Langmuir model (1) is as follows:

$$q_e = (q_0 \times K_L \times C_e)/(1 + K_L \times C_e), \quad (1)$$

where “ q_e ” is the adsorbed amount of pollutant at equilibrium in mg/g, “ q_0 ” is the maximum adsorption of pollutants to a given adsorbent in mg/g, and “ K_L ” is the Langmuir constant in L/mg, which means the affinity of adsorbate to the adsorbent (Rezakazemi and Zhang, 2018). “ C_e ” is the equilibrium concentration of adsorbate.

The expression of the Freundlich model (2) is as follows:

$$q_e = b \times C_e^{1/n}, \quad (2)$$

where “ q_e ” and “ C_e ” are the same variables as in the Langmuir model, “ b ” and “ n ” are constants for a given adsorbate and adsorbent at a given experimental condition, in which “ b ” means the adsorption affinity and “ n ” means the heterogeneity of the adsorbent surface (Lesmana et al., 2009).

6.3 Results and Discussion

6.3.1 DOM and Granular Activated Carbon Prepared

After the centrifugation process, five different DOM fractions were obtained (>100 kDa, 30–100 kDa, 10–30 kDa, 3–10 kDa, and <3 kDa). The DOM fractionation results showed that the majority of the obtained DOM belonged to the fractions >100 kDa (60.8%), 10–30 kDa (15.4%) and 3–10 kDa (20.6%), where they accounted for 96.8% of total DOM, while the fractions in the range of 30–100 kDa (1.4%) and <3 kDa (1.8%) exhibited significantly lower values. Hence, we decided to only use the more significant part of the DOM fractions, in this case >100 kDa, 10–30 kDa, and 3–10 kDa.

The separation of GAC according to particle size was successfully achieved by sieving. We thus obtained five different fractions, which were classified as: >1.4 mm, 1.0–1.4 mm, 0.71–1.0 mm, 0.5–0.71 mm, and <0.5 mm. The respective fractions accounted for $23.3 \pm 2.8\%$, $39.4 \pm 0.6\%$, $26.0 \pm 1.7\%$, $9.3 \pm 1.3\%$, and $1.9 \pm 0.5\%$ of the total GAC. It was noteworthy that no single fraction accounted for more than 50% by itself. This last finding made it necessary to mix at least two fractions together in order to prepare a representative GAC for the experiments. We therefore selected the fractions 1.0–1.4 mm and 0.71–1.0 mm, which together accounted for around 65.4% of the total GAC. Given its large size, the fraction >1.4 mm was not appropriate for our experiments, thus leading to weighing difficulties along with uniformity issues when compared with the whole set of GAC. We also found difficulties in working with fractions in the range of <0.71 mm, which was scarce and not representative of the experiment. Therefore, both fractions were discarded.

6.3.2 The Adsorption of DOM onto GAC

Figure 6.1A shows the results of the adsorption of DOM fractions >100 kDa, 10–30 kDa, and 3–10 kDa onto GAC. Unsurprisingly, DOM adsorption exhibited a correlation with concentration. The 3–10 kDa fraction appears to have reached a saturation at 400–500 mgC/L, whereas the other fractions continued to adsorb DOM at the concentrations studied. Applying DOM at a concentration <400 mgC/L clearly showed a descending adsorption tendency of the DOM fractions onto the GAC, in which the 3–10 kDa fraction was the most efficient, followed by 10–30 kDa, and >100 kDa. Such a tendency

6. Adsorption of Heavy Metals and Biocides from Building Runoff onto Granular Activated Carbon—The Influence of Different Fractions of Dissolved Organic Matter

was also reflected by the half adsorption of DOM, where 50% adsorption for DOM fraction 3–10 kDa, 10–30 kDa, and >100 kDa was found at around 20 mgC/L, 8 mgC/L, and 5 mgC/L, respectively.

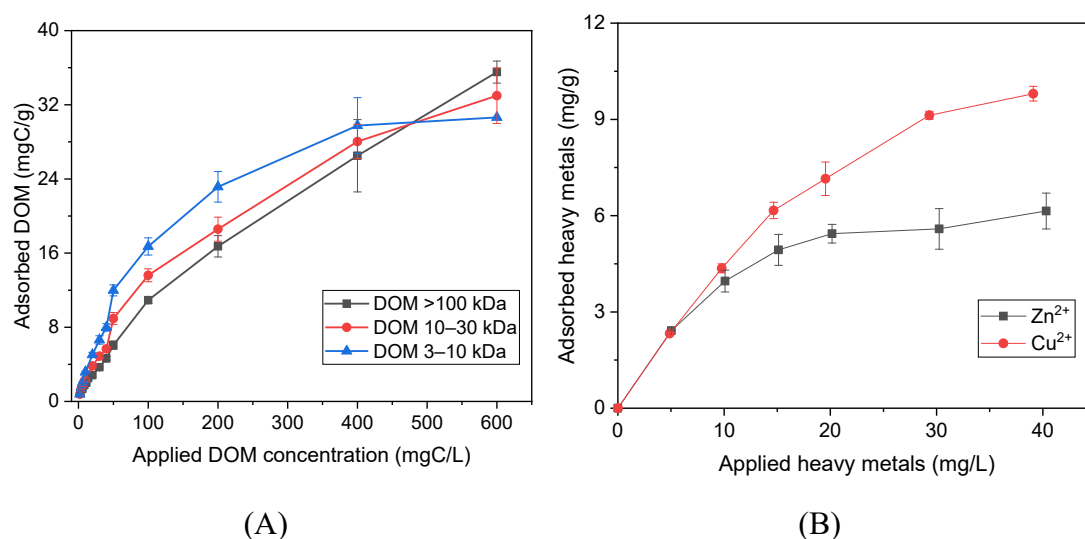


Figure 6.1. Adsorption curve for DOM and heavy metals. **(A)** The adsorption of different DOM fractions to 200 mg GAC at various concentrations in 100 mL Milli-Q water (The data point at 600 mgC/L for the 3–10 kDa fraction is an estimated result according to the Langmuir modelling equation, because the stock solution concentration of this fraction was only 567 mgC/L). **(B)** The adsorption of Cu²⁺ and Zn²⁺ to 200 mg GAC at various concentration in 100 mL Milli-Q water.

The preferential adsorption of small-size DOM fraction onto GAC has also been reported by (Schreiber et al., 2005) and (Shimabuku et al., 2017). The reason is that GAC is a porous material, which facilitates the interaction with the smaller DOM fraction (3–10 kDa) due to its size. As a result, it is quite likely that the smaller DOM fraction is able to access binding sites in the GAC pores not available to the large molecules. By increasing the concentration from 2 to 600 mgC/L, the adsorption difference between different fractions onto the GAC grows until 200 mgC/L; above 200 mgC/L, the variance initially shrinks before reversing at around 500 mgC/L, finally exhibiting the highest adsorption tendency from the >100 kDa fraction, with the lowest being the 3–10 kDa fraction. The change during the adsorption process is very likely due to the gradual saturation of GAC. The added DOM concentration was initially low, which meant that the binding sites at the surface of the GAC were sufficient to adsorb the DOM fractions. It is therefore proposed that, at low concentrations, a substantial

amount of DOM is attached on the surface of GAC, while a minor portion of DOM is accessing the pores of the GAC. Considering the low DOM concentration added (2 mgC/L), the difference between DOM fractions adsorption was very small. For example, at 2 mgC/L, the 3–10 kDa fraction adsorbed 79%, while the 10–30 kDa fraction adsorbed 78%. The >100 kDa fraction adsorbed an amount of around 70%. By increasing the DOM concentration, the surface binding sites are gradually occupied. Due to the clogging effect, which prevents the entrance of other large DOM molecules into the GAC pores, however, smaller DOM fractions are still able to access the binding sites inside the pores. The result was an adsorption difference between DOM fractions, which reached a maximum at 200 mgC/L in the experiment. At this concentration, the GAC adsorbed 3.35 mg/g more DOM of 3–10 kDa than of >100 kDa. When the DOM concentration continued to increase, the MW of DOM began to play an important role, i.e., that a large molecular weight for DOM will produce more carbon absorption due to its polymeric carbon contain. As before, at concentrations larger than 200 mgC/L, an increasing DOM concentration enhances the adsorption of all DOM fractions onto the GAC. However, the feature of large DOM fraction containing more carbon atoms in one molecule outweighs the adsorption enhancement by accessing the pores. Consequently, at 600 mgC/L, the highest adsorption was observed for the DOM fraction >100 kDa of 35.5 mg/g, followed by 33.0 mg/g for 10–30 kDa. In the case of the 3–10 kDa fraction, we estimated the value of 30.5 mg/g using the Langmuir equation (**Figure 6.1A**) because the stock solution concentration of this fraction was only 567 mgC/L.

The Langmuir modelling results determined the estimated maximum adsorption of each DOM fraction onto the GAC, whereby we found that the >100 kDa fraction can adsorb 59.4 ± 5.2 mg/g. The DOM 10–30 kDa fraction can adsorb 41.3 ± 2.4 mg/g, and the amount able to be adsorbed in the 3–10 kDa fraction was 34.3 ± 1.7 mg/g. These results are in accordance with previous research studying the adsorption of algal organic matter onto GAC, which obtained an adsorption of 31.45 mg/g (Zhao et al., 2022). The affinity of the adsorbate to the adsorbent (“ K_L ” value) increases with a decreasing DOM MW, which means that the smaller DOM fraction has a higher affinity for the GAC. The minimum R^2 value in the Langmuir modelling is 0.985, which suggests that the adsorption processes are well-fitted using the Langmuir equation. The “n” constant based on Freundlich modelling for the adsorption of DOM >100 kDa fraction onto the

GAC was 1.50 ± 0.03 . The results from the DOM 10–30 kDa and 3–10 kDa fractions were 1.89 ± 0.08 and 2.15 ± 0.14 , respectively. Since the “n” value represents the heterogeneity in the adsorption process, a larger value means that the system is more heterogeneous (Lesmana et al., 2009). The difference between “n” values implies that the smallest DOM fraction had different binding sites than the large ones. This conclusion is supported by the result in **Figure 6.1A**, which shows that, at the same concentration below 200 mgC/L, the pore structure in the GAC provided additional binding sites for the smaller DOM fractions. The ascending “b” values along with the descending DOM MW leads to the same conclusion of the Langmuir modelling, i.e., that the smaller fraction interacts more with the GAC than the large fractions. The R^2 values of the Freundlich modelling are above 0.975, which meant a good adsorption fitting result for each fraction.

6.3.3 The Adsorption of Heavy Metals onto GAC

The adsorption of heavy metals onto the GAC behaves similarly to the adsorption of DOM onto the GAC (**Figure 6.1B**). Strong adsorption was observed at the beginning, with a low concentration of heavy metals. For both Cu^{2+} and Zn^{2+} , at 5 mg/L, only 5% of the heavy metals was still found in the dissolved form. With the increase in the heavy metal concentration, the adsorption increased gradually for both Cu^{2+} and Zn^{2+} . In the experiment at concentrations higher than 5 mg/L, Cu^{2+} exhibited a higher affinity to the GAC than Zn^{2+} . At 40 mg/L heavy metal concentration, we observed the largest affinity difference in the adsorption of 60 $\mu\text{mol/g}$; at this concentration, 50% of applied Cu^{2+} was adsorbed and the amount adsorbed for Zn^{2+} was 30%. The Langmuir and Freundlich modelling results are shown in **Table 6.2**. According to the Langmuir modelling, the estimated maximum adsorption of Cu^{2+} and Zn^{2+} onto the GAC is around 157 and 85.7 $\mu\text{mol/g}$, respectively. This result is in accordance with the results found by (Sountharajah et al., 2015), who reported a Langmuir maximum adsorption of Cu^{2+} and Zn^{2+} onto the GAC at 186 and 50.5 $\mu\text{mol/g}$, respectively. It has been noted that the adsorption of Cu^{2+} onto the GAC is always stronger than that of Zn^{2+} . The higher adsorption affinity of Cu^{2+} has also been reported by studies investigating Cu^{2+} and Zn^{2+} adsorption onto biochars (Cibati et al., 2017; Jiang et al., 2016). Interestingly, the adsorption affinity difference between Cu^{2+} and Zn^{2+} is well described by the “b” value in the Freundlich model (a higher value represents a stronger adsorption), but the “ K_L ”

values in the Langmuir model failed to explain the absorption difference between the Cu^{2+} and Zn^{2+} . This is because several kinds of polar functional groups in the GAC are involved in the adsorption of Cu^{2+} and Zn^{2+} , e.g., phenolic and carboxylic groups (D.-W. Kim et al., 2020). Different functional groups provide different binding sites, i.e., a heterogeneous GAC surface to catch heavy metal cations. As previously mentioned, the Freundlich model is proposed for heterogeneous adsorption, and the Langmuir model is more appropriate for homogeneous adsorption. Therefore, the Freundlich model fits the $\text{Cu}^{2+}/\text{Zn}^{2+}$ adsorption data well ($R^2 = 0.984/0.961$), as expected. Theoretically, the Langmuir model should provide a less satisfactory result for both Cu^{2+} and Zn^{2+} . However, the fitting for Cu^{2+} adsorption onto GAC was still quite good and was due to the strong binding affinity of Cu^{2+} toward GAC (the heterogeneity at the GAC surface becomes relatively not significant for Cu^{2+}). At the same time, this was not the case for the Zn^{2+} for reason of its weaker binding capability (the GAC surface is heterogeneous for Zn^{2+}). Consequently, the Langmuir model poorly describes the adsorption affinity difference between Cu^{2+} and Zn^{2+} onto the GAC by way of the “ K_L ” value. The relative difference at the surface of the GAC for Cu^{2+} and Zn^{2+} is proved by the “ n ” values from the Freundlich model, in which case the Zn^{2+} had a higher value, i.e., a more heterogeneous surface.

6. Adsorption of Heavy Metals and Biocides from Building Runoff onto Granular Activated Carbon—The Influence of Different Fractions of Dissolved Organic Matter

Table 6.2. Pollutants GAC adsorption modelling results by the Langmuir and Freundlich equations.

Compounds	Langmuir Modelling			Freundlich Modelling		
	q_0 (mg/g, $\mu\text{mol/g}$)	K_L	R^2	b	n	R^2
DOM >100 K	59.4 ± 5.2^a	$(2.58 \pm 0.42) \times 10^{-3}$	0.991	0.55 ± 0.04	1.50 ± 0.03	0.998
DOM 10–30 K	41.4 ± 2.4^a	$(6.33 \pm 0.92) \times 10^{-3}$	0.986	1.23 ± 0.15	1.89 ± 0.08	0.990
DOM 3–10 K	34.3 ± 1.7^a	$(15.6 \pm 2.02) \times 10^{-3}$	0.985	2.09 ± 0.31	2.15 ± 0.14	0.975
Cu^{2+}	157.4 ± 0.5^b	0.72 ± 0.16	0.974	4.42 ± 0.25	3.52 ± 0.31	0.984
Zn^{2+}	85.7 ± 4.6^b	2.56 ± 1.15	0.823	3.49 ± 0.17	5.72 ± 0.61	0.961
Diuron	1621.7 ± 437.6^b	0.026 ± 0.01	0.978	1.41 ± 0.25	1.35 ± 0.11	0.983
Mecoprop	N.A.	N.A.	N.A.	0.222 ± 0.06	0.992 ± 0.09	0.981
Terbutryn	219.2 ± 46.0^b	0.29 ± 0.27	0.707	23.7 ± 11.0	4.96 ± 4.01	0.623
DCPMU	2506.2 ± 310.4^b	0.021 ± 0.004	0.997	14.8 ± 1.2	1.25 ± 0.05	0.997
DHT	495.6 ± 362.9^b	0.04 ± 0.05	0.763	5.0 ± 3.6	1.56 ± 0.61	0.785
DCPU	304.3 ± 17.9^b	0.64 ± 0.20	0.970	34.2 ± 6.0	5.65 ± 2.26	0.919
DCA	2888.8 ± 191.3^b	0.059 ± 0.01	0.997	35.4 ± 1.5	1.48 ± 0.04	0.998
HAT	N.A.	N.A.	N.A.	9.76 ± 1.7	1.52 ± 0.13	0.982

Notes: N.A. means not available; a: the unit is mg/g; b: the unit is $\mu\text{mol/g}$

6.3.4 The Adsorption of Biocides and Biocide Transformation Products onto GAC

Figure 6.2 illustrates the results of biocides and biocides transformation products (TPs) being adsorbed onto GAC. In our study, we applied three biocides with different chemical natures. We therefore used two main groups, benzene and triazine derivatives (**Figure 6.2C**). Hence, we tested terbutryn, diuron, and MCP. In the case of TPs, we used diuron (DCPMU, DCPU DCA) and terbutryn (DHT, HAT) derivatives.

In contrast to the adsorption of DOM or heavy metals onto GAC, the adsorption of biocides and TPs toward GAC commonly exhibits no clear saturation trend, except for terbutryn, which had a saturation point at 0.125 mmol/L (**Figure 6.2B**). At higher concentrations, DHT presented a behaviour which was not informative in determining whether GAC reached a saturation point (**Figure 6.2B**). For the other biocides and transformation products, we observed a collinearity between concentration and absorption (**Figure 6.2A, B**). In the experiment, the highest adsorption onto GAC was found for the chemical DCA, followed by (in decreasing order) DCPMU, diuron, DCPU, HAT, MCP, DHT, and terbutryn. It is noteworthy that the parent biocide and its transformation products presented similar adsorption capacities. In addition, the benzene-derived biocides (**Figure 6.2C**: diuron related chemicals) exhibited a higher adsorption ability than triazine-derived biocides (**Figure 6.2D**: terbutryn-related chemicals). The discovery of an adsorption difference between biocide groups (benzene and triazine derivatives) is similar to the result obtained by (Baup et al., 2002), who reported a higher adsorption for diuron onto the GAC than atrazine (the atrazine has the same core structure as terbutryn).

6. Adsorption of Heavy Metals and Biocides from Building Runoff onto Granular Activated Carbon—The Influence of Different Fractions of Dissolved Organic Matter

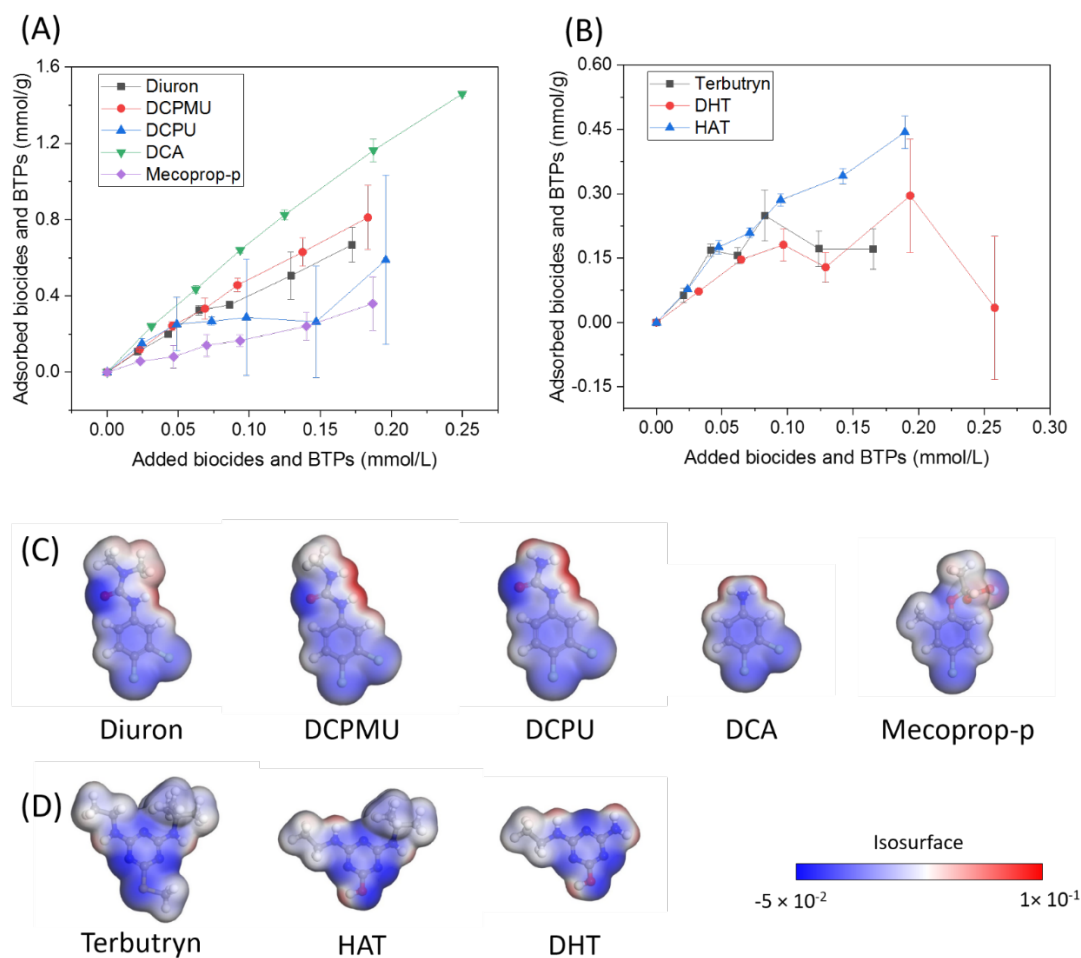


Figure 6.2. The adsorption of biocides/TPs onto GAC and biocides/TPs charge distribution. (A) The adsorption of benzene related biocides and TPs onto 10 mg GAC in 100 mL Milli-Q water; (B) The adsorption of triazine related biocides and TPs onto 10 mg GAC in 100 mL Milli-Q water. (C, D) Charge distribution of biocides and their TPs used in this study, calculated via Materials Studio with module DMol3; blue indicates a charge abundant area.

The analysis also found that the difference between chemicals adsorption onto GAC cannot be explained by their different LogD values, which is in accordance with findings by (Tang et al., 2020). Usually, a higher LogD value implies a higher hydrophobicity of a molecule and a stronger hydrophobic interaction with GAC; however, the results in this experiment did not fit the LogD prediction because the expected behaviour was not observed when compared with the adsorption. For example, the LogD values for terbutryn, diuron, and MCPP are 2.7, 2.53, and -0.25 , respectively, and the adsorption sequence for them from high to low is diuron > MCPP \geq terbutryn. This inconsistency is also found between diuron/terbutryn and their own transformation

products (TP) (see **Table 6.1** and **Figure 6.2**). This phenomenon is mainly due to the involvement of spatial hindrance from biocides and the TPs. For all three biocides and their TPs, they have benzene or triazine ring structures, thus enabling the interaction with GAC through π - π interactions (Peng et al., 2016). However, their contact with the surface of GAC is influenced by their own three-dimensional molecular structure. For example, as shown in **Figure 6.2C, D**, terbutryn, MCP, and HAT have a bulky structure, which very likely plays a detrimental role in the interaction between the molecules and the GAC surface. In contrast, diuron and DCPMU have a planar three-dimensional distribution due to the absence of bulky groups (iso-propyl at terbutryn), which enhances the interaction between the adsorbent surface (GAC) and diuron and DCPMU. Consequently, diuron-like compounds can attach to the GAC surface more easily and exhibit a higher adsorption capacity—despite benzene and triazine derived biocides supposedly having a similar π - π interaction ability based on the similar charge distribution around the ring structures. The DCA exhibited the highest adsorption among these compounds, which further confirms the above assumption that planar three-dimensional distribution can directly affect the interaction between biocides/TPs and the GAC. The influence of the three-dimensional molecular structure was also proposed by (Apul et al., 2013) after they normalized the properties of phenanthrene and biphenyl and found that the hydrophobic interaction was not the only factor controlling the adsorption process. MCP, which has a negative LogD value (-0.25), nevertheless presented a higher adsorption ability than terbutryn; this outcome can be attributed to the carboxylic acid-related hydrogen bonding (Bhadra et al., 2016) and the possible anion- π interaction (Xiaozhen et al., 2022) with GAC.

The Langmuir and Freundlich fitting results of biocides and TPs adsorption onto GAC are listed in **Table 6.2**. Not all of the data were as satisfactory as those obtained from the DOM fractions and heavy metals adsorption experiments, but the data still described most of the adsorption processes in a quantitative way. The estimated diuron adsorption capacity was around $1622 \mu\text{mol/g}$, which is higher than the result reported by (Al Bahri et al., 2016), but closer to the data from (De Souza and dos Santos, 2020) using commercial organophilic clay as an adsorbent. The estimated adsorption capacity for DCA, the chemical with the highest adsorption, was around $2900 \mu\text{mol/g}$, which was significantly higher than the data from terbutryn ($219 \mu\text{mol/g}$). By comparing the Langmuir and Freundlich modelling results, we observed that the Freundlich model fits

better than the Langmuir model due to the heterogeneity in the adsorption process (GAC surface), which is similar to the result obtained by (McGinley et al., 2022), who claimed that the Freundlich model was the best one for describing the adsorption of herbicides onto GAC.

6.3.5 The Influence of Co-Presence on the Adsorption Processes

In evaluating the influence of other substances (DOM and heavy metals) also present in the building runoff on the adsorption of target substance onto GAC, the concentration of the influencing factor was designed to mimic that found in the runoff, as shown in **Figure 6.3**.

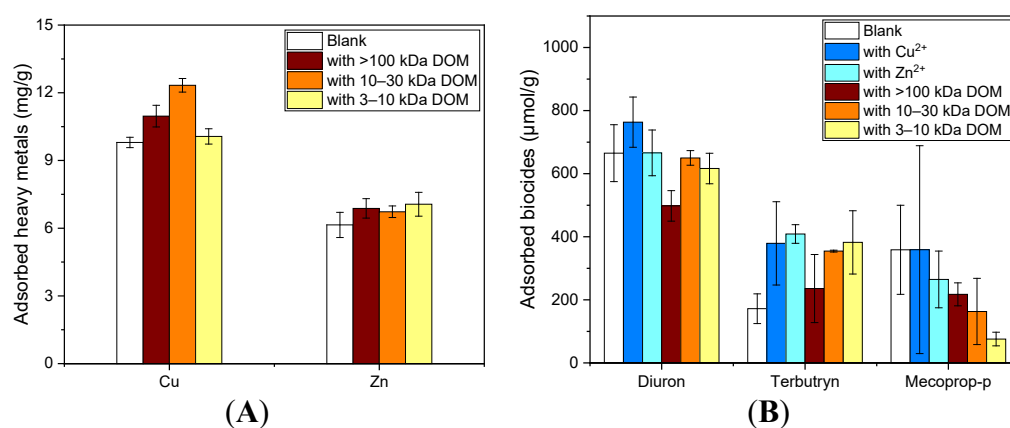


Figure 6.3. Influence of co-presence on the adsorption processes. (A) The influence of the presence of various DOM fractions (5 mg/L) on the adsorption of heavy metals (40 mg/L) onto 200 mg GAC in 100 mL Milli-Q water. (B) The influence of the presence of heavy metals (2 mg/L) and various DOM fractions (5 mg/L) on the adsorption of diuron, terbutryn, and MCP (40 mg/L) onto 10 mg GAC in 100 mL Milli-Q water. The large deviation for MCP could also be a result of methodological error.

According to the adsorption curves in **Figure 6.1A**, the application of 5 mgC/L of various DOM fractions were easily absorbed by 200 mg GAC, which means that more than 50% of the DOM fractions were adsorbed. It is also noteworthy that, as shown in **Figure 6.3A**, the presence of DOM was able to enhance the adsorption of heavy metals. For Cu²⁺, the greatest enhancement was found in the 10–30 kDa fraction (25.8%) followed by >100 kDa fraction (11.9%) and 3–10 kDa fraction (2.7%). This outcome is likely due to the oxygen-containing functional groups in the adsorbed DOM providing additional binding sites for Cu²⁺ (M. Huang et al., 2018), thus increasing its

adsorption onto the GAC. The slightly smaller adsorption of the >100 kDa fraction than the 10–30 kDa fraction can be explained by the severer blockage effect of larger DOM molecules at the entrance of GAC pores, which results in a higher loss of binding sites inside the GAC pore structures for Cu^{2+} , thus leading to the observation of a reduced Cu^{2+} adsorption. The 3–10 kDa fraction showed no clear enhancement in the Cu^{2+} adsorption because it presents a more severe blockage effect than the other two fractions. The 3–10 kDa fraction has the smallest molecular size. When applying DOM fractions at the same concentration (milligram carbon per liter), it provides the largest number of molecules, i.e., the most severe blockage effect. Furthermore, the increased binding sites from 3–10 kDa fraction cannot offset the above side effect. Eventually, the presence of the smallest DOM fraction exhibits little promotion of Cu^{2+} adsorption. By way of comparison with previous studies, (Genç-Fuhrman et al., 2016) and (Esfandiar et al., 2022) reported a negative impact of DOM on the adsorption of Cu^{2+} to adsorbents, which is the opposite of the results obtained in this study. The main reason for these conflicting results is the higher concentration of the applied DOM (around 20 mgC/L) or the use of a less active adsorbent such as biochar. As a result, a major part of DOM was in dissolved form; thus, DOM and GAC competed for Cu^{2+} , which reduced the Cu^{2+} adsorption. Given that Zn^{2+} showed a minor affinity to adsorption onto the GAC, it was less affected (average adsorption increase of 0.75 mg/g) by the presence of DOM and the blockage effect in the small pores.

Figure 6.3B illustrates the influence of heavy metals on the adsorption of biocides onto the GAC. The adsorption of diuron onto GAC was enhanced by 14.8% in the presence of Cu^{2+} but almost unaffected by the Zn^{2+} . Regarding terbutryn, the presence of heavy metals doubled its adsorption onto the GAC (increasing 120% for Cu^{2+} and 138% for Zn^{2+}). As for MCPP, the presence of Cu^{2+} did not considerably affect its average adsorption (with a big deviation in the data set). However, in the presence of Zn^{2+} , MCPP decreased the adsorption by 26.2%. As previously mentioned, the heavy metals interact with the GAC through the oxygen-containing functional groups. In fact, these functional groups are related to hydrogen bonding, which can be formed inter- and intramolecularly. The binding of heavy metals with GAC means the destruction of intramolecular hydrogen bonding inside the GAC, as well the hydrogen bonding between the GAC and the biocides. The result of the H bonding destruction is the exposure of electric charge abundant interaction sites. This change explains the

alteration of biocide adsorption onto the GAC in the presence of heavy metals. For example, diuron and its slightly improved adsorption in the presence of Cu^{2+} is the result of increased π - π interaction sites due to the destruction of intramolecular hydrogen bonding. The minor affinity of Zn^{2+} toward the GAC led to insignificant changes in the adsorption of diuron onto GAC, with values almost identical to those found in the control condition (blank). Correspondingly, the significant enhancement of terbutryn adsorption can also be explained by the increased interaction sites originating from the intramolecular hydrogen bonding due to the binding of heavy metals. The reason for an adverse effect of the Zn^{2+} presence on the MCPP adsorption is that some binding sites at the GAC surface were no longer able to act as hydrogen bonding donor because they were occupied by Zn^{2+} . The role that Cu^{2+} plays in the MCPP adsorption is complex, as it competes with the MCPP for the functional groups. At the same time, it can be assumed that Cu^{2+} is able to build a cation bridge to connect the MCPP and the GAC. An insignificant effect on the adsorption of MCPP caused by the presence of Cu^{2+} is therefore also reasonable. It should be noted that the different reaction of biocides adsorbing onto the GAC in the presence of heavy metals is due to the combined effect of π - π interaction and hydrogen bonding. A few similar positive and negative effects have been reported in previous studies. For instance, (Zheng et al., 2018) found that Cu^{2+} increased the adsorption of methyl orange onto a modified GAC material. The presence of heavy metals reduced the adsorption of polycyclic aromatic hydrocarbons onto the GAC (Eeshwarasinghe et al., 2019). Cr(III) and atrazine together exhibited a competitive adsorption onto the activated carbons (Wei et al., 2018), and others.

Similar to the influence of heavy metals on the adsorption of biocides onto the GAC, DOM fractions have a differing effect on the biocide adsorption processes (**Figure 6.3B**). The adsorption of diuron was inhibited by 25.1% in the presence of the DOM >100 kDa fraction. The 10–30 kDa fraction did not exhibit much inhibition, and an inhibition of 7.3% was observed in the 3–10 kDa fraction. For terbutryn, the adsorption onto GAC was enhanced by all three DOM fractions. It was observed that the smaller MW of DOM has the best enhancement for the terbutryn adsorption onto GAC. The enhanced adsorptions were 37% (>100 kDa), 106% (10–30 kDa), and 122% (3–10 kDa), respectively. In contrast with terbutryn adsorption, the adsorption of MCPP was clearly inhibited by the DOM fractions. The smaller of DOM MW the more

inhibition was found. These three DOM fractions inhibited the MCPP adsorption by 39.4% (>100 kDa), 54.5% (10–30 kDa), and 78.9% (3–10 kDa), respectively. Of all three biocides, the less affected adsorption of diuron in the presence of DOM is because of its strong π - π interaction with the GAC, which resists the competition from DOM (except for >100 kDa DOM, since the polymeric form covers up some active sites). The enhanced terbutryn adsorption was due to the intramolecular hydrogen bonding inside the GAC being destroyed by forming new intermolecular hydrogen bonding between the GAC and the DOM. As a result, the GAC provides additional π - π interaction binding sites for terbutryn. The inhibition of MCPP adsorption resulted from the direct competition of hydrogen bonding sites at the GAC surface with DOM. The varying influence of DOM on the adsorption of biocides onto the GAC was similar to that observed in previous studies. For example, (Radian and Mishael, 2012) found that the GAC adsorption kinetic of pyrene at equilibrium did not exhibit much difference when the DOM was added. However, a study by (L. Lin et al., 2017) reported that the presence of DOM hindered the removal of ibuprofen and sulfamethoxazole by way of the biochar. At the same time, the result by (Jin et al., 2018) implied that the presence of humic acid increased the adsorption of tetracycline and ciprofloxacin onto the activated carbon. Overall, the DOM affects the biocides adsorption by competing and providing the hydrogen bonding/ π - π interaction sites at the same time, thus resulting in different or even adverse biocide adsorption responses.

6.4 Conclusions

The adsorption of DOM onto GAC is related to both their MW and the DOM concentration applied in the adsorption experiment. At low DOM concentrations, the smaller fraction of DOM adsorbs more because it is able to access to the small pores inside the GAC. At high DOM concentrations, the larger fraction adsorbs more because the larger DOM molecule carries more carbon atoms. The adsorption behaviour of heavy metals as pollutants onto GAC differs: Cu^{2+} showed a higher affinity for GAC than Zn^{2+} . In this study, the Langmuir and Freundlich equations were good models for describing the adsorption of DOM and heavy metals onto GAC. The Langmuir equation successfully provided the estimated maximum adsorption of pollutants onto GAC. The Freundlich equation effectively described the heterogeneity of the GAC surface to the adsorbates. Regarding the adsorption of biocides and the corresponding TPs as

pollutants onto GAC, they had a strong correlation in their adsorption capacity. At the same time, we conclude that the LogD values of biocides/TPs themselves were not enough to explain the adsorption differences. Another key factor in describing the biocides/TPs adsorption is their three-dimensional molecular structure. Biocides/TPs having a more planar 3D structure, which will tend to facilitate the π - π interactions between GAC and the biocides/TPs.

The influence of the simultaneous occurrence of different substances on the adsorption of target pollutants onto GAC was able to be demonstrated. (1) The presence of DOM enhanced the adsorption of heavy metals onto GAC at low DOM concentrations. (2) The DOM influence on the adsorption of biocides differs depending on the compounds used because both hydrophobic interaction and hydrogen bonding are involved in the adsorption process and these two mechanisms respond differently to the presence of DOM. As a result, no clear trend was observed. (3) The influence of the presence of heavy metals on the adsorption of biocides also depends on the chemical structure of the biocides, which is due to the same reason as described in (2). Based on these findings, it can be stated that, in adsorption experiments used to develop decentralized stormwater treatment facilities, it is important that experiments be performed using individual substances while also taking matrix influences into consideration.

Overall, the GAC is an ideal adsorbent material for the retention of pollutants in building runoff with great potential. When analysing the adsorption of biocides, it is important to consider the influence of biocides molecular 3D structure. The effect of the presence of DOM and heavy metals on the adsorption of biocides should be carefully distinguished according to the biocides used. This study is a fundamental part of building runoff treatment system design. The follow-up work will focus on studying the adsorption of biocides at real runoff concentration, optimizing the conditions for GAC utilization, studying the effect of temperature on adsorption, and analysing the regeneration and desorption of the GAC.

6.5 Acknowledgments

Thanks for the support from Chemviron Carbon Ltd. for providing granular activated carbon Cyclecarb 301. This research was funded by a scholarship for Panfeng Zhu from China Scholarship Council.

7. Overall conclusion and outlook

7.1 Overall conclusion

The main conclusions were summarized as follows: the DOM used in this study had two different fluorescent components (namely C1 and C2), and component C1 had higher affinity in binding with heavy metals and biocides than C2. Increasing pH had a positive effect on heavy metals binding to DOM and a negative effect on biocides binding to DOM. The Ryan-Weber equation was eligible for describing $\text{Cu}^{2+}/\text{Zn}^{2+}$ -DOM interaction and the Stern-Volmer equation was eligible for MCPP/BAC-DOM interaction. Multiple mechanisms were involved in MCPP/BAC-DOM interaction, including hydrogen bonding, π - π interaction, and electrostatic effect. Among these mechanisms, hydrogen bonding plays an important role. The order of mechanisms coming into effect was dependent on pollutants; for the BAC-DOM group, the order was intermolecular hydrogen bonding > electrostatic attraction > π - π interaction > hydrogen bonding with residual free hydroxyl; for the MCPP-DOM group, it was intermolecular hydrogen bonding > π - π interaction > hydrogen bonding with residual free hydroxyl > cation bridge effect (electrostatic attraction).

In the second part of our research, to precisely determine the interaction extent between building runoff pollutants and DOM and to evaluate the influence of DOM MW as well as the presence of Cu^{2+} on biocides-DOM interaction processes, the dialysis equilibrium method was adopted and DOM was fractionated by centrifugal filtration. The DOM fractions obtained had similar UV absorbance curves, their SUVA_{254} values were in a narrow range. The binding of Cu^{2+} with DOM fraction had a positive relation with DOM fraction MW rather than the total acidity, it was assumed that valid binding sites for Cu^{2+} are more abundant in large molecules. Cu^{2+} and Zn^{2+} had different DOM binding affinities; Cu^{2+} bounds more to DOM than Zn^{2+} . For the binding of biocides to DOM, attractive electrostatic interaction was a more efficient pathway than non-covalent binding, corresponding binding capability can be more than an order of magnitude higher. In the binding of neutral or negatively charged biocides with DOM, hydrogen bonding is a mechanism that should be considered, favored by DOM fractions having higher total acidity. Additionally, parent biocides had stronger interaction with DOM than their TPs, because TPs had lower hydrophobicity and higher solubility. The

influence of Cu^{2+} on biocides-DOM interaction differed among DOM fractions. It is necessary to carefully consider the physicochemical properties of DOM fractions to have a more comprehensive understanding of the influence of Cu^{2+} .

In the third part of the research, to evaluate the adsorption of building runoff pollutants to GAC, batch tests were carried out, and adsorption processes were fitted by Langmuir and Freundlich equations. The adsorption of DOM onto GAC was impacted by both MW and DOM concentrations. In the study, smaller DOM fractions adsorbed more at concentrations <400 mgC/L due to the accessibility to small pores of GAC; at high DOM concentrations (>600 mgC/L), larger DOM fraction was adsorbed more because larger DOM molecule carries more carbon atoms. Cu^{2+} and Zn^{2+} had different affinities to GAC; GAC adsorbed more Cu^{2+} than Zn^{2+} . Both Langmuir and Freundlich equations were fitted models for describing the adsorption of DOM and heavy metals onto GAC. Langmuir equation provided an estimated maximum GAC adsorption of pollutants, and the Freundlich equation described the heterogeneity of the GAC surface to pollutants. Biocides and their corresponding TPs had a strong positive correlation in their adsorption behavior while they still had different adsorption performances. LogD values of biocides/TPs cannot fully explain their adsorption differences, so more factors, such as three-dimensional molecular structure, should be further considered. The presence of DOM at low concentration (5 mgC/L) had a positive impact on heavy metals adsorption onto GAC. However, the influence of DOM and heavy metals on biocides adsorption varied across compounds since both hydrophobic interaction and hydrogen bonding were involved in the biocides adsorption process, and these two mechanisms responded differently to DOM and heavy metals presence.

Table 7.1: Summary of hypotheses testing.

Chapter	Research hypotheses	Publications
4	#1.1: Mecoprop-p and benzyl-dimethyl-tetradecylammonium chloride can interact with DOM, indicated by decreased DOM fluorescence intensity of more than 30% at the end of titration process.	Accepted

	#1.2: Electrostatic interaction and hydrophobic interaction are the two mechanisms involved in interactions between mecoprop-p, benzyl-dimethyl-tetradecylammonium chloride and DOM.	Accepted
5	#2.1: Heavy metals and biocides/TPs prefer to bind with DOM fraction having larger molecular weight.	Rejected
	#2.2: The presence of 2mg/L Cu ²⁺ reduces 50% of binding between biocides and DOM.	Rejected
6	#3.1: Transformation products show a better adsorption onto GAC than corresponding parent biocides.	Accepted
	#3.2: The presence of 5 mgC/L DOM fractions or 2 mg/L heavy metals will inhibit the adsorption of biocides onto GAC.	Accepted

At last, according to the results obtained and to achieve building runoff contamination source control the use of adsorption-based treatment facilities is recommended. Meanwhile, utilizing adsorbent material with abundant oxygen-containing functional group is suggested. Furthermore, to improve treatment efficiency, for example, eliminating the influence from DOM on adsorption treatment (clogging adsorbent material and transferring pollutants through facilities untreated), sequential removal of pollutants by different adsorbent materials can be evaluated.

7.2 Outlook

7.2.1 Interaction of benzyl-dimethyl-tetradecylammonium chloride dihydrate (BAC) with DOM and GAC

At Chapter 4, the interaction of MCPP and BAC with DOM (represented by commercial humic substance) was revealed by excitation emission matrix analysis. BAC was found having a much stronger interaction (semi-quantification) with DOM than MCPP. To further quantify the extent of interaction, we determined the amount of biocides/TPs binding with DOM as well as their adsorption onto GAC (Chapter 5, 6), however, due to the large deviation of quantification method, the results were not solid to demonstrate the interaction extent of BAC. Therefore, further investigation on BAC interacting with DOM and adsorbing onto GAC using improved measurement methods is needed.

Additionally, hydrogen bonding and hydrophobic interaction were found to play important roles in interaction of neutral or negatively charged biocides/TPs with DOM and GAC, whereas for positively charged biocide BAC, attractive electrostatic interaction is the dominant mechanism. Understanding the influence of charged state on biocides/TPs interaction pattern with DOM and GAC is necessary to predict their environmental behaviors and can benefit the elimination of contamination. Previous studies have also reported the attractive electrostatic interaction for organic pollutant showing positive charge state due to protonation of amine group (Guillossou et al., 2020; B. Yang et al., 2021). Differently, in our study, BAC is an ammonium salt, and its charge state is not affected by H^+ concentration. As a result, BAC interaction extent with DOM and GAC cannot be simply deduced according to the results of previously reported positively charged compounds, which should be carefully addressed to fill the knowledge gap.

7.2.2 Interaction of pollutants with natural DOM in building runoff

In our study, commercial humic substance salt was used as the representative of natural DOM to keep the consistency of variable during experimental period so that results are comparable. However, the composition of commercial product is not the same as natural DOM. Study from Ma et al., 2021 and Yuan et al., 2019 showed that besides

humic-like components, natural DOM also contains protein-like component. These two components are different in molecular weight distribution and interaction with pollutants. For example, the protein-like component enriches both in the highest and lowest molecular weight fractions, and the humic-like component enriches in the middle molecular weight range (Romera-Castillo et al., 2014). Moreover, organic pollutants such as antibiotic tetracycline were found more preferable to complex with protein-like components than the humic-like components (Bai et al., 2017). Although our study using humic substance revealed pollutants-DOM interaction characteristics to a certain extent, the role of the protein-like components in interaction should still be investigated to achieve more comprehensive and representative outcomes.

Additionally, a study by Lin et al., 2022 reported that a large portion (43–77%) of natural DOM in stormwater has a molecular weight (MW) <1 kDa, whereas in our study (Chapter 5), only DOM fractions with MW >3 kDa were used to assess the interaction with heavy metals and biocides/TPs. The smaller fraction was not investigated because of its permeation through the dialysis bag. Although high MW (>1 kDa) DOM generally has higher metal and organic pollutants binding potential (Xu et al., 2019; H. Lin et al., 2017), the compounds could present greater affinity to low MW (<1 kDa) DOM dependent on the chemical structures (Garrido Reyes et al., 2021).

Hence, to better understand the interaction of building runoff pollutants (i.e., heavy metals and biocides/TPs) with DOM under realistic conditions, the influences of DOM composition and MW should be evaluated.

7.2.3 Biocides/TPs adsorption column test and desorption analysis

In Chapter 6, batch tests were carried out to investigate the adsorption performance of GAC for biocides/TPs and to evaluate the influence of DOM and heavy metals on the biocides adsorption process. As a result, the maximum adsorption of each biocide/TP onto GAC was obtained, and opposite influences from DOM (as well as heavy metals) on biocide adsorption were observed. However, the concentrations of biocides/TPs in our batch study were up to thousands of folds over the natural concentrations. Thus, to reveal the adsorption performance of GAC and the impacts of DOM under realistic conditions, column tests applying close-to-natural concentrations of pollutants and natural DOM collected from building runoff are suggested for further research. Moreover, adsorption of biocides/TPs in batch tests was conducted on individual

compounds, while in further column tests, mixed compounds could be spiked to obtain a more general performance of GAC, and the influence of biocides co-occurrence (e.g., competitive adsorption) could also be indicated.

When evaluating the retention of pollutants by adsorbent material, desorption is an important process that should be considered. Desorption usually happens when compounds are adsorbed with weak binding forces, compound concentration decreases in influent, or a compound with a higher binding force competes for binding sites (Golovko et al., 2020). Desorption can greatly affect the removal performance of biocides/TPs and heavy metals by GAC, resulting in undesired increasing effluent concentrations. DOM not only can impact the adsorption of pollutants, but can also influence the desorption phase (Corwin and Summers, 2011). Some studies have shown the effects of AC pore structure and DOM size fractions on the desorption of micropollutants (Aschermann et al., 2018; Aschermann et al., 2019), whereas studies of DOM interaction with biocides/TPs and heavy metals during desorption of GAC are rather scarce but necessary.

For further research, the elucidation of adsorption/desorption of biocides/TPs and heavy metals by GAC will improve the understanding and development of filtration as a treatment process for building runoff pollution.

7.2.4 Sequential adsorption of heavy metals and biocides

Gaining the knowledge of the independent adsorption performance of a single pollutant and the competitive adsorption of multiple heavy metals and biocides/TPs, as well as the influence of DOM, will facilitate the design of the adsorption process for treating building runoff containing diverse inorganic and organic contaminants. As indicated in our study (Chapter 6), the presence of 2 mg/L Zn^{2+} decreased the adsorption of MCPP onto GAC by around 94 $\mu\text{mol/g}$. Although, in the study, the concentration of heavy metals was similar to the environmental level, biocide concentration exceeded far from the realistic condition. Hence, validating the competitive effect of heavy metals on biocides adsorption under natural conditions is needed in further studies.

If the simultaneous adsorption is not as effective as the independent adsorption, sequential adsorption could be an alternative. As suggested by previous studies, the extent of pollutant adsorption and removal is dependent on adsorbent materials (Reddy et al., 2014; Ahmad et al., 2010). For example, in comparison with GAC, coal

combustion ash activated by steam gasification showed better adsorption capacity of cadmium and zinc in contaminated water (Erto et al., 2013). In this case, sequential adsorption of heavy metals and biocides by applying more effective heavy metal adsorbents prior to GAC might improve the overall removal performance. Moreover, to lower the costs of GAC and prolong its service lifetime, sequential adsorption combining economical adsorbents could be a promising technology, which needs further research to evaluate its capacity.

8. Supplementary information

Appendix A List of publications

Research articles

1. Zhu, P., Knoop, O., & Helmreich, B. (2022). Interaction of heavy metals and biocide/herbicide from stormwater runoff of buildings with dissolved organic matter. *Science of The Total Environment*, 814, 152599. **(Peer-reviewed)** <https://doi.org/10.1016/j.scitotenv.2021.152599>
2. Zhu, P., Sottorff, I., Bi, J., & Helmreich, B. (2025). Determining the binding of heavy metals, biocides, and their transformation products with dissolved organic matter—Understanding pollutants interactions in building façade runoff. *Ecotoxicology and Environmental Safety*, 291, 117887. **(Peer-reviewed)** <https://doi.org/10.1016/j.ecoenv.2025.117887>
3. Zhu, P., Sottorff, I., Zhang, T., & Helmreich, B. (2023). Adsorption of Heavy Metals and Biocides from Building Runoff onto Granular Activated Carbon—The Influence of Different Fractions of Dissolved Organic Matter. *Water*, 15(11), 2099. **(Peer-reviewed)** <https://doi.org/10.3390/w15112099>

Appendix B Supplementary information for Chapter 4

1. Measurement the content of dissolved organic carbon (DOC) by UV254

Based on the strong correlation between DOC concentration and UV absorbance at 254 nm (Edzwald et al., 1985), measuring the DOC concentration of each DOM sample can be replaced by detecting its UV absorbance at 254 nm. The linear relationship between DOC concentration and UV absorbance at 254 nm is shown in **Figure 8.1**.

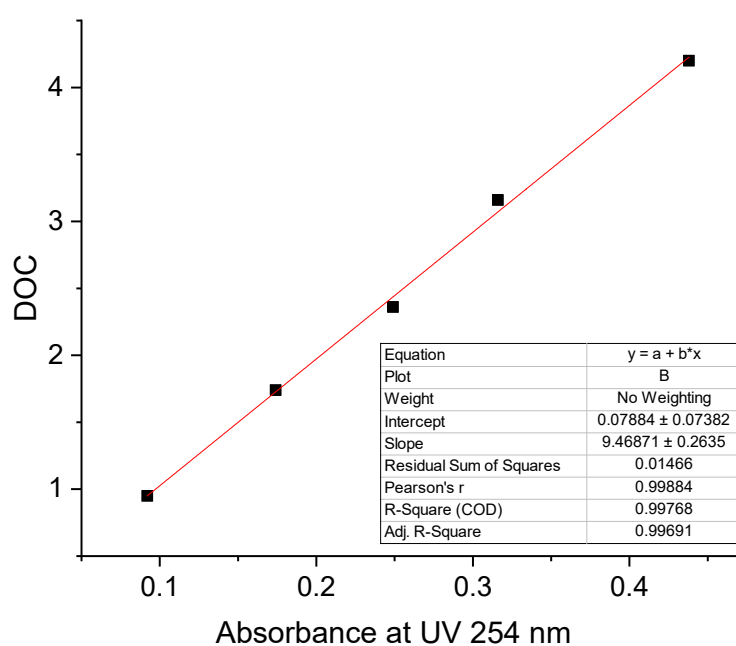


Figure 8.1. Linear correlation between UV absorbance at 254nm and DOC concentration.

2. EEM spectrum of the applied commercial humic substance

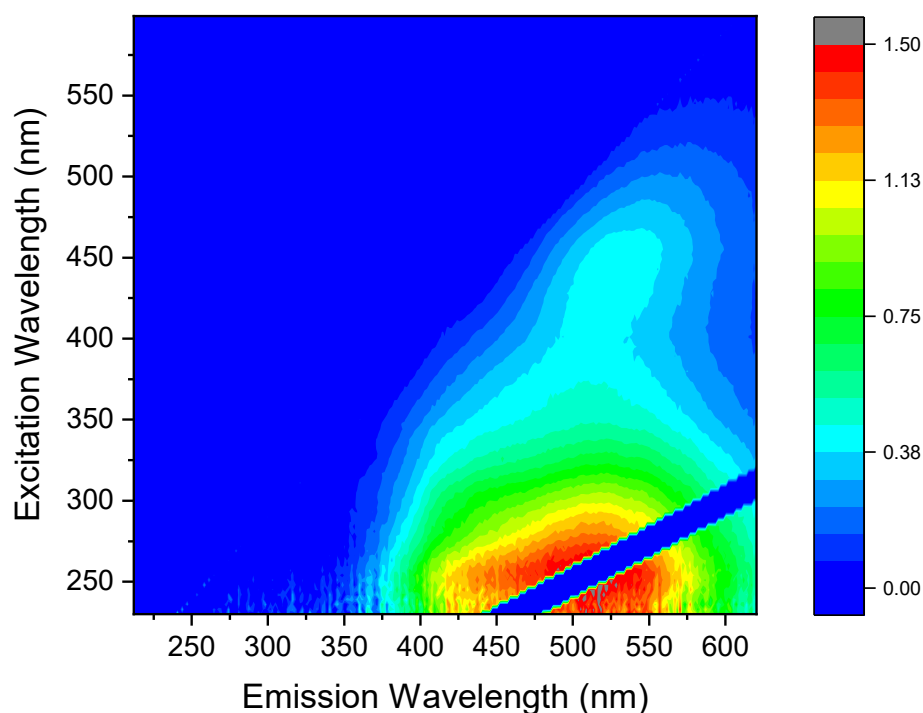


Figure 8.2. Fluorescence spectrum of the applied commercial humic substance (DOM) at pH7, 2mgC/L.

3. Changes of fluorescence from dissolved organic matter (DOM) after dialysis equilibrium

To verify whether cation bridge effect exists in interaction between mecoprop-p and DOM, a high retention dialysis bag with the molecular weight cutoff (MWCO) of 12400 (Sigma-aldrich, Germany) was used to remove the cations in the humic substance (HS) stock solution. In dialysis treatment, about 50 mL of HS stock solution was placed in 1 L Milli-Q water (pH 4) for 24 hours. To remove as much cations as possible, dialysis treatment was repeated three times. Due to the high MWCO of the dialysis bag, a small part of DOM went through the dialysis membrane as well. The transport process was detected by analyzing the fluorescence of dialysis samples. The change of DOM fluorescence before and after dialysis is shown in **Figure 8.3**.

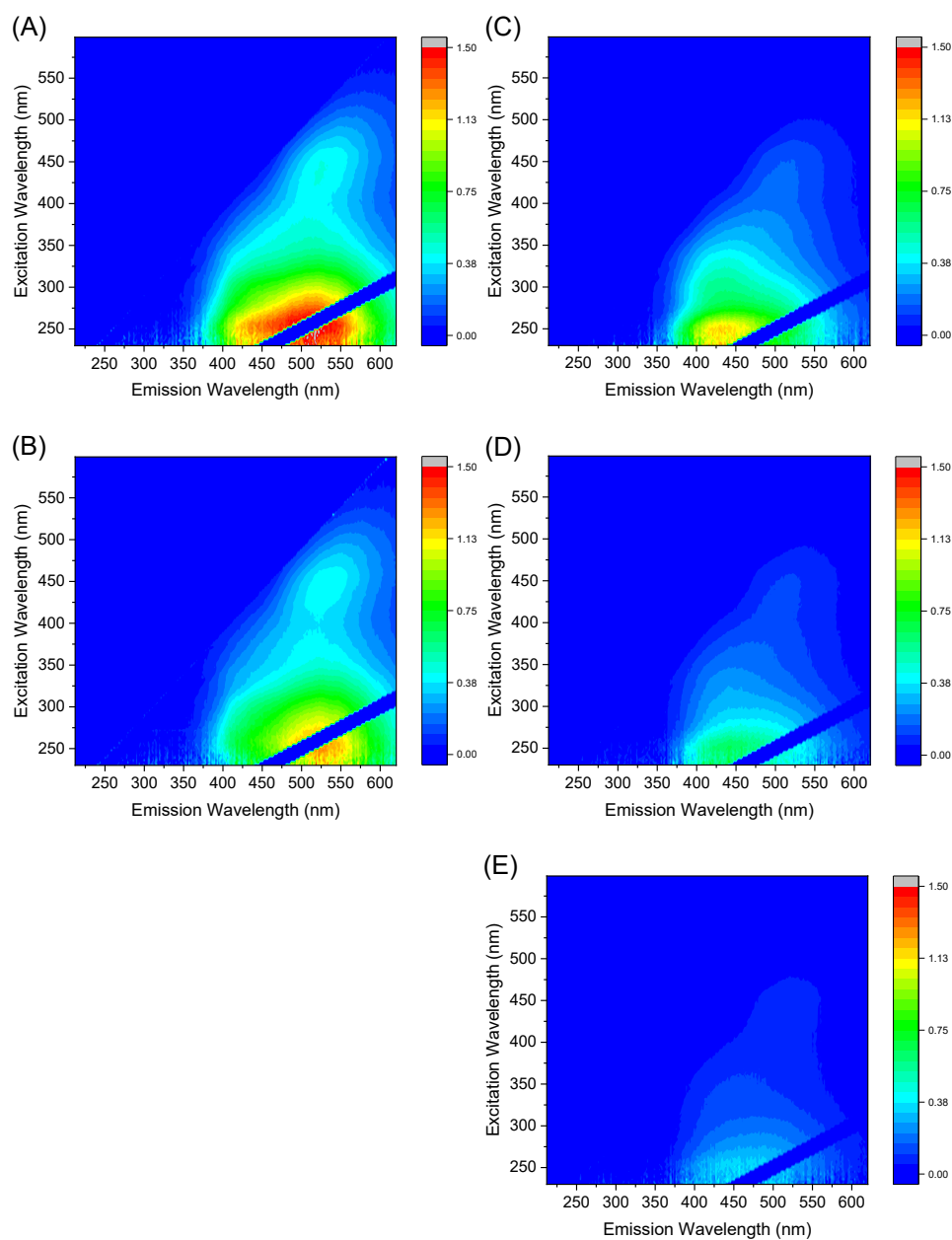


Figure 8.3. Fluorescence of DOM (2mgC/L) before (A) and after (B) dialysis treatment. C, D, and E were fluorescence of Milli-Q water after dialysis treatment for the first, second, and third time.

The change of DOM fluorescence was analyzed by PARAFAC model (paper, Section 3.1). The result demonstrated that after dialysis treatment the content of fluorescent component C1 was increased in the DOM sample. Data from Milli-Q water samples indicated a higher content of fluorescent component C2 than C1 when compared to the

DOM sample (**Figure 8.4**). A conclusion was made that component C2 has a smaller molecular weight than component C1.

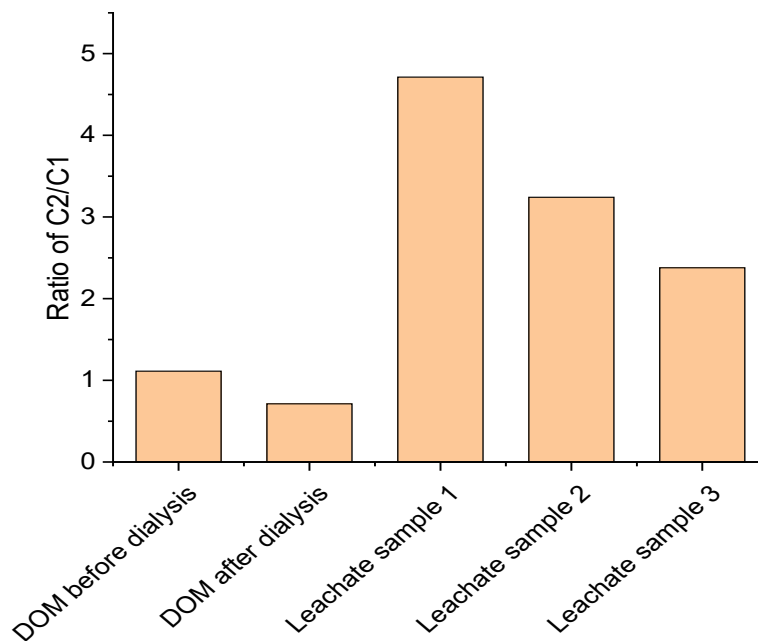


Figure 8.4. Ratio of DOM fluorescent components C1 and C2 in dialysis samples. The first two columns are data from DOM before and after dialysis treatment; the following three columns represent samples collected outside the dialysis bag in three sequential dialysis treatments.

4. The change of remaining fluorescence of C1 and C2 after dialysis treatment

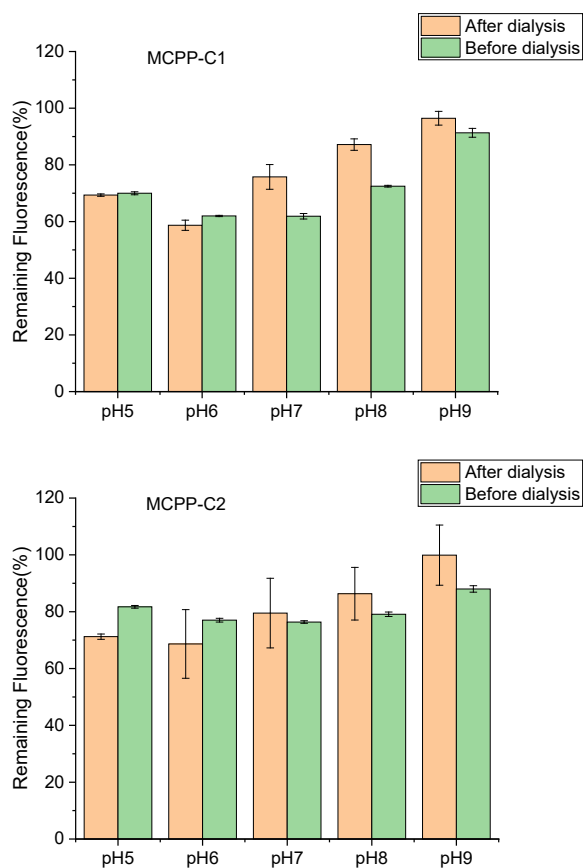
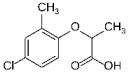
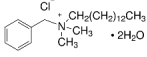


Figure 8.5. Remaining fluorescence of HS component C1 and C2 (before and after the removal of cations by dialysis) with the addition of 46.6 $\mu\text{mol/L}$ MCPP at various pH conditions. Left side: MCPP-C1 interaction; right side: MCPP-C2 interaction.

5. Physicochemical properties of mecoprop-P (MCPP) and Benzyl-dimethyl-tetradecylammonium chloride dihydrate (BAC)

8. Supplementary information

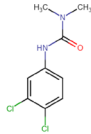
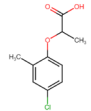
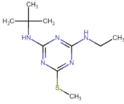
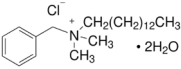
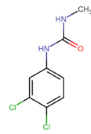
Table 8.1. Molecular structures and chemical properties of MCPP and BAC

Name	Molecular formula ^a	Molecular structure ^a	Molecular weight ^a (g/mol)	logK _{ow} ^a	Solubility in water ^a (mg/L)	pKa ^a
Mecoprop-p	C ₁₀ H ₁₁ ClO ₃		214.64	3.13 / -0.19	880	3.1- 3.78
Benzyl-dimethyl-tetradecylammonium chloride dihydrate	CH ₃ (CH ₂) ₁₃ N ⁺ (Cl) ⁻ (CH ₃) ₂ CH ₂ C ₆ H ₅ · 2H ₂ O		404.07	3.91	>1000 mg/L	/

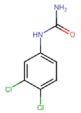
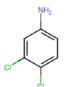
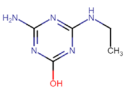
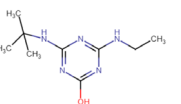
a: <https://pubchem.ncbi.nlm.nih.gov/>

Appendix C Supplementary information for Chapter 5

Table 8.2. The biocides/TPs used in dialysis study and their physicochemical properties.

Chemicals	Molecular Structure ^b	Molecular Formula ^a	Molecular Weight ^a	Water Solubility (mg/L) ^a	LogD (pH = 7) ^b
Diuron		C ₉ H ₁₀ Cl ₂ N ₂ O	233.09	37.4–42 (-3.11) ^c	2.53
Mecoprop-p		C ₁₀ H ₁₁ ClO ₃	214.64	880 (0.0) ^c	-0.25
Terbutryn		C ₁₀ H ₁₉ N ₅ S	241.36	35.9 (-3.65) ^c	2.7
benzyl-dimethyl- tetradecylammonium chloride dihydrate		C ₂₃ H ₄₆ ClNO ₂	404.07	/	/
1-(3,4-Dichlorophenyl)-3- methylurea (DCPMU)		C ₈ H ₈ Cl ₂ N ₂ O	219.06	(-3.08) ^c	2.31

8. Supplementary information

1-(3,4-Dichlorophenyl)urea (DCPU)		$C_7H_6Cl_2N_2O$	205.04	$(-3.08)^c$	2.09
3,4-Dichloroaniline (DCA)		$C_6H_5Cl_2N$	162.01	$(-2.75)^c$	2.35
Atrazine-desisopropyl-2-hydroxy (DHT)		$C_5H_9N_5O$	155.16	$(-1.8)^c$	0.59
Terbutylazine-2-hydroxy (HAT)		$C_9H_{17}N_5O$	211.26	$(-2.67)^c$	1.94

Notes: a: data from Pubchem; b: calculated data from ChemAxon; c: calculated solubility LogS from ChemAxon.

A part of content has been published in our previous research (<https://doi.org/10.3390/w15112099>)

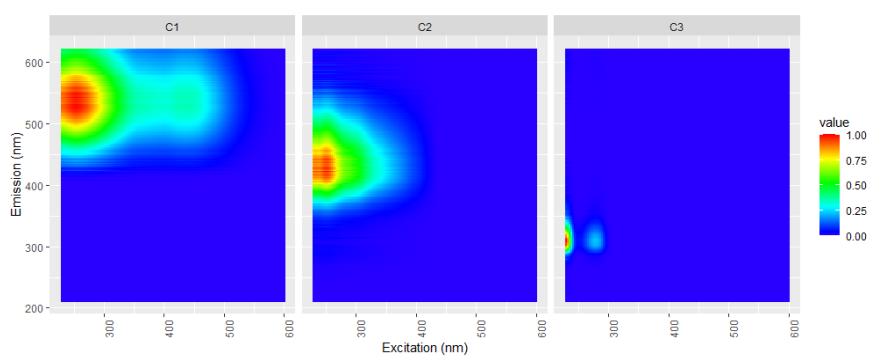
8. Supplementary information

Table 8.3. UV absorbance of DOM fractions at 280 nm before and after dialysis equilibrium.

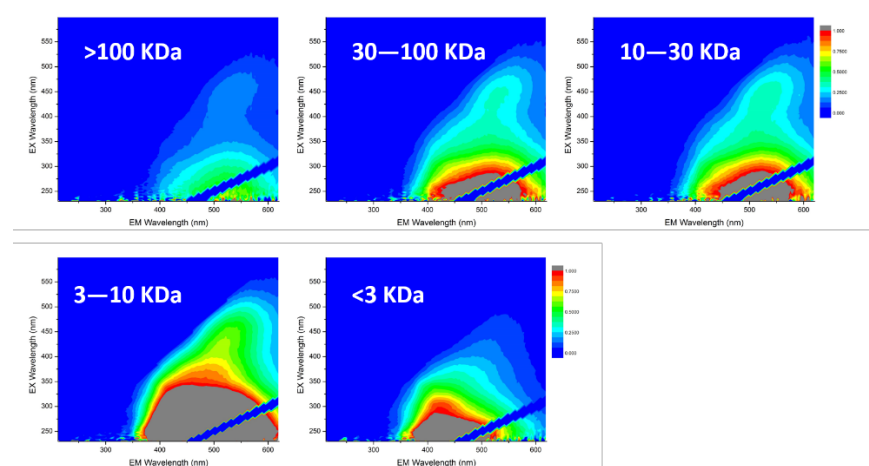
DOM fractions	>100 kDa			30–100 kDa			10–30 kDa			3–10 kDa		
before dialysis	0.206	0.198	0.197	0.180	0.178	0.177	0.158	0.159	0.159	0.103	0.102	0.103
after dialysis	0.197	0.189	0.188	0.174	0.171	0.171	0.153	0.154	0.155	0.088	0.086	0.088
%	95.63	95.45	95.43	96.67	96.07	96.61	96.84	96.86	97.48	85.44	84.31	85.44
Ave (%)	95.51			96.45			97.06			85.06		
Std (%)	0.11			0.33			0.37			0.65		

Dialysis equilibrium of DOM fractions >10 kDa was completed in dialysis bag with molecular weight cutoff (MWCO) of 12400 Dalton, for DOM fraction 3–10 kDa its equilibrium was carried out in bag with MWCO 2000 Dalton.

(A)



(B)



(C)

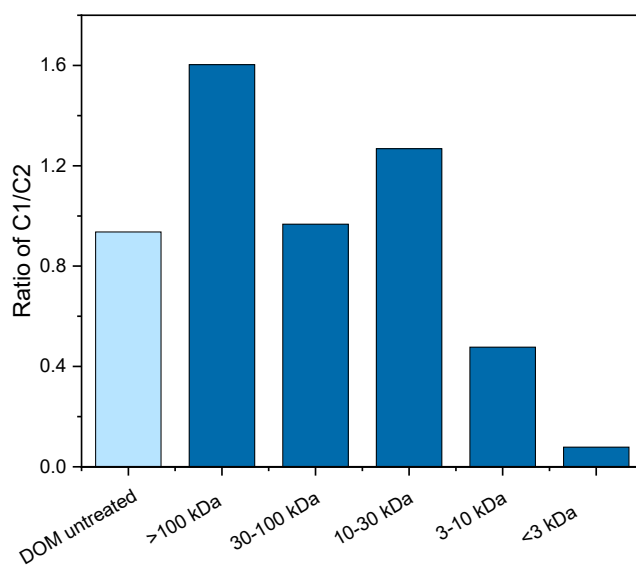


Figure 8.6. Characterization of fractionated DOM. (A) Fluorescent components identified by PARAFAC model, C1 and C2 are from DOM used and C3 is from

mecoprop. (B) excitation emission matrix of DOM fractions. (C) fluorescent component ratio (C1/C2) of fractionated DOM.

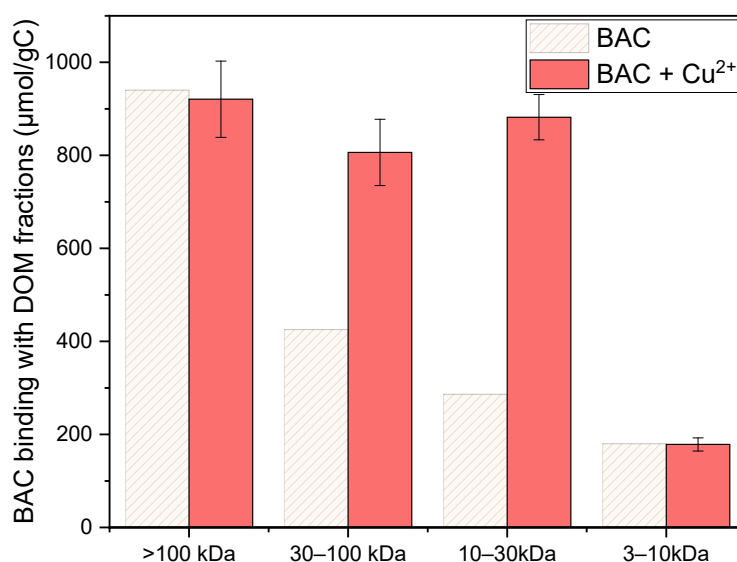


Figure 8.7. Determined binding of benzyl-dimethyl-tetradecylammonium chloride dihydrate (BAC) with different DOM fractions, with and without the presence of Cu²⁺.

Note: Due to the limitation in measuring, the binding of BAC to DOM without Cu²⁺ was not precisely determined, involved bias was indicated by too low BAC binding to DOM fractions 30–100 kDa and 10–30 kDa. Comparatively, result of BAC binding to DOM in presence of Cu²⁺ is more meaningful. In **Figure 8.7**, a conclusion can be obtained that attractive electrostatic interaction was a much stronger binding pathway than non-covalent binding, representing by observed hundreds of μmol/gC binding capability for BAC to DOM, generally, corresponding binding capabilities for biocides/TPs to DOM are no larger than 60 μmol/gC. Because of the measuring deviation of BAC interacting with DOM, the influence of Cu²⁺ on BAC interaction with DOM was not distinguished.

References

- Abreu, F.E.L., Martins, S.E., Fillmann, G., 2021. Ecological risk assessment of booster biocides in sediments of the Brazilian coastal areas. *Chemosphere* 276, 130155. <https://doi.org/10.1016/j.chemosphere.2021.130155>
- Adusei-Gyamfi, J., Ouddane, B., Rietveld, L., Cornard, J.-P., Criquet, J., 2019. Natural organic matter-cations complexation and its impact on water treatment: A critical review. *Water Research* 160, 130–147. <https://doi.org/10.1016/j.watres.2019.05.064>
- AHMAD, T., RAFATULLAH, M., GHAZALI, A., SULAIMAN, O., HASHIM, R., AHMAD, A., 2010. Removal of Pesticides from Water and Wastewater by Different Adsorbents: A Review. *Journal of Environmental Science and Health, Part C* 28, 231–271. <https://doi.org/10.1080/10590501.2010.525782>
- Aju, C.D., Achu, A.L., Raicy, M.C., Reghunath, R., 2021. Identification of suitable sites and structures for artificial groundwater recharge for sustainable water resources management in Vamanapuram River Basin, South India. *HydroResearch* 4, 24–37. <https://doi.org/10.1016/j.hydres.2021.04.001>
- Akbari, H., Rose, L.S., 2008. Urban Surfaces and Heat Island Mitigation Potentials. *JHES* 11, 85–101. <https://doi.org/10.1618/jhes.11.85>
- Akbari, H., Shea, L., 2002. Characterizing the Fabric of the Urban Environment: A Case Study of Metropolitan Chicago, Illinois 1.
- Al Bahri, M., Calvo, L., Gilarranz, M.A., Rodriguez, J.J., 2016. Diuron Multilayer Adsorption on Activated Carbon from CO₂ Activation of Grape Seeds. *Chemical Engineering Communications* 203, 103–113. <https://doi.org/10.1080/00986445.2014.934447>
- Albers, C.N., Johnsen, A.R., Bollmann, U.E., 2023. Urban areas as sources of the groundwater contaminants *N,N*-dimethylsulfamide (*N,N*-DMS) and 1,2,4-triazole. *Science of The Total Environment* 881, 163377. <https://doi.org/10.1016/j.scitotenv.2023.163377>
- Alvarez, P., Velescu, A., Pierick, K., Homeier, J., Wilcke, W., 2023. Carbon Stable Isotope Ratio of Dissolved Organic Matter as a Tool To Identify Its Sources and Transformations in a Tropical Montane Forest in Ecuador. *Environ. Sci. Technol.* 57, 14983–14993. <https://doi.org/10.1021/acs.est.3c01623>
- Apul, O.G., Wang, Q., Zhou, Y., Karanfil, T., 2013. Adsorption of aromatic organic contaminants by graphene nanosheets: Comparison with carbon nanotubes and activated carbon. *Water Research* 47, 1648–1654. <https://doi.org/10.1016/j.watres.2012.12.031>
- Aschermann, G., Neubert, L., Zietzschmann, F., Jekel, M., 2019. Impact of different DOM size fractions on the desorption of organic micropollutants from activated carbon. *Water Research* 161, 161–170. <https://doi.org/10.1016/j.watres.2019.05.039>
- Aschermann, G., Zietzschmann, F., Jekel, M., 2018. Influence of dissolved organic matter and activated carbon pore characteristics on organic micropollutant desorption. *Water Research* 133, 123–131. <https://doi.org/10.1016/j.watres.2018.01.015>
- Ataguba, C.O., Brink, I., 2020. Metals removal from automobile workshop stormwater runoff using rice husk, GAC and gravel filtration. *Water Science and Technology* 83, 184–197. <https://doi.org/10.2166/wst.2020.565>

- Athanasiadis, K., Helmreich, B., Horn, H., 2007. On-site infiltration of a copper roof runoff: Role of clinoptilolite as an artificial barrier material. *Water Research* 41, 3251–3258. <https://doi.org/10.1016/j.watres.2007.05.019>
- Athanasiadis, K., Helmreich, B., Wilderer, P.A., 2006. Infiltration of a copper roof runoff through artificial barriers. *Water Science and Technology* 54, 281–289. <https://doi.org/10.2166/wst.2006.599>
- Athanasiadis, K., Helmreich, B., Wilderer, P.A., 2004. Elimination of Zinc from Roof Runoff through Geotextile and Clinoptilolite Filters. *Acta hydrochimica et hydrobiologica* 32, 419–428. <https://doi.org/10.1002/aheh.200200547>
- Athanasiadis, K., Horn, H., Helmreich, B., 2010. A field study on the first flush effect of copper roof runoff. *Corrosion Science* 52, 21–29. <https://doi.org/10.1016/j.corsci.2009.08.048>
- Bai, L., Zhao, Z., Wang, Chunliu, Wang, Changhui, Liu, X., Jiang, H., 2017. Multi-spectroscopic investigation on the complexation of tetracycline with dissolved organic matter derived from algae and macrophyte. *Chemosphere* 187, 421–429. <https://doi.org/10.1016/j.chemosphere.2017.08.112>
- Bañas, K., Robles, M.E., Maniquiz-Redillas, M., 2023. Stormwater Harvesting from Roof Catchments: A Review of Design, Efficiency, and Sustainability. *Water* 15, 1774. <https://doi.org/10.3390/w15091774>
- Bauer, S., Linke, H.J., Wagner, M., 2020. Combining industrial and urban water-reuse concepts for increasing the water resources in water-scarce regions. *Water Environment Research* 92, 1027–1041. <https://doi.org/10.1002/wer.1298>
- Baup, S., Wolbert, D., Laplanche, A., 2002. Importance of Surface Diffusivities in Pesticide Adsorption Kinetics onto Granular Versus Powdered Activated Carbon: Experimental Determination and Modeling. *Environmental Technology* 23, 1107–1117. <https://doi.org/10.1080/09593332308618339>
- Becouze-Lareure, C., Dembélé, A., Coquery, M., Cren-Olivé, C., Bertrand-Krajewski, J.-L., 2019. Assessment of 34 dissolved and particulate organic and metallic micropollutants discharged at the outlet of two contrasted urban catchments. *Science of The Total Environment* 651, 1810–1818. <https://doi.org/10.1016/j.scitotenv.2018.10.042>
- Belkouteb, N., Franke, V., McCleaf, P., Köhler, S., Ahrens, L., 2020. Removal of per- and polyfluoroalkyl substances (PFASs) in a full-scale drinking water treatment plant: Long-term performance of granular activated carbon (GAC) and influence of flow-rate. *Water Research* 182, 115913. <https://doi.org/10.1016/j.watres.2020.115913>
- Berardi, U., GhaffarianHoseini, AmirHosein, GhaffarianHoseini, Ali, 2014. State-of-the-art analysis of the environmental benefits of green roofs. *Applied Energy* 115, 411–428. <https://doi.org/10.1016/j.apenergy.2013.10.047>
- Bhadra, B.N., Seo, P.W., Jung, S.H., 2016. Adsorption of diclofenac sodium from water using oxidized activated carbon. *Chemical Engineering Journal* 301, 27–34. <https://doi.org/10.1016/j.cej.2016.04.143>
- Bolan, N.S., Adriano, D.C., Kunhikrishnan, A., James, T., McDowell, R., Senesi, N., 2011. Chapter One - Dissolved Organic Matter: Biogeochemistry, Dynamics, and Environmental Significance in Soils, in: Sparks, D.L. (Ed.), *Advances in Agronomy*. Academic Press, pp. 1–75. <https://doi.org/10.1016/B978-0-12-385531-2.00001-3>
- Bollmann, U.E., Fernández-Calviño, D., Brandt, K.K., Storgaard, M.S., Sanderson, H., Bester, K., 2017a. Biocide Runoff from Building Facades: Degradation Kinetics

- in *Soil. Environ. Sci. Technol.* 51, 3694–3702. <https://doi.org/10.1021/acs.est.6b05512>
- Bollmann, U.E., Minelgaite, G., Schlüsener, M., Ternes, T., Vollertsen, J., Bester, K., 2016. Leaching of Terbutryn and Its Photodegradation Products from Artificial Walls under Natural Weather Conditions. *Environ. Sci. Technol.* 50, 4289–4295. <https://doi.org/10.1021/acs.est.5b05825>
- Bollmann, U.E., Minelgaite, G., Schlüsener, M., Ternes, T.A., Vollertsen, J., Bester, K., 2017b. Photodegradation of octylisothiazolinone and semi-field emissions from facade coatings. *Sci Rep* 7, 41501. <https://doi.org/10.1038/srep41501>
- Bork, M., Lange, J., Graf-Rosenfellner, M., Hensen, B., Olsson, O., Hartung, T., Fernández-Pascual, E., Lang, F., 2021. Urban storm water infiltration systems are not reliable sinks for biocides: evidence from column experiments. *Sci Rep* 11, 7242. <https://doi.org/10.1038/s41598-021-86387-9>
- Boysen, B., Cristóbal, J., Hilbig, J., Güldemund, A., Schebek, L., Rudolph, K.-U., 2020. Economic and environmental assessment of water reuse in industrial parks: case study based on a Model Industrial Park. *Journal of Water Reuse and Desalination* 10, 475–489. <https://doi.org/10.2166/wrd.2020.034>
- Bucheli, T.D., Müller, S.R., Voegelin, A., Schwarzenbach, R.P., 1998. Bituminous Roof Sealing Membranes as Major Sources of the Herbicide (R,S)-Mecoprop in Roof Runoff Waters: Potential Contamination of Groundwater and Surface Waters. *Environ. Sci. Technol.* 32, 3465–3471. <https://doi.org/10.1021/es980318f>
- Burkhardt, M., Kupper, T., Hean, S., Haag, R., Schmid, P., Kohler, M., Boller, M., 2007. Biocides used in building materials and their leaching behavior to sewer systems. *Water Science and Technology* 56, 63–67. <https://doi.org/10.2166/wst.2007.807>
- Burkhardt, M., Zuleeg, S., Vonbank, R., Bester, K., Carmeliet, J., Boller, M., Wangler, T., 2012. Leaching of Biocides from Façades under Natural Weather Conditions. *Environ. Sci. Technol.* 46, 5497–5503. <https://doi.org/10.1021/es2040009>
- Burkhardt, M., Zuleeg, S., Vonbank, R., Schmid, P., Hean, S., Lamani, X., Bester, K., Boller, M., 2011. Leaching of additives from construction materials to urban storm water runoff. *Water Science and Technology* 63, 1974–1982. <https://doi.org/10.2166/wst.2011.128>
- Caglayan, M.G., Kasap, E., Cetin, D., Suludere, Z., Tamer, U., 2017. Fabrication of SERS active gold nanorods using benzalkonium chloride, and their application to an immunoassay for potato virus X. *Microchim Acta* 184, 1059–1067. <https://doi.org/10.1007/s00604-017-2102-x>
- Cai, Q.Q., Wu, M.Y., Hu, L.M., Lee, B.C.Y., Ong, S.L., Wang, P., Hu, J.Y., 2020. Organics removal and in-situ granule activated carbon regeneration in FBR-Fenton/GAC process for reverse osmosis concentrate treatment. *Water Research* 183, 116119. <https://doi.org/10.1016/j.watres.2020.116119>
- Cai, Y., Koning, J.T., Bester, K., Bollmann, U.E., 2021. Abiotic fate of tolylfluanid and dichlofluanid in natural waters. *Science of The Total Environment* 752, 142160. <https://doi.org/10.1016/j.scitotenv.2020.142160>
- Cantoni, B., Turolla, A., Wellmitz, J., Ruhl, A.S., Antonelli, M., 2021. Perfluoroalkyl substances (PFAS) adsorption in drinking water by granular activated carbon: Influence of activated carbon and PFAS characteristics. *Science of The Total Environment* 795, 148821. <https://doi.org/10.1016/j.scitotenv.2021.148821>
- Carpenter, C.M.G., Todorov, D., Driscoll, C.T., Montesdeoca, M., 2016. Water quantity and quality response of a green roof to storm events: Experimental and

- monitoring observations. *Environmental Pollution* 218, 664–672. <https://doi.org/10.1016/j.envpol.2016.07.056>
- Chakraborty, R., Asthana, A., Singh, A.K., Jain, B., Susan, A.B.H., 2022. Adsorption of heavy metal ions by various low-cost adsorbents: a review. *International Journal of Environmental Analytical Chemistry* 102, 342–379. <https://doi.org/10.1080/03067319.2020.1722811>
- Chand, R., Tulucan, T., Aburlacitei, M., 2017. Investigation of Biocide Biodegradation in Wastewater under Laboratory Set-Up in Anaerobic, Aerobic and Aerobic with Substrate Conditions. *Journal of Civil & Environmental Engineering* 08. <https://doi.org/10.4172/2165-784X.1000295>
- Charters, F.J., Carai, N.G., Cochrane, T.A., 2021a. Performance of downpipe treatment system for removal of dissolved metals from roof runoff. *Environmental Technology & Innovation* 22, 101472. <https://doi.org/10.1016/j.eti.2021.101472>
- Charters, F.J., Cochrane, T.A., O’Sullivan, A.D., 2021b. The influence of urban surface type and characteristics on runoff water quality. *Science of The Total Environment* 755, 142470. <https://doi.org/10.1016/j.scitotenv.2020.142470>
- Charters, F.J., Cochrane, T.A., O’Sullivan, A.D., 2016. Untreated runoff quality from roof and road surfaces in a low intensity rainfall climate. *Science of The Total Environment* 550, 265–272. <https://doi.org/10.1016/j.scitotenv.2016.01.093>
- Chen, G., Lin, C., Chen, L., Yang, H., 2010. Effect of size-fractionation dissolved organic matter on the mobility of prometryne in soil. *Chemosphere* 79, 1046–1055. <https://doi.org/10.1016/j.chemosphere.2010.03.038>
- Chen, W., Westerhoff, P., Leenheer, J.A., Booksh, K., 2003. Fluorescence Excitation–Emission Matrix Regional Integration to Quantify Spectra for Dissolved Organic Matter. *Environ. Sci. Technol.* 37, 5701–5710. <https://doi.org/10.1021/es034354c>
- Chen, W.B., Smith, D.S., Guéguen, C., 2013. Influence of water chemistry and dissolved organic matter (DOM) molecular size on copper and mercury binding determined by multiresponse fluorescence quenching. *Chemosphere* 92, 351–359. <https://doi.org/10.1016/j.chemosphere.2012.12.075>
- Chianese, S., Fenti, A., Iovino, P., Musmarra, D., Salvestrini, S., 2020. Sorption of Organic Pollutants by Humic Acids: A Review. *Molecules* 25, 918. <https://doi.org/10.3390/molecules25040918>
- Christl, I., Ruiz, M., Schmidt, J.R., Pedersen, J.A., 2016. Clarithromycin and Tetracycline Binding to Soil Humic Acid in the Absence and Presence of Calcium. *Environ. Sci. Technol.* 50, 9933–9942. <https://doi.org/10.1021/acs.est.5b04693>
- Chukwu, K.B., Abafe, O.A., Amoako, D.G., Essack, S.Y., Abia, A.L.K., 2023. Antibiotic, Heavy Metal, and Biocide Concentrations in a Wastewater Treatment Plant and Its Receiving Water Body Exceed PNEC Limits: Potential for Antimicrobial Resistance Selective Pressure. *Antibiotics* 12, 1166. <https://doi.org/10.3390/antibiotics12071166>
- Cibati, A., Foereid, B., Bissessur, A., Hapca, S., 2017. Assessment of *Miscanthus × giganteus* derived biochar as copper and zinc adsorbent: Study of the effect of pyrolysis temperature, pH and hydrogen peroxide modification. *Journal of Cleaner Production* 162, 1285–1296. <https://doi.org/10.1016/j.jclepro.2017.06.114>
- Clark, S.E., Lator, M., Pratap, M., Field, R., Pitt, R., 2005. Wet-Weather Pollution from Commonly-Used Building Materials, in: *Impacts of Global Climate Change*.

- Presented at the World Water and Environmental Resources Congress 2005, American Society of Civil Engineers, Anchorage, Alaska, United States, pp. 1–12. [https://doi.org/10.1061/40792\(173\)239](https://doi.org/10.1061/40792(173)239)
- Corwin, C.J., Summers, R.S., 2011. Adsorption and desorption of trace organic contaminants from granular activated carbon adsorbers after intermittent loading and throughout backwash cycles. *Water Research* 45, 417–426. <https://doi.org/10.1016/j.watres.2010.08.039>
- Cui, N., Zhang, X., Xie, Q., Wang, S., Chen, J., Huang, L., Qiao, X., Li, X., Cai, X., 2011. Toxicity profile of labile preservative bronopol in water: The role of more persistent and toxic transformation products. *Environmental Pollution* 159, 609–615. <https://doi.org/10.1016/j.envpol.2010.09.036>
- D’Acunha, B., Johnson, M.S., 2019. Water quality and greenhouse gas fluxes for stormwater detained in a constructed wetland. *Journal of Environmental Management* 231, 1232–1240. <https://doi.org/10.1016/j.jenvman.2018.10.106>
- D’Andrilli, J., Silverman, V., Buckley, S., Rosario-Ortiz, F.L., 2022. Inferring Ecosystem Function from Dissolved Organic Matter Optical Properties: A Critical Review. *Environ. Sci. Technol.* 56, 11146–11161. <https://doi.org/10.1021/acs.est.2c04240>
- De Buyck, P.-J., Van Hulle, S.W.H., Dumoulin, A., Rousseau, D.P.L., 2021. Roof runoff contamination: a review on pollutant nature, material leaching and deposition. *Rev Environ Sci Biotechnol* 20, 549–606. <https://doi.org/10.1007/s11157-021-09567-z>
- de Souza, F.M., dos Santos, O.A.A., 2020. Adsorption of Diuron from aqueous solution onto commercial organophilic clay: kinetic, equilibrium and thermodynamic study. *Environmental Technology* 41, 603–616. <https://doi.org/10.1080/09593330.2018.1505967>
- Degenhart, J., Helmreich, B., 2022. Review on inorganic pollutants in stormwater runoff of non-metal roofs. *Front. Environ. Chem.* 3. <https://doi.org/10.3389/fenvc.2022.884021>
- Demiral, İ., Samdan, C., Demiral, H., 2021. Enrichment of the surface functional groups of activated carbon by modification method. *Surfaces and Interfaces* 22, 100873. <https://doi.org/10.1016/j.surfin.2020.100873>
- Dilling, J., Kaiser, K., 2002. Estimation of the hydrophobic fraction of dissolved organic matter in water samples using UV photometry. *Water Research* 36, 5037–5044. [https://doi.org/10.1016/S0043-1354\(02\)00365-2](https://doi.org/10.1016/S0043-1354(02)00365-2)
- Ding, L., Luo, Y., Yu, X., Ouyang, Z., Liu, P., Guo, X., 2022. Insight into interactions of polystyrene microplastics with different types and compositions of dissolved organic matter. *Science of The Total Environment* 824, 153883. <https://doi.org/10.1016/j.scitotenv.2022.153883>
- Ding, Y., Liu, M., Peng, S., Li, J., Liang, Y., Shi, Z., 2019. Binding characteristics of heavy metals to humic acid before and after fractionation by ferrihydrite. *Chemosphere* 226, 140–148. <https://doi.org/10.1016/j.chemosphere.2019.03.124>
- Dinh, Q.T., Zhou, F., Wang, Mengke, Peng, Q., Wang, Min, Qi, M., Tran, T.A.T., Chen, H., Liang, D., 2021. Assessing the potential availability of selenium in the soil-plant system with manure application using diffusive gradients in thin-films technique (DGT) and DOM-Se fractions extracted by selective extractions. *Science of The Total Environment* 763, 143047. <https://doi.org/10.1016/j.scitotenv.2020.143047>

- Dong, S., Gong, Y., Zeng, Z., Chen, S., Ye, J., Wang, Z., Dionysiou, D.D., 2023. Dissolved organic matter promotes photocatalytic degradation of refractory organic pollutants in water by forming hydrogen bonding with photocatalyst. *Water Research* 242, 120297. <https://doi.org/10.1016/j.watres.2023.120297>
- Du, Y., Zhang, Y., Chen, F., Chang, Y., Liu, Z., 2016. Photochemical reactivities of dissolved organic matter (DOM) in a sub-alpine lake revealed by EEM-PARAFAC: An insight into the fate of allochthonous DOM in alpine lakes affected by climate change. *Science of The Total Environment* 568, 216–225. <https://doi.org/10.1016/j.scitotenv.2016.06.036>
- Edzwald, J.K., Becker, W.C., Wattier, K.L., 1985. Surrogate Parameters for Monitoring Organic Matter and THM Precursors. *Journal (American Water Works Association)* 77, 122–132.
- Eeshwarasinghe, D., Loganathan, P., Vigneswaran, S., 2019. Simultaneous removal of polycyclic aromatic hydrocarbons and heavy metals from water using granular activated carbon. *Chemosphere* 223, 616–627. <https://doi.org/10.1016/j.chemosphere.2019.02.033>
- Ekanayake, D., Loganathan, P., Johir, M.A.H., Kandasamy, J., Vigneswaran, S., 2021. Enhanced Removal of Nutrients, Heavy Metals, and PAH from Synthetic Stormwater by Incorporating Different Adsorbents into a Filter Media. *Water Air Soil Pollut* 232, 96. <https://doi.org/10.1007/s11270-021-05059-6>
- Elkins, K.M., Dickerson, M.A., Traudt, E.M., 2011. Fluorescence characterization of the interaction Suwannee river fulvic acid with the herbicide dichlorprop (2-(2,4-dichlorophenoxy)propionic acid) in the absence and presence of aluminum or erbium. *Journal of Inorganic Biochemistry* 105, 1469–1476. <https://doi.org/10.1016/j.jinorgbio.2011.08.009>
- Engel, M., Chefetz, B., 2015. Adsorptive fractionation of dissolved organic matter (DOM) by carbon nanotubes. *Environmental Pollution* 197, 287–294. <https://doi.org/10.1016/j.envpol.2014.11.020>
- Erto, A., Giraldo, L., Lancia, A., Moreno-Piraján, J.C., 2013. A Comparison Between a Low-Cost Sorbent and an Activated Carbon for the Adsorption of Heavy Metals from Water. *Water Air Soil Pollut* 224, 1531. <https://doi.org/10.1007/s11270-013-1531-3>
- Esfandiari, N., Suri, R., McKenzie, E.R., 2022. Competitive sorption of Cd, Cr, Cu, Ni, Pb and Zn from stormwater runoff by five low-cost sorbents; Effects of co-contaminants, humic acid, salinity and pH. *Journal of Hazardous Materials* 423, 126938. <https://doi.org/10.1016/j.jhazmat.2021.126938>
- Fan, T., Yao, X., Ren, H., Ma, F., Liu, L., Huo, X., Lin, T., Zhu, H., Zhang, Y., 2022. Multi-spectroscopic investigation of the molecular weight distribution and copper binding ability of dissolved organic matter in Dongping Lake, China. *Environmental Pollution* 300, 118931. <https://doi.org/10.1016/j.envpol.2022.118931>
- Fang, W., Wei, Y., Liu, J., 2016. Comparative characterization of sewage sludge compost and soil: Heavy metal leaching characteristics. *Journal of Hazardous Materials* 310, 1–10. <https://doi.org/10.1016/j.jhazmat.2016.02.025>
- Fardel, A., Peyneau, P.-E., Béchet, B., Lakel, A., Rodriguez, F., 2020. Performance of two contrasting pilot swale designs for treating zinc, polycyclic aromatic hydrocarbons and glyphosate from stormwater runoff. *Science of The Total Environment* 743, 140503. <https://doi.org/10.1016/j.scitotenv.2020.140503>

- Feng, W., Liu, Y., Gao, L., 2022. Stormwater treatment for reuse: Current practice and future development – A review. *Journal of Environmental Management* 301, 113830. <https://doi.org/10.1016/j.jenvman.2021.113830>
- Fernández-Calviño, D., Rousk, J., Bååth, E., Bollmann, U.E., Bester, K., Brandt, K.K., 2023. Isothiazolinone inhibition of soil microbial activity persists despite biocide dissipation. *Soil Biology and Biochemistry* 178, 108957. <https://doi.org/10.1016/j.soilbio.2023.108957>
- FitzGerald, K.P., Nairn, J., Skennerton, G., Atrens, A., 2006. Atmospheric corrosion of copper and the colour, structure and composition of natural patinas on copper. *Corrosion Science* 48, 2480–2509. <https://doi.org/10.1016/j.corsci.2005.09.011>
- Fu, Q.-L., He, J.-Z., Blaney, L., Zhou, D.-M., 2016. Roxarsone binding to soil-derived dissolved organic matter: Insights from multi-spectroscopic techniques. *Chemosphere* 155, 225–233. <https://doi.org/10.1016/j.chemosphere.2016.04.033>
- Galster, S., Helmreich, B., 2022. Copper and Zinc as Roofing Materials—A Review on the Occurrence and Mitigation Measures of Runoff Pollution. *Water* 14, 291. <https://doi.org/10.3390/w14030291>
- Garrido, E.M., Santos, M., Silva, P., Cagide, F., Garrido, J., Borges, F., 2012. Host-guest complexes of phenoxy alkyl acid herbicides and cyclodextrins. MCPA and β -cyclodextrin. *Journal of Environmental Science and Health, Part B* 47, 869–875. <https://doi.org/10.1080/03601234.2012.693867>
- Garrido Reyes, T.I., Mendoza Crisosto, J.E., Varela Echeverria, P.S., Mejías Barrios, E.G., Álvarez Salgado, X.A., 2021. Interaction between polychlorinated biphenyls and dissolved organic matter of different molecular weights from natural and anthropic sources. *Journal of Environmental Management* 299, 113645. <https://doi.org/10.1016/j.jenvman.2021.113645>
- Gayathiri, M., Pulingam, T., Lee, K.T., Sudesh, K., 2022. Activated carbon from biomass waste precursors: Factors affecting production and adsorption mechanism. *Chemosphere* 294, 133764. <https://doi.org/10.1016/j.chemosphere.2022.133764>
- Genç-Fuhrman, H., Mikkelsen, P.S., Ledin, A., 2016. Simultaneous removal of As, Cd, Cr, Cu, Ni and Zn from stormwater using high-efficiency industrial sorbents: Effect of pH, contact time and humic acid. *Science of The Total Environment* 566–567, 76–85. <https://doi.org/10.1016/j.scitotenv.2016.04.210>
- Golovko, O., de Brito Anton, L., Cascone, C., Ahrens, L., Lavonen, E., Köhler, S.J., 2020. Sorption Characteristics and Removal Efficiency of Organic Micropollutants in Drinking Water Using Granular Activated Carbon (GAC) in Pilot-Scale and Full-Scale Tests. *Water* 12, 2053. <https://doi.org/10.3390/w12072053>
- Gong, Y., Zhang, X., Li, J., Fang, X., Yin, D., Xie, P., Nie, L., 2020. Factors affecting the ability of extensive green roofs to reduce nutrient pollutants in rainfall runoff. *Science of The Total Environment* 732, 139248. <https://doi.org/10.1016/j.scitotenv.2020.139248>
- Grdadolnik, J., Merzel, F., Avbelj, F., 2017. Origin of hydrophobicity and enhanced water hydrogen bond strength near purely hydrophobic solutes. *Proceedings of the National Academy of Sciences* 114, 322–327. <https://doi.org/10.1073/pnas.1612480114>
- Gromaire, M.C., Garnaud, S., Saad, M., Chebbo, G., 2001. Contribution of different sources to the pollution of wet weather flows in combined sewers. *Water Research* 35, 521–533. [https://doi.org/10.1016/S0043-1354\(00\)00261-X](https://doi.org/10.1016/S0043-1354(00)00261-X)

- Gromaire, M.C., Van de Voorde, A., Lorgeoux, C., Chebbo, G., 2015. Benzalkonium runoff from roofs treated with biocide products – In situ pilot-scale study. *Water Research* 81, 279–287. <https://doi.org/10.1016/j.watres.2015.05.060>
- Guillossou, R., Le Roux, J., Mailler, R., Pereira-Derome, C.S., Varrault, G., Bressy, A., Vulliet, E., Morlay, C., Nauleau, F., Rocher, V., Gasperi, J., 2020. Influence of dissolved organic matter on the removal of 12 organic micropollutants from wastewater effluent by powdered activated carbon adsorption. *Water Research* 172, 115487. <https://doi.org/10.1016/j.watres.2020.115487>
- Guo, X., Xie, X., Liu, Y., Wang, C., Yang, M., Huang, Y., 2020. Effects of digestate DOM on chemical behavior of soil heavy metals in an abandoned copper mining areas. *Journal of Hazardous Materials* 393, 122436. <https://doi.org/10.1016/j.jhazmat.2020.122436>
- He, C., Liu, Z., Wu, J., Pan, X., Fang, Z., Li, J., Bryan, B.A., 2021. Future global urban water scarcity and potential solutions. *Nat Commun* 12, 1–11. <https://doi.org/10.1038/s41467-021-25026-3>
- He, S., Liu, T., Kang, C., Xue, H., Sun, S., Yu, S., 2021. Photodegradation of dissolved organic matter of chicken manure: Property changes and effects on Zn²⁺/Cu²⁺ binding property. *Chemosphere* 276, 130054. <https://doi.org/10.1016/j.chemosphere.2021.130054>
- He, X.-S., Xi, B.-D., Pan, H.-W., Li, X., Li, D., Cui, D.-Y., Tang, W.-B., Yuan, Y., 2014. Characterizing the heavy metal-complexing potential of fluorescent water-extractable organic matter from composted municipal solid wastes using fluorescence excitation–emission matrix spectra coupled with parallel factor analysis. *Environ Sci Pollut Res* 21, 7973–7984. <https://doi.org/10.1007/s11356-014-2751-9>
- Hedberg, Y.S., Hedberg, J.F., Herting, G., Goidanich, S., Odnevall Wallinder, I., 2014. Critical Review: Copper Runoff from Outdoor Copper Surfaces at Atmospheric Conditions. *Environ. Sci. Technol.* 48, 1372–1381. <https://doi.org/10.1021/es404410s>
- Hellauer, K., Martínez Mayerlen, S., Drewes, J.E., Hübner, U., 2019. Biotransformation of trace organic chemicals in the presence of highly refractory dissolved organic carbon. *Chemosphere* 215, 33–39. <https://doi.org/10.1016/j.chemosphere.2018.09.166>
- Hensen, B., Lange, J., Jackisch, N., Zieger, F., Olsson, O., Kümmerer, K., 2018. Entry of biocides and their transformation products into groundwater via urban stormwater infiltration systems. *Water Research* 144, 413–423. <https://doi.org/10.1016/j.watres.2018.07.046>
- Hensen, B., Olsson, O., Kümmerer, K., 2020. A strategy for an initial assessment of the ecotoxicological effects of transformation products of pesticides in aquatic systems following a tiered approach. *Environment International* 137, 105533. <https://doi.org/10.1016/j.envint.2020.105533>
- Hensen, B., Olsson, O., Kümmerer, K., 2019. The role of irradiation source setups and indirect phototransformation: Kinetic aspects and the formation of transformation products of weakly sunlight-absorbing pesticides. *Science of The Total Environment* 695, 133808. <https://doi.org/10.1016/j.scitotenv.2019.133808>
- Hou, J., Bian, L., Li, T., 2013. Characteristics and sources of polycyclic aromatic hydrocarbons in impervious surface run-off in an urban area in Shanghai, China. *J. Zhejiang Univ. Sci. A* 14, 751–759. <https://doi.org/10.1631/jzus.A1300155>

- Huang, L., Li, M., Ngo, H.H., Guo, W., Xu, W., Du, B., Wei, Q., Wei, D., 2018. Spectroscopic characteristics of dissolved organic matter from aquaculture wastewater and its interaction mechanism to chlorinated phenol compound. *Journal of Molecular Liquids* 263, 422–427. <https://doi.org/10.1016/j.molliq.2018.05.025>
- Huang, M., Li, Z., Huang, B., Luo, N., Zhang, Q., Zhai, X., Zeng, G., 2018. Investigating binding characteristics of cadmium and copper to DOM derived from compost and rice straw using EEM-PARAFAC combined with two-dimensional FTIR correlation analyses. *Journal of Hazardous Materials* 344, 539–548. <https://doi.org/10.1016/j.jhazmat.2017.10.022>
- Hussan, K.P.S., Thayyil, M.S., Deshpande, S.K., Jinitha, T.V., Rajan, V.K., Ngai, K.L., 2016. Synthesis and molecular dynamics of double active pharmaceutical ingredient-benzalkonium ibuprofenate. *Journal of Molecular Liquids* 223, 1333–1339. <https://doi.org/10.1016/j.molliq.2016.09.054>
- Jeon, M., Guerra, H.B., Choi, H., Kwon, D., Kim, H., Kim, L.-H., 2021. Stormwater Runoff Treatment Using Rain Garden: Performance Monitoring and Development of Deep Learning-Based Water Quality Prediction Models. *Water* 13, 3488. <https://doi.org/10.3390/w13243488>
- Ji, W.-X., Tian, Y.-C., Li, A., Gu, X.-M., Sun, H.-F., Cai, M.-H., Shen, S.-Q., Zuo, Y.-T., Li, W.-T., 2022. Unravelling relationships between fluorescence spectra, molecular weight distribution and hydrophobicity fraction of dissolved organic matter in municipal wastewater. *Chemosphere* 308, 136359. <https://doi.org/10.1016/j.chemosphere.2022.136359>
- Jiang, S., Huang, L., Nguyen, T.A.H., Ok, Y.S., Rudolph, V., Yang, H., Zhang, D., 2016. Copper and zinc adsorption by softwood and hardwood biochars under elevated sulphate-induced salinity and acidic pH conditions. *Chemosphere, Biochars multifunctional role as a novel technology in the agricultural, environmental, and industrial sectors* 142, 64–71. <https://doi.org/10.1016/j.chemosphere.2015.06.079>
- Jin, J., Feng, T., Gao, R., Ma, Y., Wang, W., Zhou, Q., Li, A., 2018. Ultrahigh selective adsorption of zwitterionic PPCPs both in the absence and presence of humic acid: Performance and mechanism. *Journal of Hazardous Materials* 348, 117–124. <https://doi.org/10.1016/j.jhazmat.2018.01.036>
- Jjagwe, J., Olupot, P.W., Menya, E., Kalibbala, H.M., 2021. Synthesis and Application of Granular Activated Carbon from Biomass Waste Materials for Water Treatment: A Review. *Journal of Bioresources and Bioproducts* 6, 292–322. <https://doi.org/10.1016/j.jobab.2021.03.003>
- Juksu, K., Zhao, J.-L., Liu, Y.-S., Yao, L., Sarin, C., Sreesai, S., Klomjek, P., Jiang, Y.-X., Ying, G.-G., 2019. Occurrence, fate and risk assessment of biocides in wastewater treatment plants and aquatic environments in Thailand. *Science of The Total Environment* 690, 1110–1119. <https://doi.org/10.1016/j.scitotenv.2019.07.097>
- Junginger, T., Payraudeau, S., Imfeld, G., 2023. Emissions of the Urban Biocide Terbutryn from Facades: The Contribution of Transformation Products. *Environ. Sci. Technol.* 57, 14319–14329. <https://doi.org/10.1021/acs.est.2c08192>
- Junginger, T., Payraudeau, S., Imfeld, G., 2022. Transformation and stable isotope fractionation of the urban biocide terbutryn during biodegradation, photodegradation and abiotic hydrolysis. *Chemosphere* 305, 135329. <https://doi.org/10.1016/j.chemosphere.2022.135329>

- Kaal, J., Cortizas, A.M., Biester, H., 2017. Downstream changes in molecular composition of DOM along a headwater stream in the Harz mountains (Central Germany) as determined by FTIR, Pyrolysis-GC-MS and THM-GC-MS. *Journal of Analytical and Applied Pyrolysis* 126, 50–61. <https://doi.org/10.1016/j.jaap.2017.06.025>
- Kalaruban, M., Loganathan, P., Nguyen, T.V., Nur, T., Hasan Johir, M.A., Nguyen, T.H., Trinh, M.V., Vigneswaran, S., 2019. Iron-impregnated granular activated carbon for arsenic removal: Application to practical column filters. *Journal of Environmental Management* 239, 235–243. <https://doi.org/10.1016/j.jenvman.2019.03.053>
- Karlén, C., Odnevall Wallinder, I., Heijerick, D., Leygraf, C., 2002. Runoff rates, chemical speciation and bioavailability of copper released from naturally patinated copper. *Environmental Pollution* 120, 691–700. [https://doi.org/10.1016/S0269-7491\(02\)00179-3](https://doi.org/10.1016/S0269-7491(02)00179-3)
- Katsigiannis, A., Noutsopoulos, C., Mantziaras, J., Gioldasi, M., 2015. Removal of emerging pollutants through Granular Activated Carbon. *Chemical Engineering Journal* 280, 49–57. <https://doi.org/10.1016/j.cej.2015.05.109>
- Kennedy, A., Hausmann, J., Corwin, C., Summers, R.S., 2021. DOM removal is more important than the specific DOM removal pretreatment process for GAC adsorption of TrOCs. *Environ. Sci.: Water Res. Technol.* 7, 1707–1713. <https://doi.org/10.1039/D1EW00375E>
- Keshavarz, F., Alavianmehr, M.M., Yousefi, R., 2013. Molecular Interaction of Benzalkonium Ibuprofenate and its Discrete Ingredients with Human Serum Albumin. *Physical Chemistry Research* 1, 111–116. <https://doi.org/10.22036/pcr.2013.3039>
- Kiefer, N., Nichterlein, M., Reiß, F., Runge, M., Biermann, U., Wieland, T., Noll, M., Kalkhof, S., 2024. Eluates from façades at the beginning of their service time affect aquatic and sediment organisms. *Science of The Total Environment* 906, 167531. <https://doi.org/10.1016/j.scitotenv.2023.167531>
- Kikuchi, T., Fujii, M., Terao, K., Jiwei, R., Lee, Y.P., Yoshimura, C., 2017. Correlations between aromaticity of dissolved organic matter and trace metal concentrations in natural and effluent waters: A case study in the Sagami River Basin, Japan. *Science of The Total Environment* 576, 36–45. <https://doi.org/10.1016/j.scitotenv.2016.10.068>
- Kim, D.-W., Wee, J.-H., Yang, C.-M., Yang, K.S., 2020. Efficient removals of Hg and Cd in aqueous solution through NaOH-modified activated carbon fiber. *Chemical Engineering Journal* 392, 123768. <https://doi.org/10.1016/j.cej.2019.123768>
- Kim, H.-B., Kim, J.-G., Kim, T., Alessi, D.S., Baek, K., 2020. Mobility of arsenic in soil amended with biochar derived from biomass with different lignin contents: Relationships between lignin content and dissolved organic matter leaching. *Chemical Engineering Journal* 393, 124687. <https://doi.org/10.1016/j.cej.2020.124687>
- Ko, D., Mines, P.D., Jakobsen, M.H., Yavuz, C.T., Hansen, H.Chr.B., Andersen, H.R., 2018. Disulfide polymer grafted porous carbon composites for heavy metal removal from stormwater runoff. *Chemical Engineering Journal* 348, 685–692. <https://doi.org/10.1016/j.cej.2018.04.192>
- Koning, Jasper.T., Bollmann, Ulla.E., Bester, K., 2021. Biodegradation of third-generation organic antifouling biocides and their hydrolysis products in marine

- model systems. *Journal of Hazardous Materials* 406, 124755. <https://doi.org/10.1016/j.jhazmat.2020.124755>
- Kresmann, S., Arokia, A.H.R., Koch, C., Sures, B., 2018. Ecotoxicological potential of the biocides terbutryn, othilinone and methylisothiazolinone: Underestimated risk from biocidal pathways? *Science of The Total Environment* 625, 900–908. <https://doi.org/10.1016/j.scitotenv.2017.12.280>
- Lakowicz, J.R., 2013. *Principles of Fluorescence Spectroscopy*. Springer Science & Business Media.
- Lebow, S.T., 2014. Evaluating the Leaching of Biocides from Preservative-Treated Wood Products, in: *Deterioration and Protection of Sustainable Biomaterials*, ACS Symposium Series. American Chemical Society, pp. 239–254. <https://doi.org/10.1021/bk-2014-1158.ch014>
- Lee, B.-M., Seo, Y.-S., Hur, J., 2015. Investigation of adsorptive fractionation of humic acid on graphene oxide using fluorescence EEM-PARAFAC. *Water Research* 73, 242–251. <https://doi.org/10.1016/j.watres.2015.01.020>
- Lesmana, S.O., Febriana, N., Soetaredjo, F.E., Sunarso, J., Ismadji, S., 2009. Studies on potential applications of biomass for the separation of heavy metals from water and wastewater. *Biochemical Engineering Journal, Invited Review Issue 2009* 44, 19–41. <https://doi.org/10.1016/j.bej.2008.12.009>
- Li, C., Peng, C., Chiang, P.-C., Cai, Y., Wang, X., Yang, Z., 2019. Mechanisms and applications of green infrastructure practices for stormwater control: A review. *Journal of Hydrology* 568, 626–637. <https://doi.org/10.1016/j.jhydrol.2018.10.074>
- Li, D., Lin, H., Guo, L., 2023. Comparisons in molecular weight distributions and size-dependent optical properties among model and reference natural dissolved organic matter. *Environ Sci Pollut Res* 30, 57638–57652. <https://doi.org/10.1007/s11356-023-26398-3>
- Li, L., Li, J., Zhu, C., Yu, S., 2020. Study of the binding regularity and corresponding mechanism of drinking water odorous compound 2-MIB with coexisting dissolved organic matter. *Chemical Engineering Journal* 395, 125015. <https://doi.org/10.1016/j.cej.2020.125015>
- Li, Yuanhang, Gong, X., Sun, Y., Shu, Y., Niu, D., Ye, H., 2022. High molecular weight fractions of dissolved organic matter (DOM) determined the adsorption and electron transfer capacity of DOM on iron minerals. *Chemical Geology* 604, 120907. <https://doi.org/10.1016/j.chemgeo.2022.120907>
- Li, Yu, Liu, M., Wu, X., 2022. Reclaimed Water Reuse for Groundwater Recharge: A Review of Hot Spots and Hot Moments in the Hyporheic Zone. *Water* 14, 1936. <https://doi.org/10.3390/w14121936>
- Lin, H., Guo, L., 2020. Variations in Colloidal DOM Composition with Molecular Weight within Individual Water Samples as Characterized by Flow Field-Flow Fractionation and EEM-PARAFAC Analysis. *Environ. Sci. Technol.* 54, 1657–1667. <https://doi.org/10.1021/acs.est.9b07123>
- Lin, H., Xia, X., Bi, S., Jiang, X., Wang, H., Zhai, Y., Wen, W., 2017. Quantifying Bioavailability of Pyrene Associated with Dissolved Organic Matter of Various Molecular Weights to *Daphnia magna* [WWW Document]. ACS Publications. <https://doi.org/10.1021/acs.est.7b05520>
- Lin, L., Jiang, W., Xu, P., 2017. Comparative study on pharmaceuticals adsorption in reclaimed water desalination concentrate using biochar: Impact of salts and organic matter. *Science of The Total Environment* 601–602, 857–864. <https://doi.org/10.1016/j.scitotenv.2017.05.203>

- Lin, S., Chu, W., Liu, A., 2022. Characteristics of dissolved organic matter in two alternative water sources: A comparative study between reclaimed water and stormwater. *Science of The Total Environment* 851, 158235. <https://doi.org/10.1016/j.scitotenv.2022.158235>
- Linke, F., Olsson, O., Preusser, F., Kümmerer, K., Schnarr, L., Bork, M., Lange, J., 2021. Sources and pathways of biocides and their transformation products in urban storm water infrastructure of a 2 ha urban district. *Hydrology and Earth System Sciences* 25, 4495–4512. <https://doi.org/10.5194/hess-25-4495-2021>
- Linke, F., Olsson, O., Schnarr, L., Kümmerer, K., Preusser, F., Bork, M., Leistert, H., Lange, J., 2022. Discharge and fate of biocide residuals to ephemeral stormwater retention pond sediments. *Hydrology Research* 53, 1441–1453. <https://doi.org/10.2166/nh.2022.075>
- Linke, F., Skodras, D., Leistert, H., Zimmermann, F., Lange, J., 2024. Biocides in urban groundwater – modeling entry pathways at a district level (No. EGU24-12147). Presented at the EGU24, Copernicus Meetings. <https://doi.org/10.5194/egusphere-egu24-12147>
- Liu, H., Tang, J., Zhang, X., Wang, R., Zhu, B., Li, N., Liang, C., Zhao, P., 2021. Seasonal variations of groundwater recharge in a small subtropical agroforestry watershed with horizontal sedimentary bedrock. *Journal of Hydrology* 596, 125703. <https://doi.org/10.1016/j.jhydrol.2020.125703>
- Liu, K., Lin, X., Chen, L., Huang, L., Cao, S., Wang, H., 2013. Preparation of Microfibrillated Cellulose/Chitosan–Benzalkonium Chloride Biocomposite for Enhancing Antibacterium and Strength of Sodium Alginate Films. *J. Agric. Food Chem.* 61, 6562–6567. <https://doi.org/10.1021/jf4010065>
- Liu, X.-Y., Chen, W., Qian, C., Yu, H.-Q., 2017. Interaction between Dissolved Organic Matter and Long-Chain Ionic Liquids: A Microstructural and Spectroscopic Correlation Study. *Environ. Sci. Technol.* 51, 4812–4820. <https://doi.org/10.1021/acs.est.6b05228>
- Liu, Z., Delgado-Moreno, L., Lu, Z., Zhang, S., He, Y., Gu, X., Chen, Z., Ye, Q., Gan, J., Wang, W., 2019. Inhibitory effects of dissolved organic matter on erythromycin bioavailability and possible mechanisms. *Journal of Hazardous Materials* 375, 255–263. <https://doi.org/10.1016/j.jhazmat.2019.04.073>
- Lu, Y., Allen, H., 2002. Characterization of copper complexation with natural dissolved organic matter (DOM)—link to acidic moieties of DOM and competition by Ca and Mg. *Water Research* 36, 5083–5101. [https://doi.org/10.1016/S0043-1354\(02\)00240-3](https://doi.org/10.1016/S0043-1354(02)00240-3)
- Luthy, R.G., Sharvelle, S., Dillon, P., 2019. Urban Stormwater to Enhance Water Supply. *Environ. Sci. Technol.* 53, 5534–5542. <https://doi.org/10.1021/acs.est.8b05913>
- Ma, L., Yates, S.R., 2018. Dissolved organic matter and estrogen interactions regulate estrogen removal in the aqueous environment: A review. *Science of The Total Environment* 640–641, 529–542. <https://doi.org/10.1016/j.scitotenv.2018.05.301>
- Ma, Y., Mao, R., Li, S., 2021. Hydrological seasonality largely contributes to riverine dissolved organic matter chemical composition: Insights from EEM-PARAFAC and optical indicators. *Journal of Hydrology* 595, 125993. <https://doi.org/10.1016/j.jhydrol.2021.125993>
- Machate, O., Dellen, J., Schulze, T., Wentzky, V.C., Krauss, M., Brack, W., 2021. Evidence for antifouling biocides as one of the limiting factors for the recovery

- of macrophyte communities in lakes of Schleswig-Holstein. *Environ Sci Eur* 33, 57. <https://doi.org/10.1186/s12302-021-00500-3>
- Madgett, A.S., Yates, K., Webster, L., McKenzie, C., Moffat, C.F., 2021. The concentration and biomagnification of trace metals and metalloids across four trophic levels in a marine food web. *Marine Pollution Bulletin* 173, 112929. <https://doi.org/10.1016/j.marpolbul.2021.112929>
- McFarland, A.R., Larsen, L., Yeshitela, K., Engida, A.N., Love, N.G., 2019. Guide for using green infrastructure in urban environments for stormwater management. *Environ. Sci.: Water Res. Technol.* 5, 643–659. <https://doi.org/10.1039/C8EW00498F>
- McGinley, J., Healy, M.G., Ryan, P.C., Mellander, P.-E., Morrison, L., O’Driscoll, J.H., Siggins, A., 2022. Batch adsorption of herbicides from aqueous solution onto diverse reusable materials and granulated activated carbon. *Journal of Environmental Management* 323, 116102. <https://doi.org/10.1016/j.jenvman.2022.116102>
- McIntyre, J.K., Winters, N., Rozmyn, L., Haskins, T., Stark, J.D., 2019. Metals leaching from common residential and commercial roofing materials across four years of weathering and implications for environmental loading. *Environmental Pollution* 255, 113262. <https://doi.org/10.1016/j.envpol.2019.113262>
- Meerow, S., Newell, J.P., 2017. Spatial planning for multifunctional green infrastructure: Growing resilience in Detroit. *Landscape and Urban Planning* 159, 62–75. <https://doi.org/10.1016/j.landurbplan.2016.10.005>
- Mei, Y., Bai, Y., Wang, L., 2016. Effect of pH on binding of pyrene to hydrophobic fractions of dissolved organic matter (DOM) isolated from lake water. *Acta Geochim* 35, 288–293. <https://doi.org/10.1007/s11631-016-0094-6>
- Milovanović, I., Hedström, A., Herrmann, I., Viklander, M., 2022. Performance of a zeolite filter treating copper roof runoff. *Urban Water Journal* 19, 499–508. <https://doi.org/10.1080/1573062X.2022.2031230>
- Minelgaite, G., Nielsen, A.H., Pedersen, M.L., Vollertsen, J., 2017. Photodegradation of three stormwater biocides. *Urban Water Journal* 14, 53–60. <https://doi.org/10.1080/1573062X.2015.1076489>
- Müller, A., Österlund, H., Nordqvist, K., Marsalek, J., Viklander, M., 2019. Building surface materials as sources of micropollutants in building runoff: A pilot study. *Science of The Total Environment* 680, 190–197. <https://doi.org/10.1016/j.scitotenv.2019.05.088>
- Murphy, K.R., Stedmon, C.A., Graeber, D., Bro, R., 2013. Fluorescence spectroscopy and multi-way techniques. *PARAFAC. Anal. Methods* 5, 6557. <https://doi.org/10.1039/c3ay41160e>
- Nebbioso, A., Piccolo, A., 2013. Molecular characterization of dissolved organic matter (DOM): a critical review. *Anal Bioanal Chem* 405, 109–124. <https://doi.org/10.1007/s00216-012-6363-2>
- Noda, I., 1990. Two-dimensional infrared (2D IR) spectroscopy: theory and applications. *Applied Spectroscopy* 44, 550–561.
- Odnevall Wallinder, I., Verbiest, P., He, W., Leygraf, C., 2000. Effects of exposure direction and inclination on the runoff rates of zinc and copper roofs. *Corrosion Science* 42, 1471–1487. [https://doi.org/10.1016/S0010-938X\(99\)00145-6](https://doi.org/10.1016/S0010-938X(99)00145-6)
- Okamura, H., 2002. Photodegradation of the antifouling compounds Irgarol 1051 and Diuron released from a commercial antifouling paint. *Chemosphere* 48, 43–50. [https://doi.org/10.1016/S0045-6535\(02\)00025-5](https://doi.org/10.1016/S0045-6535(02)00025-5)

- Ouellet, V., Khamis, K., Croghan, D., Hernandez Gonzalez, L.M., Rivera, V.A., Phillips, C.B., Packman, A.I., Miller, W.M., Hawke, R.G., Hannah, D.M., Krause, S., 2021. Green roof vegetation management alters potential for water quality and temperature mitigation. *Ecohydrology* 14. <https://doi.org/10.1002/eco.2321>
- Pacholak, A., Burlaga, N., Frankowski, R., Zgoła-Grześkowiak, A., Kaczorek, E., 2022. Azole fungicides: (Bio)degradation, transformation products and toxicity elucidation. *Science of The Total Environment* 802, 149917. <https://doi.org/10.1016/j.scitotenv.2021.149917>
- Paijens, C., Bressy, A., Frère, B., Moilleron, R., 2020. Biocide emissions from building materials during wet weather: identification of substances, mechanism of release and transfer to the aquatic environment. *Environ Sci Pollut Res* 27, 3768–3791. <https://doi.org/10.1007/s11356-019-06608-7>
- Paijens, C., Bressy, A., Frère, B., Tedoldi, D., Mailler, R., Rocher, V., Neveu, P., Moilleron, R., 2021. Urban pathways of biocides towards surface waters during dry and wet weathers: Assessment at the Paris conurbation scale. *Journal of Hazardous Materials* 402, 123765. <https://doi.org/10.1016/j.jhazmat.2020.123765>
- Pan, B., Qiu, M., Wu, M., Zhang, D., Peng, H., Wu, D., Xing, B., 2012. The opposite impacts of Cu and Mg cations on dissolved organic matter-ofloxacin interaction. *Environmental Pollution* 161, 76–82. <https://doi.org/10.1016/j.envpol.2011.09.040>
- Pan, J., Gao, B., Guo, K., Gao, Y., Xu, X., Yue, Q., 2022. Insights into selective adsorption mechanism of copper and zinc ions onto biogas residue-based adsorbent: Theoretical calculation and electronegativity difference. *Science of The Total Environment* 805, 150413. <https://doi.org/10.1016/j.scitotenv.2021.150413>
- Panettieri, M., Guigue, J., Chemidlin Prevost-Bouré, N., Thévenot, M., Lévêque, J., Le Guillou, C., Maron, P.-A., Santoni, A.-L., Ranjard, L., Mounier, S., Menasseri, S., Viaud, V., Mathieu, O., 2020. Grassland-cropland rotation cycles in crop-livestock farming systems regulate priming effect potential in soils through modulation of microbial communities, composition of soil organic matter and abiotic soil properties. *Agriculture, Ecosystems & Environment* 299, 106973. <https://doi.org/10.1016/j.agee.2020.106973>
- Pappalardo, V., La Rosa, D., Campisano, A., La Greca, P., 2017. The potential of green infrastructure application in urban runoff control for land use planning: A preliminary evaluation from a southern Italy case study. *Ecosystem Services, Putting ES into practice* 26, 345–354. <https://doi.org/10.1016/j.ecoser.2017.04.015>
- Park, J., Cho, K.H., Lee, E., Lee, S., Cho, J., 2018. Sorption of pharmaceuticals to soil organic matter in a constructed wetland by electrostatic interaction. *Science of The Total Environment* 635, 1345–1350. <https://doi.org/10.1016/j.scitotenv.2018.04.212>
- Parker, B.A., Kanalos, C.A., Radniecki, T.S., Simonich, S.L.M., Field, J.A., 2023. Evaluation of sorbents and matrix effects for treating heavy metals and per- and polyfluoroalkyl substances as co-contaminants in stormwater. *Environ. Sci.: Water Res. Technol.* 9, 3281–3289. <https://doi.org/10.1039/D3EW00028A>
- Pastor, A., Gámiz, B., Cruz-Yusta, M., Sánchez, L., Pavlovic, I., 2020. Carbendazim-clay complexes for its potential use as antimicrobial additives in mortars.

- Building and Environment 183, 107214.
<https://doi.org/10.1016/j.buildenv.2020.107214>
- Paun, I., Pirvu, F., Iancu, V.I., Chiriac, F.L., 2022. Occurrence and Transport of Isothiazolinone-Type Biocides from Commercial Products to Aquatic Environment and Environmental Risk Assessment. *International Journal of Environmental Research and Public Health* 19, 7777. <https://doi.org/10.3390/ijerph19137777>
- Peñafiel, M.E., Matesanz, J.M., Vanegas, E., Bermejo, D., Mosteo, R., Ormad, M.P., 2021. Comparative adsorption of ciprofloxacin on sugarcane bagasse from Ecuador and on commercial powdered activated carbon. *Science of The Total Environment* 750, 141498. <https://doi.org/10.1016/j.scitotenv.2020.141498>
- Peng, B., Chen, L., Que, C., Yang, K., Deng, F., Deng, X., Shi, G., Xu, G., Wu, M., 2016. Adsorption of Antibiotics on Graphene and Biochar in Aqueous Solutions Induced by π - π Interactions. *Sci Rep* 6, 31920. <https://doi.org/10.1038/srep31920>
- Peter, P.O., Ifon, B.E., Nkinahamira, F., Lasisi, K.H., Li, J., Hu, A., Yu, C.-P., 2024. Harnessing the composition of dissolved organic matter in lagoon sediment in association with rare earth elements using fluorescence and UV-visible absorption spectroscopy. *Science of The Total Environment* 908, 168139. <https://doi.org/10.1016/j.scitotenv.2023.168139>
- Plaza, C., Brunetti, G., Senesi, N., Polo, A., 2006. Fluorescence characterization of metal ion-humic acid interactions in soils amended with composted municipal solid wastes. *Anal Bioanal Chem* 386, 2133–2140. <https://doi.org/10.1007/s00216-006-0844-0>
- Polkowska, Ż., Tobiszewski, M., Górecki, T., Namieśnik, J., 2009. Pesticides in rain and roof runoff waters from an urban region. *Urban Water Journal* 6, 441–448. <https://doi.org/10.1080/15730620902972405>
- Pucher, M., Wunsch, U., Weigelhofer, G., Murphy, K., Hein, T., Graeber, D., 2019. staRdom: Versatile Software for Analyzing Spectroscopic Data of Dissolved Organic Matter in R. *Water* 11, 2366. <https://doi.org/10.3390/w11112366>
- Qiao, C., Shen, L., Hao, L., Mu, X., Dong, J., Ke, W., Liu, J., Liu, B., 2019. Corrosion kinetics and patina evolution of galvanized steel in a simulated coastal-industrial atmosphere. *Journal of Materials Science & Technology* 35, 2345–2356. <https://doi.org/10.1016/j.jmst.2019.05.039>
- Quang, V.L., Kim, H.-C., Maqbool, T., Hur, J., 2016. Fate and fouling characteristics of fluorescent dissolved organic matter in ultrafiltration of terrestrial humic substances. *Chemosphere* 165, 126–133. <https://doi.org/10.1016/j.chemosphere.2016.09.029>
- Quon, H., Jiang, S., 2023. Decision making for implementing non-traditional water sources: a review of challenges and potential solutions. *npj Clean Water* 6, 1–14. <https://doi.org/10.1038/s41545-023-00273-7>
- Radian, A., Mishaal, Y., 2012. Effect of Humic Acid on Pyrene Removal from Water by Polycation-Clay Mineral Composites and Activated Carbon. *Environ. Sci. Technol.* 46, 6228–6235. <https://doi.org/10.1021/es300964d>
- Reddy, K.R., Xie, T., Dastgheibi, S., 2014. Removal of heavy metals from urban stormwater runoff using different filter materials. *Journal of Environmental Chemical Engineering* 2, 282–292. <https://doi.org/10.1016/j.jece.2013.12.020>
- Reiß, F., Kiefer, N., Noll, M., Kalkhof, S., 2021. Application, release, ecotoxicological assessment of biocide in building materials and its soil microbial response.

- Ecotoxicology and Environmental Safety 224, 112707. <https://doi.org/10.1016/j.ecoenv.2021.112707>
- Reiß, F., Kiefer, N., Purahong, W., Borcken, W., Kalkhof, S., Noll, M., 2024. Active soil microbial composition and proliferation are directly affected by the presence of biocides from building materials. *Science of The Total Environment* 912, 168689. <https://doi.org/10.1016/j.scitotenv.2023.168689>
- Ren, H., Fan, T., Yao, X., Ma, F., Liu, L., Ming, J., Wang, S., Zhang, Y., Deng, H., 2022. Investigation of the variations in dissolved organic matter properties and complexations with two typical heavy metals under the influence of biodegradation: A survey of an entire lake. *Science of The Total Environment* 806, 150485. <https://doi.org/10.1016/j.scitotenv.2021.150485>
- Ren, J., Fan, W., Wang, X., Ma, Q., Li, X., Xu, Z., Wei, C., 2017. Influences of size-fractionated humic acids on arsenite and arsenate complexation and toxicity to *Daphnia magna*. *Water Research* 108, 68–77. <https://doi.org/10.1016/j.watres.2016.10.052>
- Rezakazemi, M., Zhang, Z., 2018. 2.29 Desulfurization Materials, in: Dincer, I. (Ed.), *Comprehensive Energy Systems*. Elsevier, Oxford, pp. 944–979. <https://doi.org/10.1016/B978-0-12-809597-3.00263-7>
- Rizzuto, S., Baho, D.L., Jones, K.C., Zhang, H., Leu, E., Nizzetto, L., 2021a. Binding of waterborne pharmaceutical and personal care products to natural dissolved organic matter. *Science of The Total Environment* 784, 147208. <https://doi.org/10.1016/j.scitotenv.2021.147208>
- Rizzuto, S., Jones, K.C., Zhang, H., Baho, D.L., Leu, E., Nizzetto, L., 2021b. Critical assessment of an equilibrium-based method to study the binding of waterborne organic contaminants to natural dissolved organic matter (DOM). *Chemosphere* 285, 131524. <https://doi.org/10.1016/j.chemosphere.2021.131524>
- Romera-Castillo, C., Chen, M., Yamashita, Y., Jaffé, R., 2014. Fluorescence characteristics of size-fractionated dissolved organic matter: Implications for a molecular assembly based structure? *Water Research* 55, 40–51. <https://doi.org/10.1016/j.watres.2014.02.017>
- Romero, C.M., Engel, R.E., D'Andrilli, J., Miller, P.R., Wallander, R., 2019. Compositional tracking of dissolved organic matter in semiarid wheat-based cropping systems using fluorescence EEMs-PARAFAC and absorbance spectroscopy. *Journal of Arid Environments* 167, 34–42. <https://doi.org/10.1016/j.jaridenv.2019.04.013>
- Rommel, S.H., Ebert, V., Huber, M., Drewes, J.E., Helmreich, B., 2019. Spatial distribution of zinc in the topsoil of four vegetated infiltration swales treating zinc roof runoff. *Science of The Total Environment* 672, 806–814. <https://doi.org/10.1016/j.scitotenv.2019.04.016>
- Ryan, D.K., Weber, J.H., 1982. Fluorescence quenching titration for determination of complexing capacities and stability constants of fulvic acid. *Anal. Chem.* 54, 986–990. <https://doi.org/10.1021/ac00243a033>
- Sage, J., El Oreibi, E., Saad, M., Gromaire, M.-C., 2016. Modeling the temporal variability of zinc concentrations in zinc roof runoff—experimental study and uncertainty analysis. *Environ Sci Pollut Res* 23, 16552–16566. <https://doi.org/10.1007/s11356-016-6827-6>
- Saidon, N.B., Szabó, R., Budai, P., Lehel, J., 2024. Trophic transfer and biomagnification potential of environmental contaminants (heavy metals) in aquatic ecosystems. *Environmental Pollution* 340, 122815. <https://doi.org/10.1016/j.envpol.2023.122815>

- Schmidt, M.P., Ashworth, D.J., Ibekwe, A.M., 2024. Cephalixin interaction with biosolids-derived dissolved organic matter: binding mechanism and implications for adsorption by biochar and clay. *Environ. Sci.: Water Res. Technol.* <https://doi.org/10.1039/D3EW00590A>
- Schmidt, M.P., Martínez, C.E., 2019. The influence of tillage on dissolved organic matter dynamics in a Mid-Atlantic agroecosystem. *Geoderma* 344, 63–73. <https://doi.org/10.1016/j.geoderma.2019.03.001>
- Schoknecht, U., Gruycheva, J., Mathies, H., Bergmann, H., Burkhardt, M., 2009. Leaching of Biocides Used in Façade Coatings under Laboratory Test Conditions. *Environ. Sci. Technol.* 43, 9321–9328. <https://doi.org/10.1021/es9019832>
- Schoknecht, U., Mathies, H., Lisek, J., 2021. Leaching and Transformation of Film Preservatives in Paints Induced by Combined Exposure to Ultraviolet Radiation and Water Contact under Controlled Laboratory Conditions. *Water* 13, 2390. <https://doi.org/10.3390/w13172390>
- Schoknecht, U., Mathies, H., Wegner, R., 2016. Biocide leaching during field experiments on treated articles. *Environ Sci Eur* 28, 6. <https://doi.org/10.1186/s12302-016-0074-9>
- Schreiber, B., Brinkmann, T., Schmalz, V., Worch, E., 2005. Adsorption of dissolved organic matter onto activated carbon—the influence of temperature, absorption wavelength, and molecular size. *Water Research* 39, 3449–3456. <https://doi.org/10.1016/j.watres.2005.05.050>
- Schriewer, A., Horn, H., Helmreich, B., 2008. Time focused measurements of roof runoff quality. *Corrosion Science* 50, 384–391. <https://doi.org/10.1016/j.corsci.2007.08.011>
- Schwerd, R.; Hübner, S.; Schwitalla, C.; Scherer, C. Freisetzung von Mecoprop aus Polymerbitumendachbahnen. In *Aqua Urbana Congerence Proceedings 2018*; Technical University of Kaiserslautern: Kaiserslautern, Germany, 2018; pp. 317–320.
- Sharma, R., Malaviya, P., 2021. Management of stormwater pollution using green infrastructure: The role of rain gardens. *WIREs Water* 8, e1507. <https://doi.org/10.1002/wat2.1507>
- Shimabuku, K.K., Kennedy, A.M., Mulhern, R.E., Summers, R.S., 2017. Evaluating Activated Carbon Adsorption of Dissolved Organic Matter and Micropollutants Using Fluorescence Spectroscopy. *Environ. Sci. Technol.* 51, 2676–2684. <https://doi.org/10.1021/acs.est.6b04911>
- Smith, M.A., Kominoski, J.S., Gaiser, E.E., Price, R.M., Troxler, T.G., 2021. Stormwater Runoff and Tidal Flooding Transform Dissolved Organic Matter Composition and Increase Bioavailability in Urban Coastal Ecosystems. *Journal of Geophysical Research: Biogeosciences* 126, e2020JG006146. <https://doi.org/10.1029/2020JG006146>
- Solanki, A., Boyer, T.H., 2019. Physical-chemical interactions between pharmaceuticals and biochar in synthetic and real urine. *Chemosphere* 218, 818–826. <https://doi.org/10.1016/j.chemosphere.2018.11.179>
- Sounthararajah, D.P., Loganathan, P., Kandasamy, J., Vigneswaran, S., 2015. Effects of Humic Acid and Suspended Solids on the Removal of Heavy Metals from Water by Adsorption onto Granular Activated Carbon. *International Journal of Environmental Research and Public Health* 12, 10475–10489. <https://doi.org/10.3390/ijerph120910475>

- Sowers, T.D., Adhikari, D., Wang, J., Yang, Y., Sparks, D.L., 2018a. Spatial Associations and Chemical Composition of Organic Carbon Sequestered in Fe, Ca, and Organic Carbon Ternary Systems. *Environ. Sci. Technol.* 52, 6936–6944. <https://doi.org/10.1021/acs.est.8b01158>
- Sowers, T.D., Stuckey, J.W., Sparks, D.L., 2018b. The synergistic effect of calcium on organic carbon sequestration to ferrihydrite. *Geochem Trans* 19, 4. <https://doi.org/10.1186/s12932-018-0049-4>
- Styszko, K., Bollmann, U.E., Bester, K., 2015. Leaching of biocides from polymer renders under wet/dry cycles – Rates and mechanisms. *Chemosphere* 138, 609–615. <https://doi.org/10.1016/j.chemosphere.2015.07.029>
- Szabó, Z., Pedretti, D., Masetti, M., Ridavits, T., Csiszár, E., Falus, G., Palcsu, L., Mádl-Szőnyi, J., 2023. Rooftop rainwater harvesting by a shallow well – Impacts and potential from a field experiment in the Danube-Tisza Interfluvium, Hungary. *Groundwater for Sustainable Development* 20, 100884. <https://doi.org/10.1016/j.gsd.2022.100884>
- Taguchi, V.J., Weiss, P.T., Gulliver, J.S., Klein, M.R., Hozalski, R.M., Baker, L.A., Finlay, J.C., Keeler, B.L., Nieber, J.L., 2020. It Is Not Easy Being Green: Recognizing Unintended Consequences of Green Stormwater Infrastructure. *Water* 12, 522. <https://doi.org/10.3390/w12020522>
- Tang, J., Zhuang, L., Yu, Z., Liu, X., Wang, Y., Wen, P., Zhou, S., 2019. Insight into complexation of Cu(II) to hyperthermophilic compost-derived humic acids by EEM-PARAFAC combined with heterospectral two dimensional correlation analyses. *Science of The Total Environment* 656, 29–38. <https://doi.org/10.1016/j.scitotenv.2018.11.357>
- Tang, L., Ma, X.Y., Wang, Y., Zhang, S., Zheng, K., Wang, X.C., Lin, Y., 2020. Removal of trace organic pollutants (pharmaceuticals and pesticides) and reduction of biological effects from secondary effluent by typical granular activated carbon. *Science of The Total Environment* 749, 141611. <https://doi.org/10.1016/j.scitotenv.2020.141611>
- Tu, S., Li, Q., Nie, L., Gao, H., Yu, H., 2024. Applying fluorescence spectroscopy with absolute principal component coefficient to explore dynamic migration of DOM fractions from an urbanized river during torrential rainfall. *Spectrochimica Acta Part A: Molecular and Biomolecular Spectroscopy* 314, 124206. <https://doi.org/10.1016/j.saa.2024.124206>
- Uhlig, S., Colson, B., Schoknecht, U., 2019. A mathematical approach for the analysis of data obtained from the monitoring of biocides leached from treated materials exposed to outdoor conditions. *Chemosphere* 228, 271–277. <https://doi.org/10.1016/j.chemosphere.2019.04.102>
- Umbría-Salinas, K., Valero, A., Martins, S.E., Wallner-Kersanach, M., 2021. Copper ecological risk assessment using DGT technique and PNEC: A case study in the Brazilian coast. *Journal of Hazardous Materials* 403, 123918. <https://doi.org/10.1016/j.jhazmat.2020.123918>
- Ungureanu, N., Vlăduț, V., Voicu, G., 2020. Water Scarcity and Wastewater Reuse in Crop Irrigation. *Sustainability* 12, 9055. <https://doi.org/10.3390/su12219055>
- Urbanczyk, M.M., Bester, K., Borho, N., Schoknecht, U., Bollmann, U.E., 2019. Influence of pigments on phototransformation of biocides in paints. *Journal of Hazardous Materials* 364, 125–133. <https://doi.org/10.1016/j.jhazmat.2018.10.018>
- Uwayezu, J.-N., Yeung, L.W.Y., Bäckström, M., 2019. Sorption of PFOS isomers on goethite as a function of pH, dissolved organic matter (humic and fulvic acid)

- and sulfate. *Chemosphere* 233, 896–904.
<https://doi.org/10.1016/j.chemosphere.2019.05.252>
- Vatankhah, H., Riley, S.M., Murray, C., Quiñones, O., Steirer, K.X., Dickenson, E.R.V., Bellona, C., 2019. Simultaneous ozone and granular activated carbon for advanced treatment of micropollutants in municipal wastewater effluent. *Chemosphere* 234, 845–854.
<https://doi.org/10.1016/j.chemosphere.2019.06.082>
- Vega-Garcia, P., Lok, C.S.C., Marhoon, A., Schwerd, R., Johann, S., Helmreich, B., 2022b. Modelling the environmental fate and behavior of biocides used in façades covered with mortars and plasters and their transformation products. *Building and Environment* 216, 108991.
<https://doi.org/10.1016/j.buildenv.2022.108991>
- Vega-Garcia, P., Schwerd, R., Johann, S., Helmreich, B., 2022a. Groundwater risk assessment of leached inorganic substances from façades coated with plasters and mortars. *Chemosphere* 287, 132176.
<https://doi.org/10.1016/j.chemosphere.2021.132176>
- Vega-Garcia, P., Schwerd, R., Scherer, C., Schwitalla, C., Johann, S., Rommel, S.H., Helmreich, B., 2020. Influence of façade orientation on the leaching of biocides from building façades covered with mortars and plasters. *Science of The Total Environment* 734, 139465. <https://doi.org/10.1016/j.scitotenv.2020.139465>
- Vermeirssen, E.L.M., Campiche, S., Dietschweiler, C., Werner, I., Burkhardt, M., 2018. Ecotoxicological Assessment of Immersion Samples from Facade Render Containing Free or Encapsulated Biocides. *Environmental Toxicology and Chemistry* 37, 2246–2256. <https://doi.org/10.1002/etc.4176>
- Vialle, C., Sablayrolles, C., Lovera, M., Jacob, S., Huau, M.-C., Montrejaud-Vignoles, M., 2011. Monitoring of water quality from roof runoff: Interpretation using multivariate analysis. *Water Research* 45, 3765–3775.
<https://doi.org/10.1016/j.watres.2011.04.029>
- Vialle, C., Sablayrolles, C., Silvestre, J., Monier, L., Jacob, S., Huau, M.-C., Montrejaud-Vignoles, M., 2013. Pesticides in roof runoff: Study of a rural site and a suburban site. *Journal of Environmental Management* 120, 48–54.
<https://doi.org/10.1016/j.jenvman.2013.02.023>
- Vione, D., Arey, J.S., Parkerton, T.F., Redman, A.D., 2024. Direct and indirect photodegradation in aquatic systems mitigates photosensitized toxicity in screening-level substance risk assessments of selected petrochemical structures. *Water Research* 121677. <https://doi.org/10.1016/j.watres.2024.121677>
- Wang, D., Peng, Q., Yang, W.-X., Dinh, Q.T., Tran, T.A.T., Zhao, X.-D., Wu, J.-T., Liu, Y.-X., Liang, D.-L., 2020. DOM derivations determine the distribution and bioavailability of DOM-Se in selenate applied soil and mechanisms. *Environmental Pollution* 259, 113899.
<https://doi.org/10.1016/j.envpol.2019.113899>
- Wang, H., Ge, X., Li, S., Huang, H., 2024. Insight into the binding characteristics of dissolved organic matter(DOM)and Fe(II)/Mn(II): Based on the spectroscopic and dialysis equilibrium analysis. *Chemosphere* 362, 142672.
<https://doi.org/10.1016/j.chemosphere.2024.142672>
- Wang, H., Wang, J., Yu, X., 2022. Wastewater irrigation and crop yield: A meta-analysis. *Journal of Integrative Agriculture* 21, 1215–1224.
[https://doi.org/10.1016/S2095-3119\(21\)63853-4](https://doi.org/10.1016/S2095-3119(21)63853-4)

- Wang, J., 2003. Modeling heavy metal uptake by sludge particulates in the presence of dissolved organic matter. *Water Research* 37, 4835–4842. <https://doi.org/10.1016/j.watres.2003.08.021>
- Wang, J., Guo, X., 2020. Adsorption isotherm models: Classification, physical meaning, application and solving method. *Chemosphere* 258, 127279. <https://doi.org/10.1016/j.chemosphere.2020.127279>
- Wang, L., Wu, X., Zhao, Z., Fan, F., Zhu, M., Wang, Y., Na, R., Li, Q.X., 2020. Interactions between Imidacloprid and Thiamethoxam and Dissolved Organic Matter Characterized by Two-Dimensional Correlation Spectroscopy Analysis, Molecular Modeling, and Density Functional Theory Calculations. *J. Agric. Food Chem.* 68, 2329–2339. <https://doi.org/10.1021/acs.jafc.9b06857>
- Wang, M., Bodirsky, B.L., Rijnveld, R., Beier, F., Bak, M.P., Batool, M., Droppers, B., Popp, A., van Vliet, M.T.H., Strokal, M., 2024. A triple increase in global river basins with water scarcity due to future pollution. *Nat Commun* 15, 880. <https://doi.org/10.1038/s41467-024-44947-3>
- Wang, S., Yuan, Y., Bi, E., 2024. The role of magnesium ion in the interactions between humic acid and tetracycline in solution. *Journal of Environmental Management* 354, 120344. <https://doi.org/10.1016/j.jenvman.2024.120344>
- Wang, Y., Liu, J., Liem-Nguyen, V., Tian, S., Zhang, S., Wang, D., Jiang, T., 2022. Binding strength of mercury (II) to different dissolved organic matter: The roles of DOM properties and sources. *Science of The Total Environment* 807, 150979. <https://doi.org/10.1016/j.scitotenv.2021.150979>
- Wang, Y., Zhang, Xinyuan, Zhang, Xing, Meng, Q., Gao, F., Zhang, Y., 2017. Characterization of spectral responses of dissolved organic matter (DOM) for atrazine binding during the sorption process onto black soil. *Chemosphere* 180, 531–539. <https://doi.org/10.1016/j.chemosphere.2017.04.063>
- Wangler, T.P., Zuleeg, S., Vonbank, R., Bester, K., Boller, M., Carmeliet, J., Burkhardt, M., 2012. Laboratory scale studies of biocide leaching from façade coatings. *Building and Environment* 54, 168–173. <https://doi.org/10.1016/j.buildenv.2012.02.021>
- Wei, J., Tu, C., Yuan, G., Zhou, Y., Wang, H., Lu, J., 2020. Limited Cu(II) binding to biochar DOM: Evidence from C K-edge NEXAFS and EEM-PARAFAC combined with two-dimensional correlation analysis. *Science of The Total Environment* 701, 134919. <https://doi.org/10.1016/j.scitotenv.2019.134919>
- Wei, X., Wu, Zhansheng, Wu, Zhilin, Ye, B.-C., 2018. Adsorption behaviors of atrazine and Cr(III) onto different activated carbons in single and co-solute systems. *Powder Technology* 329, 207–216. <https://doi.org/10.1016/j.powtec.2018.01.060>
- Weishaar, J.L., Aiken, G.R., Bergamaschi, B.A., Fram, M.S., Fujii, R., Mopper, K., 2003. Evaluation of Specific Ultraviolet Absorbance as an Indicator of the Chemical Composition and Reactivity of Dissolved Organic Carbon. *Environ. Sci. Technol.* 37, 4702–4708. <https://doi.org/10.1021/es030360x>
- Wen, L., Yang, F., Li, X., Liu, S., Lin, Y., Hu, E., Gao, L., Li, M., 2023. Composition of dissolved organic matter (DOM) in wastewater treatment plants influent affects the efficiency of carbon and nitrogen removal. *Science of The Total Environment* 857, 159541. <https://doi.org/10.1016/j.scitotenv.2022.159541>
- Wicke, D., Cochrane, T.A., O'Sullivan, A.D., Cave, S., Derksen, M., 2014. Effect of age and rainfall pH on contaminant yields from metal roofs. *Water Science and Technology* 69, 2166–2173. <https://doi.org/10.2166/wst.2014.124>

- Wicke, D., Matzinger, A., Sonnenberg, H., Caradot, N., Schubert, R.-L., Dick, R., Heinzmann, B., Dünnbier, U., von Seggern, D., Rouault, P., 2021. Micropollutants in Urban Stormwater Runoff of Different Land Uses. *Water* 13, 1312. <https://doi.org/10.3390/w13091312>
- Wicke, D., Tatis-Muvdi, R., Rouault, P., Zerbball-van Baar, P., Dünnbier, U., Rohr, M., Burkhardt, M., 2022. Emissions from Building Materials—A Threat to the Environment? *Water* 14, 303. <https://doi.org/10.3390/w14030303>
- Wiest, L., Baudot, R., Lafay, F., Bonjour, E., Becouze-Lareure, C., Aubin, J.-B., Jame, P., Barraud, S., Kouyi, G.L., Sébastien, C., Vulliet, E., 2018. Priority substances in accumulated sediments in a stormwater detention basin from an industrial area. *Environmental Pollution* 243, 1669–1678. <https://doi.org/10.1016/j.envpol.2018.09.138>
- Winters, N., Granuke, K., McCall, M., 2015. Roofing Materials Assessment: Investigation of Five Metals in Runoff from Roofing Materials. *Water Environment Research* 87, 835–844. <https://doi.org/10.2175/106143015X14362865226437>
- Wu, D., Ren, C., Jiang, L., Li, Q., Zhang, W., Wu, C., 2020. Characteristic of dissolved organic matter polar fractions with variable sources by spectrum technologies: Chemical properties and interaction with phenoxy herbicide. *Science of The Total Environment* 724, 138262. <https://doi.org/10.1016/j.scitotenv.2020.138262>
- Wu, H., Xu, X., Fu, P., Cheng, W., Fu, C., 2021. Responses of soil WEOM quantity and quality to freeze–thaw and litter manipulation with contrasting soil water content: A laboratory experiment. *CATENA* 198, 105058. <https://doi.org/10.1016/j.catena.2020.105058>
- Wu, J., Zhang, H., He, P.-J., Shao, L.-M., 2011. Insight into the heavy metal binding potential of dissolved organic matter in MSW leachate using EEM quenching combined with PARAFAC analysis. *Water Research* 45, 1711–1719. <https://doi.org/10.1016/j.watres.2010.11.022>
- Wu, J., Zhang, H., Shao, L.-M., He, P.-J., 2012. Fluorescent characteristics and metal binding properties of individual molecular weight fractions in municipal solid waste leachate. *Environmental Pollution* 162, 63–71. <https://doi.org/10.1016/j.envpol.2011.10.017>
- Xian, Q., Li, P., Liu, C., Cui, J., Guan, Z., Tang, X., 2018. Concentration and spectroscopic characteristics of DOM in surface runoff and fracture flow in a cropland plot of a loamy soil. *Science of The Total Environment* 622–623, 385–393. <https://doi.org/10.1016/j.scitotenv.2017.12.010>
- Xiao, K., Yu, J., Wang, S., Du, J., Tan, J., Xue, K., Wang, Y., Huang, X., 2020. Relationship between fluorescence excitation-emission matrix properties and the relative degree of DOM hydrophobicity in wastewater treatment effluents. *Chemosphere* 254, 126830. <https://doi.org/10.1016/j.chemosphere.2020.126830>
- Xiaozhen, F., Xing, L., Zhenglin, H., Kaiyuan, Z., Guosheng, S., 2022. DFT study of common anions adsorption at graphene surface due to anion- π interaction. *J Mol Model* 28, 225. <https://doi.org/10.1007/s00894-022-05218-4>
- Xu, H., Zou, L., Guan, D., Li, W., Jiang, H., 2019. Molecular weight-dependent spectral and metal binding properties of sediment dissolved organic matter from different origins. *Science of The Total Environment* 665, 828–835. <https://doi.org/10.1016/j.scitotenv.2019.02.186>

- Yang, B., Cheng, X., Zhang, Y., Li, W., Wang, J., Guo, H., 2021. Probing the roles of pH and ionic strength on electrostatic binding of tetracycline by dissolved organic matters: Reevaluation of modified fitting model. *Environmental Science and Ecotechnology* 8, 100133. <https://doi.org/10.1016/j.ese.2021.100133>
- Yang, D.-Q., Rochette, J.-F., Sacher, E., 2005. Spectroscopic Evidence for π - π Interaction between Poly(diallyl dimethylammonium) Chloride and Multiwalled Carbon Nanotubes. *J. Phys. Chem. B* 109, 4481–4484. <https://doi.org/10.1021/jp044511+>
- Yang, W., Wang, Z., Hua, P., Zhang, J., Krebs, P., 2021. Impact of green infrastructure on the mitigation of road-deposited sediment induced stormwater pollution. *Science of The Total Environment* 770, 145294. <https://doi.org/10.1016/j.scitotenv.2021.145294>
- Yang, X., Wan, Y., Zheng, Y., He, F., Yu, Z., Huang, J., Wang, H., Ok, Y.S., Jiang, Y., Gao, B., 2019. Surface functional groups of carbon-based adsorbents and their roles in the removal of heavy metals from aqueous solutions: A critical review. *Chemical Engineering Journal* 366, 608–621. <https://doi.org/10.1016/j.cej.2019.02.119>
- Yerli, C., Sahin, U., Ors, S., Kiziloglu, F.M., 2023. Improvement of water and crop productivity of silage maize by irrigation with different levels of recycled wastewater under conventional and zero tillage conditions. *Agricultural Water Management* 277, 108100. <https://doi.org/10.1016/j.agwat.2022.108100>
- Yi, P., Yan, Y., Kong, Y., Chen, Q., Wu, M., Liang, N., Zhang, L., Pan, B., 2023. The opposite influences of Cu and Cd cation bridges on sulfamethoxazole sorption on humic acids in wetting-drying cycles. *Science of The Total Environment* 898, 165547. <https://doi.org/10.1016/j.scitotenv.2023.165547>
- Yuan, D., An, Y., Wang, J., Chu, S., Lim, B., Chen, B., Xiong, Y., Kou, Y., Li, J., 2019. Dissolved organic matter characteristics of urban stormwater runoff from different functional regions during grassy swale treatment. *Ecological Indicators* 107, 105667. <https://doi.org/10.1016/j.ecolind.2019.105667>
- Zhang, D., Gersberg, R.M., Ng, W.J., Tan, S.K., 2017. Conventional and decentralized urban stormwater management: A comparison through case studies of Singapore and Berlin, Germany. *Urban Water Journal* 14, 113–124. <https://doi.org/10.1080/1573062X.2015.1076488>
- Zhang, F., Li, X., Duan, L., Zhang, H., Gu, W., Yang, X., Li, J., He, S., Yu, J., Ren, M., 2021. Effect of different DOM components on arsenate complexation in natural water. *Environmental Pollution* 270, 116221. <https://doi.org/10.1016/j.envpol.2020.116221>
- Zhao, X., Hu, Z., Yang, X., Cai, X., Wang, Z., Xie, X., 2019. Noncovalent interactions between fluoroquinolone antibiotics with dissolved organic matter: A ¹H NMR binding site study and multi-spectroscopic methods. *Environmental Pollution* 248, 815–822. <https://doi.org/10.1016/j.envpol.2019.02.077>
- Zhao, Z., Sun, W., Ray, M.B., 2022. Adsorption isotherms and kinetics for the removal of algal organic matter by granular activated carbon. *Science of The Total Environment* 806, 150885. <https://doi.org/10.1016/j.scitotenv.2021.150885>
- Zheng, X., Yu, N., Wang, X., Wang, Y., Wang, L., Li, X., Hu, X., 2018. Adsorption Properties of Granular Activated Carbon-Supported Titanium Dioxide Particles for Dyes and Copper Ions. *Sci Rep* 8, 6463. <https://doi.org/10.1038/s41598-018-24891-1>

- Zherebker, A., Shirshin, E., Rubekina, A., Kharybin, O., Kononikhin, A., Kulikova, N.A., Zaitsev, K.V., Roznyatovsky, V.A., Grishin, Y.K., Perminova, I.V., Nikolaev, E.N., 2020. Optical Properties of Soil Dissolved Organic Matter Are Related to Acidic Functions of Its Components as Revealed by Fractionation, Selective Deuteromethylation, and Ultrahigh Resolution Mass Spectrometry. *Environ. Sci. Technol.* 54, 2667–2677. <https://doi.org/10.1021/acs.est.9b05298>
- Zhu, P., Knoop, O., Helmreich, B., 2022. Interaction of heavy metals and biocide/herbicide from stormwater runoff of buildings with dissolved organic matter. *Science of The Total Environment* 814, 152599. <https://doi.org/10.1016/j.scitotenv.2021.152599>
- Zhu, P., Sottorff, I., Zhang, T., Helmreich, B., 2023. Adsorption of Heavy Metals and Biocides from Building Runoff onto Granular Activated Carbon—The Influence of Different Fractions of Dissolved Organic Matter. *Water* 15, 2099. <https://doi.org/10.3390/w15112099>